Fractional Flow Reserve and the Diagnosis of Coronary Artery Disease

A Thesis
Submitted for the Degree of
Master of Science (Engineering)

by

Akanksha Bohra

Engineering Mechanics Unit
Jawaharlal Nehru Centre for Advanced Scientific Research
(A Deemed University)
Bangalore – 560 064

NOVEMBER 2020

DECLARATION

I hereby declare that the matter embodied in the thesis entitled "**Fractional Flow Reserve and the Diagnosis of Coronary Artery Disease**" is the result of investigations carried out by me at the Engineering Mechanics Unit, Jawaharlal Nehru Centre for Advanced Scientific Research, Bangalore, India under the supervision of **Prof. Santosh Ansumali** and that it has not been submitted elsewhere for the award of any degree or diploma.

In keeping with the general practice in reporting scientific observations, due acknowledgment has been made whenever the work described is based on the findings of other investigators.

Akanksha Bohra

CERTIFICATE

I hereby certify that the matter embodied in this thesis entitled "**Fractional Flow Reserve and the Diagnosis of Coronary Artery Disease**" has been carried out by **Ms. Akanksha Bohra** at the Engineering Mechanics Unit, Jawaharlal Nehru Centre for Advanced Scientific Research, Bangalore, India under my supervision and that it has not been submitted elsewhere for the award of any degree or diploma.

Prof. Santosh Ansumali

(Research Supervisor)

Acknowledgements

I express my sincere gratitude to Prof. Santosh Ansumali for his patience, encouragement, and guidance during my Masters' which helped me professionally and personally. I would also like to thank Prof. P Sunthar and Prof. V Kumaran for their inputs in the thesis. I thank Dr. Ashita Barthur, Radiologist, SJICR, and Dr. Rahul Patil, Cardiologist, SJICR for their help during our collaborative work. I am also grateful to Ms. Rani B. J., Staff Nurse, SJICR and Mr. Pratheesh Kumar K.C., DEO, SJICR for their time and help during the data-collection process. I thank the faculty, my lab mates and colleagues in EMU and JNCASR for all the help and time. I would like to thank the administrative staff, employees of the library, Complab, hostel and other staff for their cooperation. I thank my family for their constant love and support.

Abstract

Coronary artery disease (CAD) is a widespread cardiovascular illness that causes high rates of mortality all around the world (World Health Organization 2016; Kaptoge *et al.* 2019). The diagnosis of coronary artery disease progressed over the years from the use of invasive coronary angiography (ICA) only procedure to the use of non-invasive coronary computed tomography angiography (CCTA) and invasive FFR for making treatment decisions. While ICA and CCTA provide an anatomical-visual assessment of the disease, the invasive FFR measures the quantitative functional effect of the disease by measuring fractional flow reserve (FFR), a pressure ratio index based on the correlation between blood flow and pressure drop in coronary arteries. To obtain both the anatomical and functional assessment of the disease using non-invasive measures, CT-FFR method was developed in last decade. The thesis presents the framework of CT-FFR methodology using open source tools. We provide a review of the clinical trials that led to the approval of CT-FFR process for clinical use. The CT-FFR method is based on the development of patient-specific coronary blood flow models created from Coronary Computed Tomography Angiography(CCTA) image datasets. To acquire the clinical data, the data-collection was undertaken and a data repository of CCTA images, ICA images and FFR data was created. The patient-specific three-dimensional geometries for two subjects from the study were constructed. The blood flow was simulated using these 3D models as the computational domain with lumped parameter models of the cardiovascular system as boundary conditions. The FFR values were computed using pressure distribution results from the simulation and compared against the invasive FFR values obtained from clinical measurement.

List of Figures

1.1 Top 10 Global Causes of Death in 2016 (World Health Organization 2016). 3
1.2 Deaths by Cardiovascular diseases in 2016 (World Health Organization 2016). . . 3
1.3 Build-up of Coronary Artery Disease (Blausen,Wikipedia 2013). 4
1.4 Conventional care-path to treat stable coronary artery disease. 5
1.5 Overview of patient treatment strategies using invasive and non-invasive methods. 5
1.6 Measurement of invasive FFR. 6
1.7 Recommended care path after FAME trials (Tonino *et al.* 2009). 6
1.8 Framework of CT-FFR process. 6
1.9 CT-FFR guided care-path. 7
1.10 The procedural outline to study the CT-FFR process for current project. 8

2.1 The Heart section as viewed from the front (Pierce 2019). Left and right side of heart are left hand and right hand side of patient. 11
2.2 Ventricular pressure-volume curve for one cardiac cycle. EDV: End-diastolic volume. ESV: End-systolic volume. Figure reproduced (Hall & Guyton (2011); Chandran *et al.* (2007)) with permission. 13
2.3 Pressure variation in systemic circulation(Pappano *et al.* 2013; Levick 1991). . . . 14
2.4 Pressure at different stages of cardiac loop. (a) during peak systole (b) during end diastole (Image sourced from OpenStax (OpenStax CNX 2013) and modified with added pressure values). 15
2.5 Flow velocity and cross-sectional area changes in systemic circulation (Pappano *et al.* 2013; Levick 1991). 16
2.6 Quantities relevant to flow in a blood vessel. 16
2.7 Coronary Circulation. Left: Anterior view. Right: Posterior view(Betts *et al.* 2013). 18
2.8 Aortic origin of Left and Right coronary arteries:L= left, R= right, NC= noncoronary, LCA= Left Circumflex Artery, RCA= Right Coronary Artery, LAD= Left Anterior Descending Artery, LM= Left Main. (Waller *et al.* 1992). 18
2.9 Proximal, Mid and Distal part of artery. 19
2.10 Phasic coronary blood flow in Left and right coronary arteries (Pappano *et al.* 2013). 20
2.11 Blood flow in Healthy artery(A) and Blocked Artery(B). Image sourced from National Heart, Lung, and Blood Institute, U.S. website (National Heart, Lung, and Blood Institute 2018). 21
2.12 Flow rate and velocity as function of degree of stenosis for a smooth and axisymmetric stenosis (Hoskins *et al.* 2016*b*; Spencer & Reid 1979). 22
2.13 Proximal and Distal Pressures in a stenosed coronary artery. 23
2.14 Change in CAD care-paths with inclusion of invasive FFR and CT-FFR. OMT stands for optimal medical therapy. 25
2.15 Left: CT-scanning tube and detector rotate around patient (Hoskins *et al.* 2016*a*); RightCT-Scan Equipment (Image source: `https://www.philips.co.in/healthcare/product/HC889407/brilliance-ct-64-channel---ds-refurbished-ct-scanner`, Retrieved on 17 Feb 2020). 26
2.16 Coronary CT-scan Axial view (left) and Curved MPR view for Artery visualization. 27

2.17 CT-Scan Images and 3D View after Image reconstruction. 28
2.18 Cath-Lab Equipment (Image source:https://avantehs.com/p/philips-allura-xper-fd10-cathangio-system/13789, Retrieved on Feb 17, 2020). 28
2.19 Plaque visualization in CT-Scan(left) and in Invasive Coronary Angiography(right) in Cath-Lab. 29
2.20 Invasive FFR measurement using Pressure wire through Catheter. 29
2.21 Invasive FFR values in using St. Jude Medical FFR measurement System. 30

3.2 Coronary Artery model colormapped with indicated FFR value from HeartFlow. Image retrieved from https://www.heartflow.com/ on Oct 2019. 35

4.1 Data-collection Process. 40
4.2 Coronary CTA Acquisition Process. OPD (Outpatient Department). 41
4.3 Invasive Angiography Procedure Protocol. 42
4.4 Invasive FFR Procedure Protocol. 43
4.5 DICOM Image Set, 2D images and 3D volume.(Image retrieved from "http://people.cas.sc.edu/rorden/ezdicom/activex/index.html" on Sept 7, 2018). 44
4.6 DICOM Data Model Structure (Damien 2015). 44
4.7 Anonymization in DicomCleaner. 47
4.8 Screenshot of database main web-page. The database is accessible at "http://www.jncasr.ac.in/dicon/". 47
4.9 Screenshot of Login-page to upload data in database. 48
4.10 Screenshot of Upload data form (left) and the data download page (right). 48

5.1 Left: Raw grey scale image; Right: Segmented region based on pixel intensity. . . 50
5.2 Active Contour Model(evolution of contour). 50
5.3 Level Set Method (Nicoguaro,Wikipedia 2018). 51
5.4 3D Slicer Ecosystem (Fedorov *et al.* 2012). 52
5.5 CT-Scan images in 3D Slicer GUI with Volume Rendering. 52
5.6 Threshold method in Slicer. 53
5.7 Model Generated in slicer using Threshold method. 53
5.8 SimVascular Pipeline (Updegrove *et al.* 2017). 54
5.9 Creating pathlines along the centreline of coronary arteries in SimVascular display window. 54
5.10 2D contour segmentation in SimVascular. 55
5.11 Model Generated in SimVascular. 55

6.1 Total resistance in series and parallel configuration (Chandran *et al.* 2007). 58
6.2 (a) Pipe flow (b) Equivalent electric circuit. 59
6.3 Windekessel models. 60
6.4 Different Modelling Scales (Shi *et al.* 2011). 61
6.5 Inflow Waveform (Absi 2018; Karmonik *et al.* 2014). 63
6.6 Aorta outlet boundary condition. 63
6.7 Boundary condition at coronary outlets. 64
6.8 Pressure variation in left and right ventricles (Hall & Guyton 2011). 64
6.9 Simulation setup with inflow, RCR and RCRCR boundary conditions. 65
6.10 Paralled artery and body circuit. 66
6.11 Parent Artery and bifurcation. 67
6.12 The lesion in LAD from CCTA images and in the 3D model for case study 1. . . 68
6.13 Flow rate at aorta inlet and outlet 69
6.14 Pressure waveform at aorta inlet and outlet. 69
6.15 Flow and pressure waveform for Left coronary artery (proximal). 69

6.16 Flow and pressure waveform for Right coronary artery (proximal). 70
6.17 Aortic Pressure, Pressure proximal and distal to lesion in LAD. 70
6.18 Flow velocity proximal and distal to lesion in LAD. 70
6.19 Average pressure distribution in coronary artery bed. 71
6.20 Streamlines at different instances of a cardiac cycle.t=0.1 is peak diastole phase and t=0.5 is peak systole phase. 71
6.21 Invasive FFR for stenosed LAD for case 01. 72
6.22 Stenosed artery fom ICA image and calculated FFR for case 01. 72
6.23 FFR values at proximal and distal points to lesion in LAD for case 01. 72
6.24 CCTA with stenosis in LAD for case 2. 73
6.25 Pressure waveform at aorta inlet and outlet for case 2. 73
6.26 Comparison of Invasive FFR with Computed FFR for case 2. 74

A.1 Pressure wire Aeris with Agile Tip from St. Jude MedicalSystems AB (abbott) (St. Jude global 2018) 78

List of Tables

1.1 Indicative average costs of various procedures in CAD care in USA, UK and Japan compared to India. In all countries, the cost of diagnosis varies greatly, and the costs mentioned here fall on the lower end of the spectrum. The cost of CT-FFR procedure in Japan is approximate cost. The countries selected are the ones listed for service in the HeartFlow website: USA (approval by FDA (Cohen 2014; HeartFlow Inc. 2019*a*)), Japan (approval by Japanese Ministry of Health, Labour and Welfare (Japan HeartFlow 2016)), UK (endorsed by National Institute for Health and Care Excellence (NICE) (NICE HeartFlow 2017)). 8

2.1 Vessel Dimensions, Volume, Area, Pressure, Velocity and Reynolds number through Systemic Circulation. Table adapted from (Hoskins *et al.* 2016*b*; Klabunde 2011; Chandran *et al.* 2007) and data also sourced from (Dawson 2005) 13
2.2 Lumen diameter of Coronary Arteries (Dodge *et al.* 1992; Waller *et al.* 1992). . . 19
2.3 Male and Female coronary artery dimensions comparison for Indian patients (Saikrishna *et al.* 2006). 20
2.4 Canadian cardiovascular Society grading of angina pectoris (Canadian Cardiovascular Society 2006). 22
2.5 Coronary Artery Disease -Reporting and Data System (CAD-RADS) for patients with stable chest pain. Table content reproduced from (Cury *et al.* 2016). 23
2.6 Hounsfield Values for different substances (Pavone *et al.* 2009; Kalra 2018). . . . 27

3.1 Comparison of results from FFR_{CT} Evaluation Studies. 36

4.1 Baseline characteristics of participants in collected-data for current study. 46

6.1 Analogy of Electrical Circuit and Cardiovascular System. 58
6.2 Blood Flow in Characteristics in Cardiovascular System (Hoskins *et al.* 2016*b*). . 62

A.1 Philips Brilliance 64-Slice CT-Scanner Specifications (Medwow 2018; Philips CT website 2018) 77
A.2 Philips Allura Xper FD10 Cath Lab System Specifications, (Phillips Medwow 2018) 78
A.3 Pressure measurement Specifications (SJM manual 2020) 78
A.4 Specifications of Wireless transmission(FCCID user manual 2019) 79

Contents

Abstract **vii**

Abbreviations **1**

1 Introduction **3**
1.1 Chapter Outline 9

2 Cardiovascular System and Coronary Artery Disease **11**
2.1 Cardiovascular System 11
2.1.1 The Cardiac Cycle 12
2.1.2 Pressure and velocity variation in Circulation 14
2.1.3 Coronary Circulation 17
2.2 Coronary Artery Disease 20
2.3 Fractional Flow Reserve(FFR) 23
2.4 Diagnosis and Treatment of Coronary Artery Disease 24
2.4.1 Coronary CT-Scan 26
2.4.2 Invasive Coronary Angiography(ICA) 28
2.4.3 Invasive FFR 29
2.4.4 Clinical Trials related to invasive FFR 30

3 CT-FFR **33**
3.1 CT-FFR Procedure 33
3.1.1 HeartFlow FFR_{CT} Software 34
3.1.2 Siemens cFFR Software 35
3.2 Research Studies evaluating CT-FFR 35
3.3 Limitations of CT-FFR 38

4 Data Collection and Medical Imaging **39**
4.1 Clinical Data Collection 39
4.1.1 Coronary CTA acquisition 40
4.1.2 ICA Images and FFR data acquisition 41
4.2 Medical Imaging 42
4.3 Database and Data storage 45

5 3D Modelling of Vascular Structures **49**
5.1 Image Segmentation 49
5.1.1 Threshold Technique 50
5.1.2 Contour Models (Deformable models) 50
5.2 Segmentation tools and reconstruction of coronary arteries 51
5.2.1 About 3D Slicer 51
5.2.2 About Simvascular 53

6 Coronary Blood Flow Simulation **57**
6.1 Analogy of the cardiovascular system with electrical circuit 57
6.1.1 Cardiovascular system as lumped parameter model 58
6.1.2 Distributed Parameter Modelling 60
6.2 Blood flow characteristics in circulatory System 61
6.3 Boundary Conditions 62
6.3.1 Inlet flow boundary conditions 63
6.3.2 Outlet boundary conditions 63
6.4 Simulation Set-up 64
6.4.1 Calculation of Vascular Resistance 65
6.4.2 Approximation of Arterial Compilance 67
6.5 Simulation Results 68
6.5.1 Case Study 01 68
6.5.2 Case Study 02 73

7 Outlook **75**

Appendix A **77**
A.1 Philips Brilliance 64-Slice CT-Scanner 77
A.2 Philips Allura Xper FD10 Cath Lab System 77
A.3 FFR Measurement System 77

Abbreviations

AC	Alternating Current
AHA	American Heart Association
CABG	Coronary Artery Bypass Grafting
CAD	Coronary Artery Disease
CAD-RADS	Coronary Artery Disease-Reporting and Data System
CCS	Canadian Cardiovascular Society
CCTA	Coronary CT Angiography
CFD	Computational Fluid Dynamics
CHD	Coronary Heart Disease
CI	Confidence Interval
CO	Cardiac Output
CT	Computed Tomography
CV	Cardiovascular
CVD	Cardiovascular Disease
DICOM	Digital Imaging and Communications in Medicine
ECG	Electrocardiogram
ECHO	Echocardiography
EDV	End-Diastolic Volume
ESV	End-Systolic Volume
FFR	Fractional Flow Reserve
HR	Heart Rate
HU	Hounsfield Unit
ICA	Invasive Coronary Angiography
IHD	Ischemic Heart Disease
LAD	Left Anterior Descending Artery
LCX	Left Circuflex Artery
LMCA	Left Main Coronary Artery
LV	Left Ventricular
MACE	Massive Adverse Cardiovascular Events
MAP	Mean Aortic Pressure

MI	Myocardial Infarction
MRI	Magnetic Resonance Imaging
NTG	Nitroglycerin
OMT	Optimum Medical Therapy
PCI	Percutaneous Coronary Intervention
PET	Positron Emission Tomography
RCA	Right Coronary Artery
RV	Right Ventricle
SCCT	Society of Cardiovascular Computed Tomography
SPECT	Single-photon Emission Computed Tomography
SV	Stroke Volume

Chapter 1
Introduction

Coronary artery disease (CAD), also known as ischaemic heart disease (IHD) or coronary heart disease (CHD) is an endemic condition with high mortality rates (Sanchis-Gomar *et al.* 2016). According to World Health Organization estimates, over 17 million people died of cardiovascular diseases in the year 2016, of which 9.4 million deaths were caused by ischaemic heart disease, making it one of the leading causes of the deaths in the world (figure 1.1 and 1.2) (World Health Organization 2016; Kaptoge *et al.* 2019). Majority of these deaths occur in low and middle income countries (Klag 2012; Kaptoge *et al.* 2019). Indeed, according to Indian Council of Medical Research report, one of the "the leading individual cause of death in India in 2016 was ischaemic heart disease, the death rate from which was twice as much as the next leading cause" (ICMR 2017).

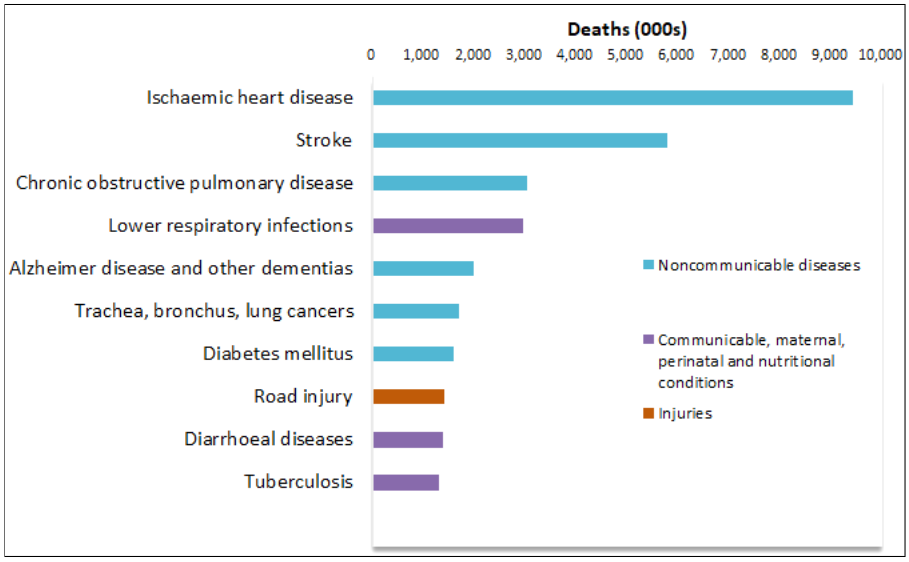

Figure 1.1: Top 10 Global Causes of Death in 2016 (World Health Organization 2016).

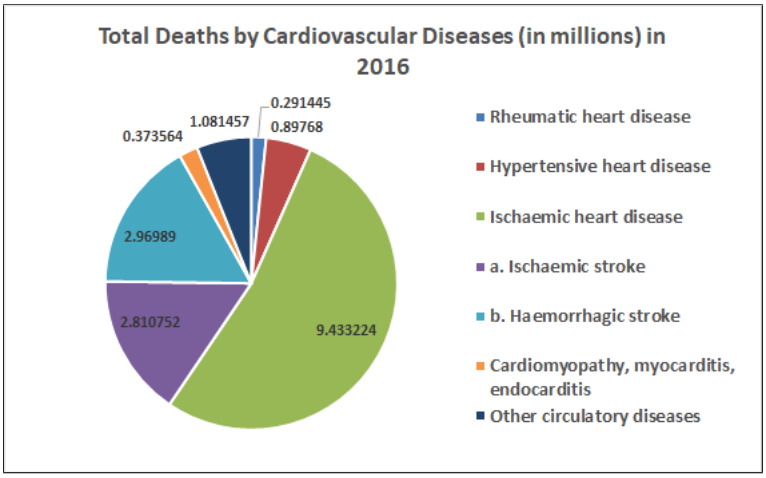

Figure 1.2: Deaths by Cardiovascular diseases in 2016 (World Health Organization 2016).

Coronary artery disease happens when fatty deposits (plaque) build up in coronary arteries (Hall & Guyton 2011)(figure 1.3). These arteries supply blood, oxygen and nutrients to heart muscles. The plaque hardens over time and constricts the arteries. A build-up of plaque on arterial walls is called atherosclerosis and the narrowing of arteries due to the atherosclerotic plaque is called stenosis (Hoskins *et al.* 2016*b*). It reduces blood flow to heart muscles. Inadequate blood supply due to partial or complete blockage of vessels is called myocardial ischaemia (Hall & Guyton 2011). The formation of plaque can also rupture and cause the formation of blood clots which disrupts the blood flow. Resulting ischaemia or lack of oxygenated blood can lead to damage or death of heart muscles. It results in chest pain and discomfort or heaviness in the jaw, shoulder, back or arm (angina pectoris) (Cassar *et al.* 2009). A Complete blockage of blood flow to an area of the heart can lead to a heart attack (myocardial infarction). Non-functioning cardiac muscles also lead to irregularity of heartbeat (arrhythmia) and heart-failure (Ashley & Niebauer 2004). A few major factors that can cause coronary artery disease include high blood pressure, smoking, high blood cholesterol, and diabetes (Pryor *et al.* 1991). Other significant factors are obesity, sedentary lifestyle, age, and family history of early heart disease (Klag 2012).

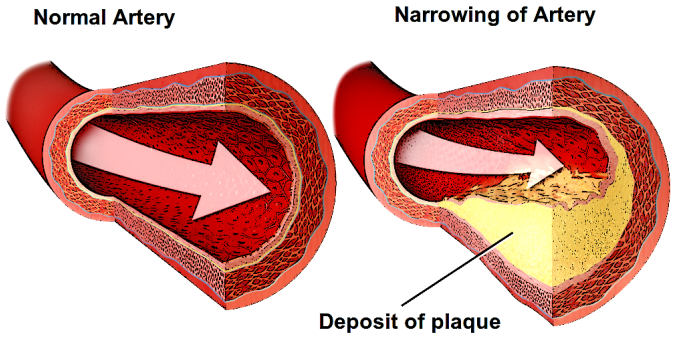

Figure 1.3: Build-up of Coronary Artery Disease (Blausen,Wikipedia 2013).

The chest pain experienced intermittently due to physical exertion or stress is called stable angina (Hall & Guyton 2011). Typically, it lasts for a short time and disappears during rest. Unstable angina is the chest pain that occurs during rest or with very little physical exertion and is a medical emergency condition which requires immediate treatment (Kern *et al.* 2018). Conventionally, patients with stable angina are diagnosed based on medical history, physical exams and diagnostic tests and procedures (figure 1.4). Initial diagnosis of patients suffering from chronic chest pain includes non-invasive tests like an echocardiogram (ECHO), electrocardiogram (ECG), coronary computed tomography angiography (CCTA), etc. Often, patients undergo exercise stress tests to induce symptoms and evaluate the effect of level of exertion on heart rate, blood pressure and heart function. The stress test can be paired up with ECG and echocardiogram. While ECG reveals the abnormalities of heart rhythm due to CAD, echocardiogram evaluates the overall function of the heart. Coronary computed tomography angiography (CCTA) is CT-scan for coronary arteries. It is an imaging test which produces images of heart and blood vessels using X-rays. Current treatment plan involves patients with evidence of CAD undergoing further diagnosis which includes Invasive Coronary Angiography (ICA)and measurement of invasive FFR during ICA procedure (Alfakih *et al.* 2018; Budoff & Nakansihi 2016). Invasive coronary angiography is an X-ray imaging procedure to visualize blood flow in vessels (Kern *et al.* 2018). Coronary artery disease is treated with medicines and medical procedures such as angioplasty and coronary artery bypass grafting (CABG).

Coronary computed tomography angiography (CCTA) and invasive coronary angiography (ICA) are used for anatomical evaluation of disease by visual assessment. Stenosis in an artery

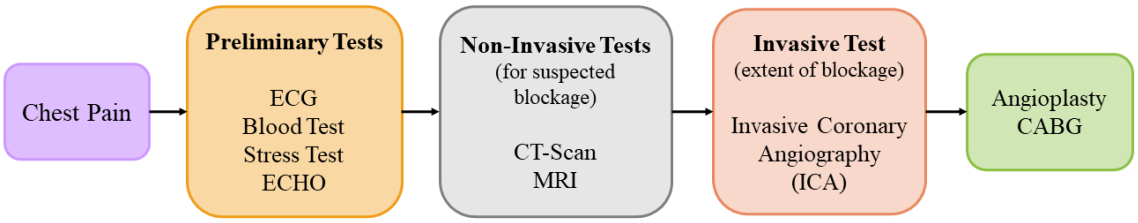

Figure 1.4: Conventional care-path to treat stable coronary artery disease.

is physiologically significant if it causes ischaemia (Sciola *et al.* 2018). Typically, any occlusion in arteries reduces coronary blood flow. As blood flow is directly proportional to the pressure gradient, the measurement of the drop in pressure across stenosis gives a quantitative indication of the reduction in blood flow, thus estimating the effect of stenosis on heart function. Invasive FFR measurement is based on this correlation between blood flow and pressure in coronary arteries (Taylor *et al.* 2013). Fractional flow reserve (FFR) is an index to quantitatively evaluate the functional significance of a stenosis. It is defined as the ratio of pressure downstream of the stenotic lesion to pressure upstream of the lesion (aortic pressure) during hyperaemia (maximal blood flow) (Hoskins *et al.* 2016*b*). FFR is invasively measured using a pressure-wire at the time of ICA in the cardiac catheterization laboratory (figure 1.6). FFR value (FFR $\leq$ 0.8) determines the need for revascularization of an artery (Tonino *et al.* 2009). Invasive FFR is considered a 'Gold Standard' for severity assessment of vessel-specific ischaemia because of its accuracy (Zimmermann *et al.* 2019)(figure 1.7). Patients with functionally non-significant stenosis are treated with optimal medical therapy(OMT) alone. A single test to determine both the anatomical and functional significance of stenosis has been a long-standing objective in the area of non-invasive assessment of CAD (Zarins *et al.* 2013). The poor correlation between visual assessment by ICA and the functional assessment by FFR ((Tonino *et al.* 2010; Park *et al.* 2012) has encouraged these efforts. Interest in developing alternatives to invasive procedures has led to the development of CT-FFR (Computed Tomography derived Fraction Flow Reserve) method.

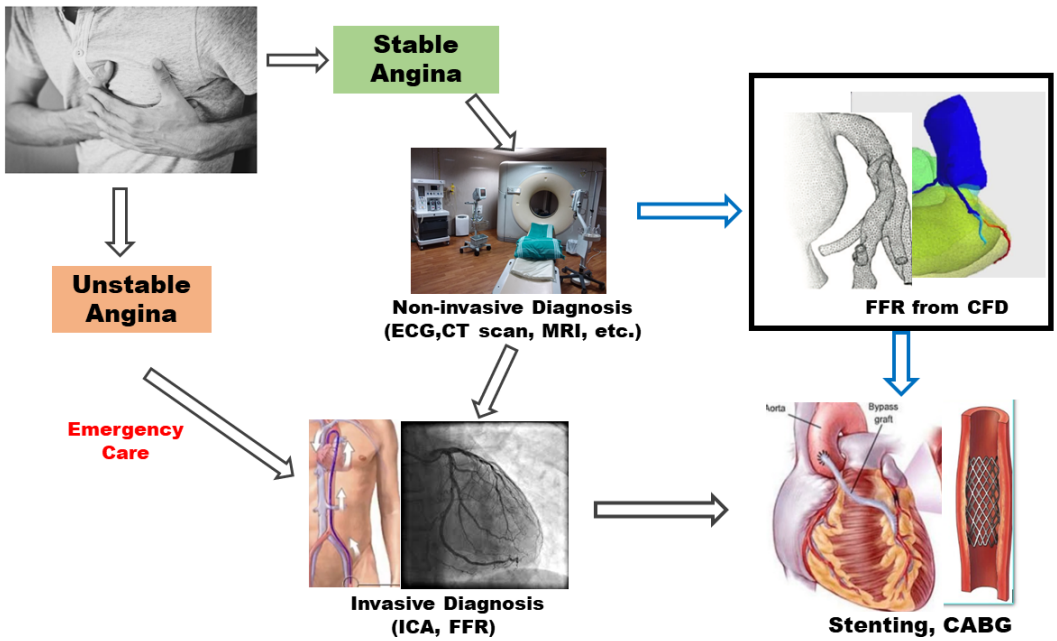

Figure 1.5: Overview of patient treatment strategies using invasive and non-invasive methods.

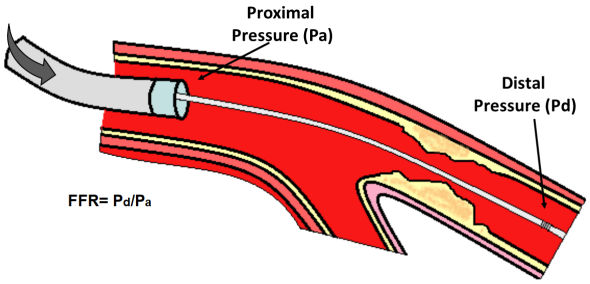

Figure 1.6: Measurement of invasive FFR.

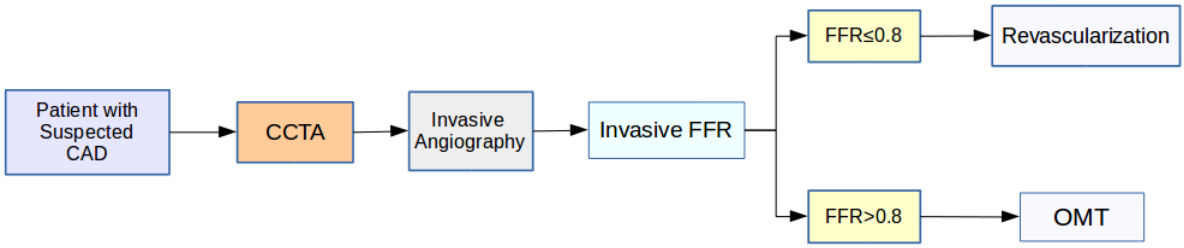

Figure 1.7: Recommended care path after FAME trials (Tonino *et al.* 2009).

CT-FFR method is one such non-invasive diagnostic technique used for assessment of coronary artery disease. For CT-FFR, image datasets from coronary computed tomography angiography (CCTA) are used to create patient-specific coronary artery models (figure 1.8). The three-dimensional mesh is generated from CT-scan images of coronary arteries. Blood flow is simulated using the Navier-Stokes equation and FFR is calculated from pressure variation in arteries. CT-FFR allows for a single non-invasive test for 'combined anatomic-functional assessment' (Zarins *et al.* 2013). The CT-FFR method is aimed at risk and cost reduction resulting from invasive procedures (Colleran *et al.* 2017). The FFR computed using CCTA data has been clinically validated by direct comparison with invasive FFR in trials like DISCOVER-FLOW(Koo *et al.* 2011) , DeFACTO (Min *et al.* 2012) and NXT(Nørgaard 2014) (Budoff & Nakansihi 2016; Curzen *et al.* 2016). The FFR_{CT} software developed by HeartFlow Inc., U.S.A is currently the only commercial software being used for prediction of FFR from CCTA images for clinical use (Cohen 2014; HeartFlow Inc. 2019*a*). The FFR_{CT} software was cleared for use in the treatment plan by the U.S. Food and Drug Administration (FDA) in 2014 (Cohen 2014; HeartFlow Inc. 2019*a*). In 2019, it was commercially available in the USA, Canada, Europe and Japan (HeartFlow Inc. 2019*a*).

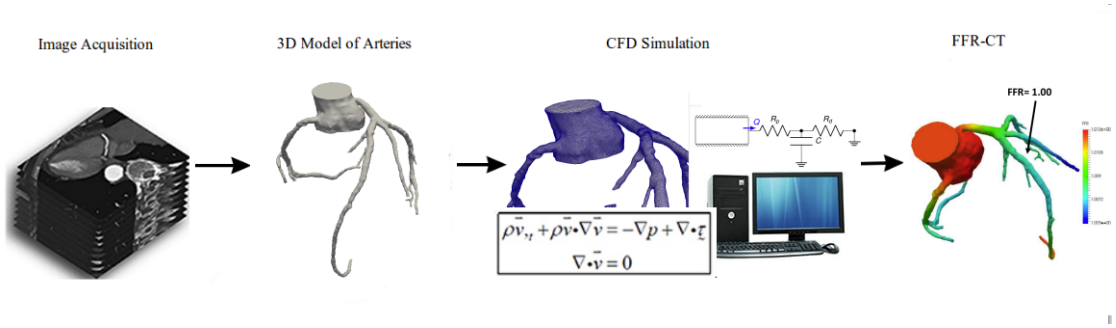

Figure 1.8: Framework of CT-FFR process.

However, in India, the main decision-making test for revascularization has been invasive coro-

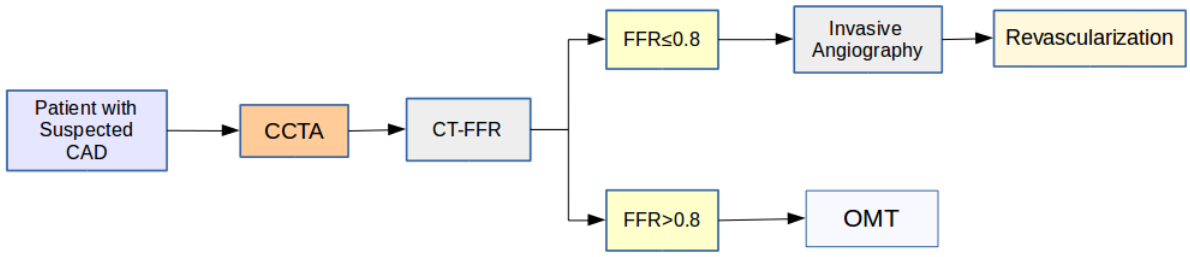

Figure 1.9: CT-FFR guided care-path.

nary angiogram for long. It is observed that only 40% of patients suffering from coronary stenosis require consequent intervention after invasive coronary angiography (Gorenoi *et al.* 2012; Patel *et al.* 2014). It has also been speculated that there is "unwarranted re-vascularization without much clinical improvement"(Prasad *et al.* 2017) for Indian patients with the borderline coronary lesion. The invasive FFR based patient management is getting used more often in diagnosis over the last few years. Invasive FFR procedure costs upwards of INR 30,000 (Sengottuvelu *et al.* 2016). While the use of invasive FFR in decision making is shown to be a cost-effective and safer measure for overall patient management process, it does put an extra economic burden on the patient (Sengottuvelu *et al.* 2016; Prasad *et al.* 2017). The availability of a non-invasive diagnostic procedure has shown to reduce the economic burden and the risk of extra invasive procedures (Whittaker & Curzen 2013). With a large population of heart patients in our country (ICMR 2017), the availability of such non-invasive FFR procedure can reduce the number of people being sent to the catheterization laboratory for ICA. The average cost of CT-scan in the USA is 1000 USD (Kincaid 2018). The reported cost of CT-FFR evaluation by HeartFlow is 1500 USD (more than INR 100,000) in United States (Douglas 2016; HeartFlow Cost 2019; Kincaid 2018), which is equivalent to per capita annual income for India (National Statistical Office India 2019). The average cost of both coronary CT angiogram (CCTA) and ICA in India, ranges between INR 6000 to INR 10,000 (average cost of 100 USD) (SJICR 2019). The coronary angioplasty costs upwards of INR 45,000 (SJICR 2019). A comparative costs of diagnostic and treatment procedures are listed in table 1.1. A non-invasive diagnostic procedure like CT-FFR is highly relevant for Indian population only if it is made available within a cost range of doing CT-scan procedure (∼100USD). Such cost-effective solution would require a dedicated software package.

Any attempt for the development of an indigenous non-invasive medical technology similar to FFR_{CT} would require a considerable number of good quality medical images and clinical data relevant to local condition. The functionality and accuracy of the tool can only be substantiated with invasive FFR. HeartFlow FFR_{CT} has been used for the diagnosis of more than 30,000 patients (HeartFlow Inc. 2019*b*). Indian patients have different size of coronary arteries than that of Caucasians and have more frequent cases of single and multivessel coronary artery disease but there is a scarcity of FFR related data from India (Sengottuvelu *et al.* 2016; Raut *et al.* 2017). There is no open or free access medical image database of Indian patients available to the best of author's knowledge. This project intends to bridge the gap by providing high-quality data.

The objective of the current project is to study the basic framework of CT-FFR based methodology. The framework includes the acquisition of CCTA images, creating three-dimensional models of coronary arteries, blood flow simulation in the models, and comparative assessment of computed FFR against invasive FFR. To acquire the necessary clinical data-set, data collection exercise is undertaken in which data is collected from patients suffering from CAD and being treated in a tertiary care hospital. Data collected under standard protocols include CT-scan

Procedure	**USA*** **(cost in USD)**	**UK*** **(cost in USD)**	**Japan**** **(cost in USD)**	**India***** **(cost in USD)**
Coronary CT-Scan	1100	600	300	110
Invasive Coronary Angiography	7088	2446	500	250
Invasive FFR	1000^{+}	800^{++}	1800	400
Angioplasty(one stent)	32229	11661	11000	3000
Heart Bypass surgery	78104	24440	29000	5000
CT-FFR procedure	1500$^{\oplus}$	900 $^{\oplus\oplus}$	1500	-

* CT-scan, Invasive Coronary Angiography, Angioplasty and Bypass Surgery cost from International Federation of Health plans Comparative Price Report (IFHP report 2019)
** Source: Tanaka *et al.* (2019) and Igarashi *et al.* (2013), National Center for Global Health Medicine (Japan NCGM 2020), and Kimura *et al.* (2015)
*** Source: Indian Healthcare Tourism, SEPC (India Healthcare Tourism 2020) and Sri Jayadeva Institute of Cardiovascular Science and Research (SJICR 2019)
$^{+}$ Source for invasive FFR Moschetti *et al.* (2014) and Hoffman (2018)
$^{++}$ Source: Moschetti *et al.* (2014)
$^{\oplus}$ Source: HeartFlow Cost (2019); Kincaid (2018)
$^{\oplus\oplus}$ Source: Alfakih *et al.* (2018), NHS England Innovation and Technology Payment (UK FFR-CT 2019); the cost of Heartflow FFR_{CT} is £700, (the conversion rate used here is £1= 1.30USD)

Table 1.1: Indicative average costs of various procedures in CAD care in USA, UK and Japan compared to India. In all countries, the cost of diagnosis varies greatly, and the costs mentioned here fall on the lower end of the spectrum. The cost of CT-FFR procedure in Japan is approximate cost. The countries selected are the ones listed for service in the HeartFlow website: USA (approval by FDA (Cohen 2014; HeartFlow Inc. 2019*a*)), Japan (approval by Japanese Ministry of Health, Labour and Welfare (Japan HeartFlow 2016)), UK (endorsed by National Institute for Health and Care Excellence (NICE) (NICE HeartFlow 2017)).

images, invasive-FFR data, invasive angiogram images and demographic information. This data set is anonymized and stored in a local database at JNCASR. Even though small in scale, the data collection is intended to create a reference data-set which can be used for investigation, evaluation, development and testing of either conventional or commercial tools for clinical use.

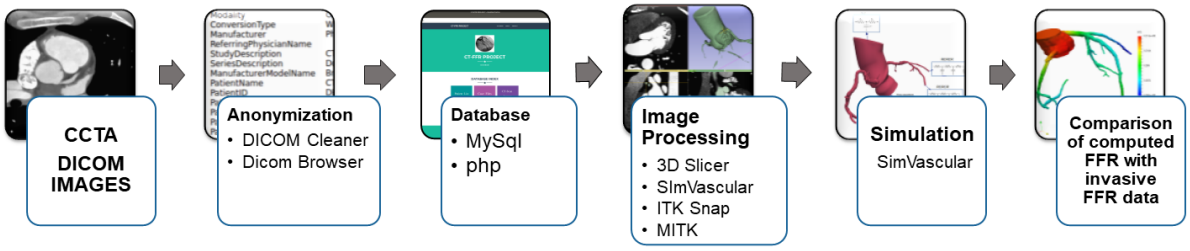

Figure 1.10: The procedural outline to study the CT-FFR process for current project.

At present, multiple image-processing software packages commercial (e.g., Mimics, AMIRA-AVIZO) and open-source (e.g., ITK, VTK, ITK-SNAP, 3D Slicer) exist to create vascular models from medical images. Similarly, a large number of dedicated CFD tools (e.g., OpenFOAM, ICEM, FLUENT) are available for flow simulation in 3D models which can be used for blood flow

simulation. Integrated three-dimensional modelling and simulation packages dedicated to cardiovascular simulation (e.g., CRIMSON, SimVascular) are also available. For the current project, the feasibility of the entire process workflow with the uses of open-source software packages is studied (figure 1.10). The thesis reviews the methodology for non-invasive computation of FFR such that the developmental and implementation framework along with medical data-sets for validation can be used for further advancement of applications for clinical use. Patient-specific image-based coronary artery models are created for two subjects from acquired CT-images during data-collection. The threshold and level-set segmentation methods are utilized for image segmentation and the three-dimensional models are generated using two different image processing software (3D Slicer and SimVascular). Blood flow is simulated by coupling 3D simulation with reduced order boundary conditions (lumped parameter models). Zero-dimensional models or lumped parameter models are a simplified representation of cardiovascular system characteristics and implemented using the hydraulic-electrical analogy. Flow pattern, pressure and velocity are obtained from simulation results and FFR value is computed from these results. Reliability of the coronary blood flow models and existing assumptions in modelling and simulation is estimated by the correlation of calculated FFR with the invasive FFR data.

1.1 Chapter Outline

The report is organised as follows:

- Chapter 2 gives the introduction to the cardiovascular circulatory system including coronary circulation. It discusses the coronary artery disease mechanism and its gradation. The utility and limitations of various diagnostic procedures for CAD and treatment methods are explained.
- Chapter 3 presents the CT-FFR method and its clinical background. It includes the discussion on past clinical trials and current research leading to the development of FFR_{CT} and its inclusion in treatment decision making. The limitations of the CT-FFR are also summarized.
- Chapter 4 presents the clinical data-collection steps, description of protocols for medical procedures involved in data-collection and method of database creation.
- Chapter 5 presents the procedure of creating a 3-dimensional geometry of the coronary artery model from CCTA images. It involves the discussion of image-segmentation methods and software tools used for the construction of the 3D model.
- Chapter 6 presents blood flow simulation in coronary artery bed and simulation results. It lists the blood flow modelling assumptions in arteries. The reduced-order models of inlet and outlet boundary conditions are discussed and the steps to set up the simulation in the computational domain in CFD solver are listed. The result of virtual FFR calculation is compared with invasive FFR results.
- Chapter 7 presents a discussion on the possible roadmaps and challenges in the development of Indian computational tool for computational FFR and its scope.

Chapter 2
Cardiovascular System and Coronary Artery Disease

In this chapter, we provide a brief overview of the cardiovascular system and coronary artery disease. The section 2.1 on cardiovascular system discusses heart function and arterial circulation relevant to the understanding of coronary artery disease and its impact. The sections 2.2 and 2.3 inlcude discussion on cornary artery disease and fractional flow reserve. The section 2.4 presents the diagnosis methods of coronary artery disease and the shift in diagnostic strategies. The section 2.4.4 discusses the clinical trials which established the relevance of invasive FFR as diagnostic procedure.

2.1 Cardiovascular System

The cardiovascular system consists of heart, blood, and blood carrying vessels like arteries, capillaries, and veins etc. Every organ of the human body receives blood due to the pumping action of the heart. The heart has four chambers, left atrium, left ventricle, right atrium and right ventricle. The septum divides the left and right side of the heart. The left side of the heart pumps blood through peripheral organs and the right side of the heart pumps blood through the lungs. Arteries carry the blood away from the heart and veins carry blood towards the heart. Capillaries allow exchange of gases and nutrients with the tissues in the body. A healthy heart pumps 5.2 litres of blood per minute (Chandran *et al.* 2007). The figure 2.1 shows the section of the heart as viewed from the front.

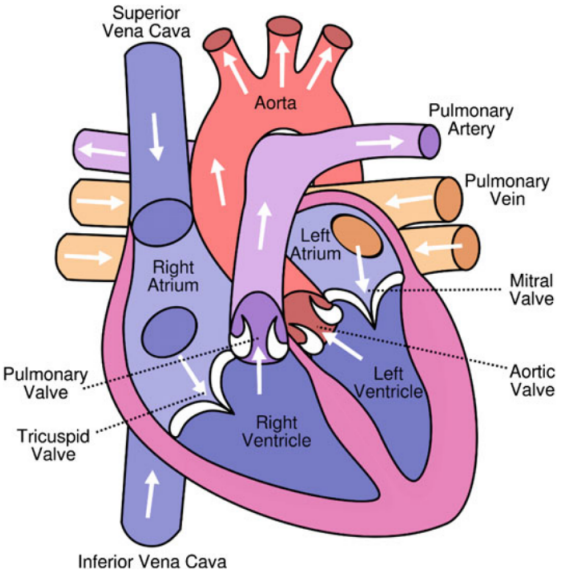

Figure 2.1: The Heart section as viewed from the front (Pierce 2019). Left and right side of heart are left hand and right hand side of patient.

Blood flow in the cardiovascular system occurs through the following circulatory routes:

1. **Pulmonary Circulation:** Right atrium receives de-oxygenated blood from vena cava,

which flows into the right ventricle. The right ventricle pumps this blood through pulmonary arteries to the lungs. The pulmonary veins return oxygenated blood from the lungs to the left atrium.

2. **Systemic Circulation:** The oxygen-rich blood from left atrium is pumped into the left ventricle. The left ventricle pumps the blood through the aorta and systemic arteries to the different organs of the body. The aorta progressively divides into smaller vessels called large and small systemic arteries. Small arteries further divide into arterioles and capillaries. Vessels after capillary bed unite into small venules to larger veins up to vena cava. Deoxygenated blood is brought back to the heart by systemic veins.

This blood flow in heart is regulated by four uni-directional valves throughout the heart which are: mitral valve(between the left atrium and left ventricle), tricuspid valve (between right atrium and the right ventricle), pulmonary valve (between right ventricle and the pulmonary veins) and aortic valve (between left ventricle and aorta). Valves between atria and ventricles are also called atrioventricular valves. Heart valves work based on the pressure difference between two chambers of the heart and prevent backflow. The arteries contain 28% of the blood in systemic circulation while veins contain 65% and capillaries contain 7% blood(Hoskins *et al.* 2016*b*). The dimensions of the vessels involved in systemic circulation are shown in table 2.1. The circulation of blood in smaller vessels like arterioles, capillaries and venules is called micro-circulation. The heart wall is made of three layers: epicardium (thin external layer), myocardium (muscular middle layer), and endocardium (endothelial inner layer). The myocardium is responsible for heart contractions. It is the thickest layer and has maximum mass. The left ventricle is thick-walled (thick myocardium) larger chamber compared to right ventricle as systemic circulation supplies blood to farther parts of the body and works under higher pressure than pulmonary circulation.

2.1.1 The Cardiac Cycle

The cardiac cycle consists of all physiological events during a single heartbeat. Heartbeat consists of two phases of heart, diastole (period of ventricular relaxation) followed by systole (period of ventricular contraction). Time of one cardiac cycle of a healthy human is around 0.8 seconds (assuming a heart rate of 72 beats per minute) with systole duration being one-third of the cardiac cycle (0.27sec) and diastole duration being two-third of the cardiac cycle (0.53sec) (Hall & Guyton 2011). The atria and ventricles contract alternatively. Ventricle diastole starts before atrial systole. At the beginning of diastole right atrium is filled by blood from vena cava and the left atrium is filled by oxygenated blood from pulmonary veins. The pressure in right and left atrium increases due to blood flow and when it exceeds the pressure in right and left ventricles respectively, tricuspid and mitral valves open. The blood fills the ventricles. During the systole phase, ventricles start contracting when blood is still flowing in. As ventricular pressure increases, atrioventricular valves close. There is isovolumetric contraction and pressure rises rapidly inside ventricles. Once the pressure is higher than aorta and pulmonary artery, aortic and pulmonary valves open. Blood flows into systemic and pulmonary circuits. Then ventricular muscles start relaxing at the end of systole and ventricular chamber pressure falls and, aortic and pulmonary valves close. Then the isovolumetric ventricular relaxation starts at the beginning of diastole. When the pressure in ventricles falls below atria pressure, atrioventricular valves open again. In a cardiac cycle, the maximum ventricular volume is at the end of diastole and it is called end-diastolic volume(EDV). Minimum ventricular volume at the end of systole is called end-systolic volume(ESV). Cardiac cycle is shown in figure 2.2.

Volume of blood pumped by left ventricle per cycle is called stroke volume (SV). Stroke volume can be obtained by:

$$SV(ml/beat) = EDV - ESV \tag{2.1}$$

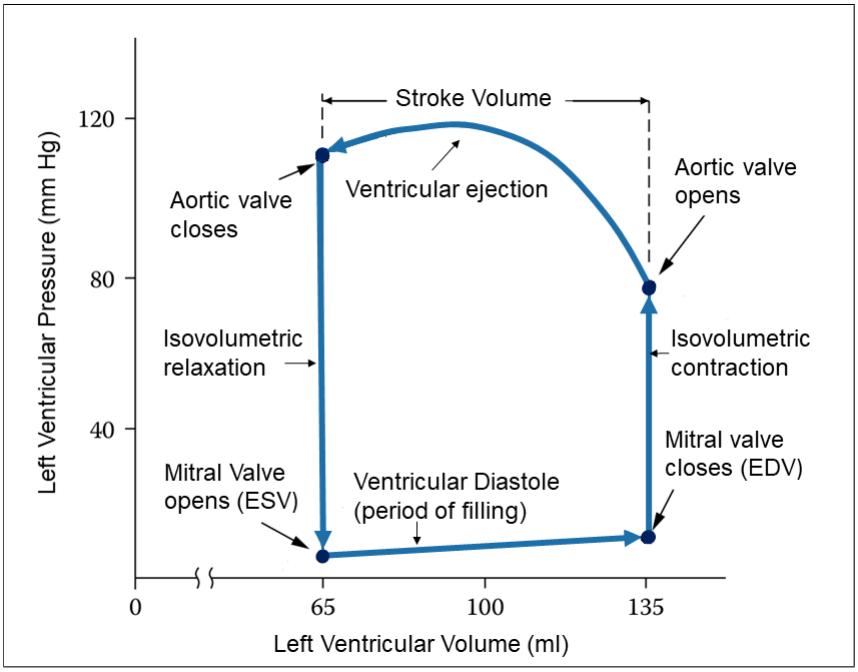

Figure 2.2: Ventricular pressure-volume curve for one cardiac cycle. EDV: End-diastolic volume. ESV: End-systolic volume. Figure reproduced (Hall & Guyton (2011); Chandran *et al.* (2007)) with permission.

The end diastolic volume for healthy heart is about 110-120ml and end systolic volume is 40 to 50ml (Hall & Guyton 2011).
Amount of the blood pumped by the heart in 1 minute is called cardiac output (CO). Cardiac Output (CO) is blood ejected from left-ventricle during a single cardiac cycle. It is calculated from stroke volume and heart rate:

$$CO(ml/min) = SV(ml/beat) \times HeartRate(beats/min) \tag{2.2}$$

The cardiac output of a healthy heart under normal conditions is 5.2l/min (Hall & Guyton 2011).

Vessel	**Diameter (mm)**	**Length (mm)**	**Number of vessels**	**Volume (mL)**	**Cross sectional area (cm^2)**	**Mean Velocity (cm/s)**	**Mean Pressure (mmHg)**	**Reynolds number (Peak)**
Aorta	22-25	600	1	228	4	25	95	5000
Large Arteries	1.0-4.0	300	40	339	11	8.3	93	
Small Arteries	0.2-1.0	50	2400	377	75	1.2	87	500
Arterioles	0.01-0.20	3	1.1×10^8	104	346	0.3	54	0.5
Capillaries	0.006-0.01	1	3.3×10^9	259	2592	0.04	25	0.0003
Venules	0.01-0.20	3	2.2×10^8	829	2765	0.03	7	0.03
Small Veins	2	50	2400	377	75	1.2	4	100
Large Veins	10	300	40	943	31	3	2	
Vena Cava	22-35	500*	2	228	4	25	0	3000-4000

* Inferior and Superior vena cava length combined

Table 2.1: Vessel Dimensions, Volume, Area, Pressure, Velocity and Reynolds number through Systemic Circulation. Table adapted from (Hoskins *et al.* 2016*b*; Klabunde 2011; Chandran *et al.* 2007) and data also sourced from (Dawson 2005)

2.1.2 Pressure and velocity variation in Circulation

Regulated blood pressure throughout the cardiovascular system facilitates the normal distribution of fluids, hormones and molecules. During systole, blood ejection from the ventricle to aorta creates pulsatile pressure wave and flow wave. Due to contraction of heart, these pressure and flow waveforms are large-amplitude highly transient wave-forms in larger arteries near the heart and relatively constant small-amplitude waveforms in small vessels which are far from the heart. As the pressure gradient between ventricles and arteries decreases, the rate of blood ejection decreases. As aorta progressively divides into arteries and smaller vessels (figure 2.4), the pressure gradually falls (figure 2.3 and figure 2.4), and the total cross-sectional area of vessels increases (figure 2.5), with flow rate in each bifurcation remaining constant. The flow velocity decrease and flow and pressure wave become steady. Blood flow is slowest in capillaries. The pulse pressure (the difference between the maximum and minimum pressure) increases as the vessels get distant from the heart while mean pressure throughout the remaining system falls with a mean pressure at the entrance of right atrium being lowest (Hoskins *et al.* 2016*b*). Pulse wave transmission velocity increases in distal vessels as the vessel wall becomes stiffer (Chandran *et al.* 2007).

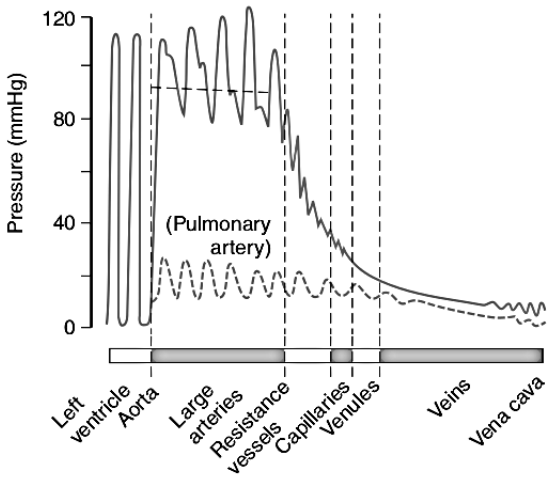

Figure 2.3: Pressure variation in systemic circulation(Pappano *et al.* 2013; Levick 1991).

The pressure gradient between aorta and right atrium is the driving force for blood flow in the circulatory system. Blood flow rate (Q) through a vessel is determined by the pressure gradient(ΔP) and vascular resistance (R).

$$Q = \Delta P/R \tag{2.3}$$

$$R = \Delta P/Q \tag{2.4}$$

Equation 2.4 is hydraulic analogue of Ohm's law ($R = E/I$, where E is the voltage drop across a segment in electric circuit and I is current).
From Poiseuille's law for fluid flow through tube,

$$R = \frac{8\eta L}{\pi r^4} \tag{2.5}$$

where,η is the dynamic viscosity,L is the length of pipe and r is radius of the pipe.

From equation 2.5,

$$R \propto \frac{1}{r^4} \tag{2.6}$$

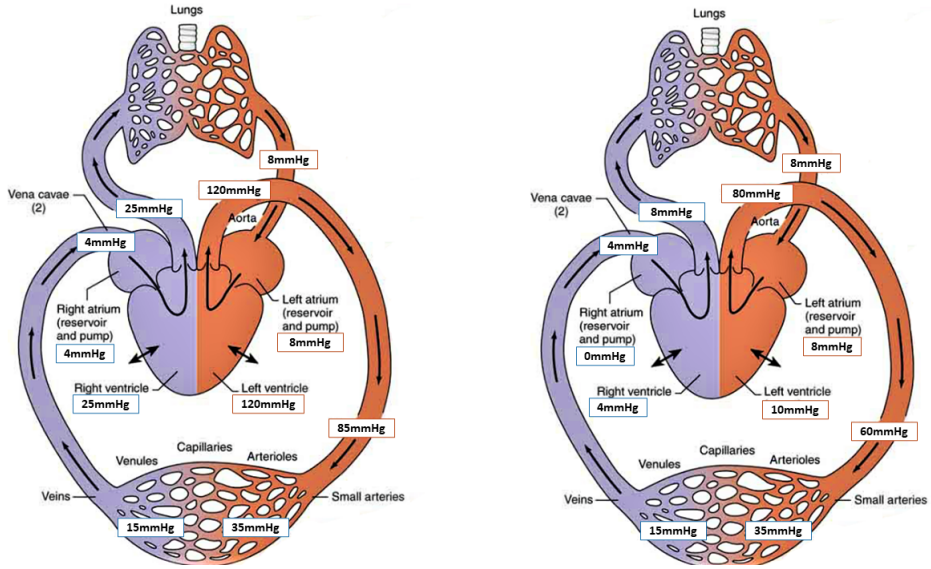

(a) (b)

Figure 2.4: Pressure at different stages of cardiac loop. (a) during peak systole (b) during end diastole (Image sourced from OpenStax (OpenStax CNX 2013) and modified with added pressure values).

It shows that even small decrease in radius can cause large increase in vascular resistance. The flow in arterial segments is pulsatile. Though, the Poiseuille's law stands for steady, laminar flow, it holds for time averaged pressure difference (ΔP) and flow rate (Q) (Chandran *et al.* 2007) in circulatory system.
At each segment of circulatory system, same volume of blood flows. The blood flow velocity,

$$v = \frac{Q}{A} \tag{2.7}$$

where, v is blood velocity and A is cross-sectional area. The flow velocity and cross-section area variation through cardiac cycle is shown in figure 2.5 and the values are listed in table 2.1.

Pressure gradient in systolic and diastolic phase is affected by heart rate, stroke volume and local characteristic impedance(Chandran *et al.* 2007). The vascular impedance is opposition to rate of change in pressure and flow and it is determined by vessel geometric and elastic properties (Marino 2014). During circulation, maximum pressure at a location occurs during systole (systolic pressure, p_s) and the minimum pressure occurs during diastole (diastolic pressure, p_d). Mean arterial pressure(p_m) is average pressure of large arteries over a cardiac cycle. It is estimated from the following formula considering that systole last $1/3^{rd}$ of cardiac cycle and diastole last twice that of systole duration:

$$p_m = \frac{p_s + 2p_d}{3} = p_d + \frac{p_s - p_d}{3} \tag{2.8}$$

pulse pressure (p_p) is defined as:

$$p_p = p_s - p_d \tag{2.9}$$

For a normal adult, the systolic pressure is 120mmHg and the diastolic pressure is 80mmHg at the root of the aorta. Pressure change across systemic circulation is the difference between mean arterial pressure and venous pressure (pressure at the end of superior vena cava or in the right atrium). Peripheral resistance of smaller arteries, arterioles and capillaries determines the mean arterial pressure. Total peripheral resistance (R) of all systemic circulation is approximated as

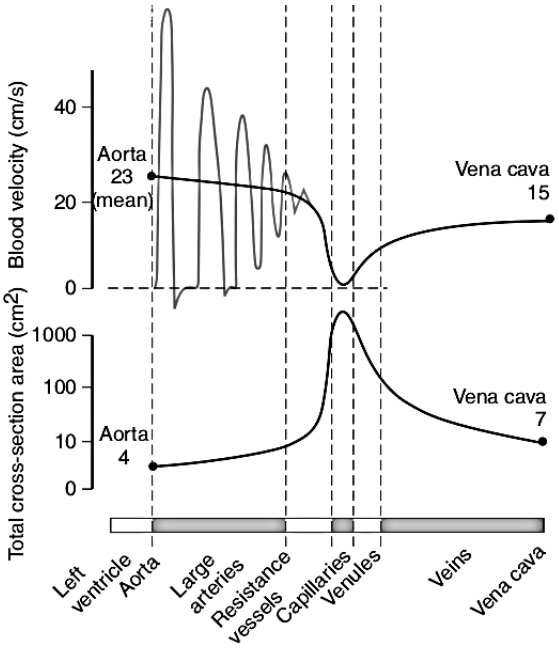

Figure 2.5: Flow velocity and cross-sectional area changes in systemic circulation (Pappano *et al.* 2013; Levick 1991).

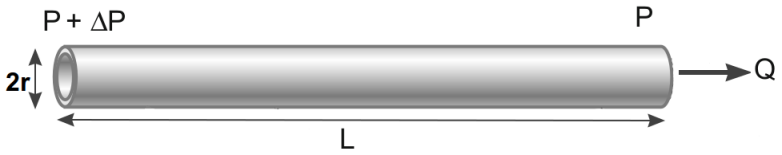

Figure 2.6: Quantities relevant to flow in a blood vessel.

(Chandran *et al.* 2007):

$$R = \frac{p_m - p_v}{Q_m} \tag{2.10}$$

where, p_v= venous pressure, and Q_m= mean flow rate= Cardiac Output(CO). If pressure difference is measured in $mmHg$ and flow rate is measured in cm^3/s, then the unit of resistance is $mmHg - s/cm^3$. The average pressure difference between aorta and vena-cava is 100mmHg and for an adult human, the average cardiac output is 100ml/sec, then total peripheral resistance is 1mmHg/ml-sec, which is called 1 peripheral resistance unit(PRU). When all vessels in the body constrict the total resistance value increase to 4 PRU and when all vessels dilate, the total resistance value decreases to 0.2PRU (Hall & Guyton 2011). Arterioles and capillaries offer maximum resistance to blood flow and cause the highest pressure drop. These are referred as **resistance vessels** while large arteries are called **conduit vessels**. Other parameters that affect blood pressure and velocity are vessel compliance and distensibility. Compliance and distensibility refer to the ability of vessel wall to contract and expand in response to the flow which maintains a continuous flow of blood through vessels.

- **Vascular Compliance (or Capacitance)(C)**: It is a measure of contraction and expansion of the vessel wall due to the pressure difference over the vessel wall (local transmural pressure). It refers to the quantity of blood that can be stored or released per unit pressure

rise in given part of circulation (Hall & Guyton 2011). It is defined as the ratio of change in end-diastolic volume to change in end-diastolic pressure (Marino 2014). Compliance is measured as

$$C = \frac{\Delta V}{\Delta P} \tag{2.11}$$

where,ΔV is change in volume and ΔP is change in transmural pressure.

- **Vascular Distensibility(D)**: It is a measure of contraction and expansion of the vessel with change in pressure due to the elastic properties of the vessel wall. Aorta and its major branches are elastic vessels with high distensibility (Hoskins *et al.* 2016*b*). Due to distensibility, the pulsatile flow becomes continuous for smaller vessels. Veins are most distensible vessels (eight times more distensible than arteries ((Hall & Guyton 2011)) and therefore, act as a reservoir for large quantities of blood. Distensibility is compliance per unit volume. A vessel with larger volume but less distensibility can have higher compliance than a more distensible vessel with a smaller volume.

$$D = \frac{\Delta V}{V \Delta P} \tag{2.12}$$

$$D = \frac{C}{V} \tag{2.13}$$

Cross-sectional distensibility is defined as

$$D = \frac{1}{A}\frac{\Delta A}{\Delta P} \tag{2.14}$$

where, A is cross sectional area and $\triangle P$ is pressure drop.

- **Blood Inertance (Ł)**: Effective mass of blood that is being accelerated or decelerated with each heartbeat is called blood inertance (or inductance).

$$\Delta P = Ł\frac{\Delta Q}{\Delta t} \tag{2.15}$$

where, $Ł = \frac{\rho L}{A}$. Here, ΔP= pressure drop,ρ is blood density, A is the cross-sectional area, L is the length of the vessel, and ΔQ is blood flow.

2.1.3 Coronary Circulation

Heart muscles receive blood and nutrients through coronary circulation which includes coronary arteries, coronary veins and the capillary bed. Coronary arteries spread over the walls of the heart supply blood to the heart muscles (figure 2.7). Coronary arteries are large conduit arteries that lie on the epicardium (i.e. the surface of the heart), thus are called epicardial arteries. These arteries divide into arterioles and capillaries. Coronary arteries originate at the root of the aorta near aortic valve (figure 2.8), branch out over heart surface and then penetrate heart muscle. Left main coronary artery (LMCA) originates from left aortic sinus. L supplies blood to the left ventricle and atrium. It divides into the left anterior descending artery (LAD) and left circumflex artery (LCX). The right coronary artery arises from right aortic sinus and divides into the posterior descending artery (PDA) and posterolateral branches. The right coronary artery(RCA) supplies blood to the right atrium and ventricle. Humans can have dominant right coronary artery (50% of population) or dominant left coronary artery (20% of population) or equal flow delivered by both arteries(remaining 30%) (Pappano *et al.* 2013; Chandran *et al.* 2007). Coronary venules and veins take impure blood from heart muscles to the right atrium through the coronary sinus. 85% of the returning blood returns through the coronary sinus and the remaining 15% directly enters the cardiac chambers(Chandran *et al.* 2007). Coronary

blood flow for a human being in resting conditions is about 4-5% of total cardiac output (Hall & Guyton 2011).

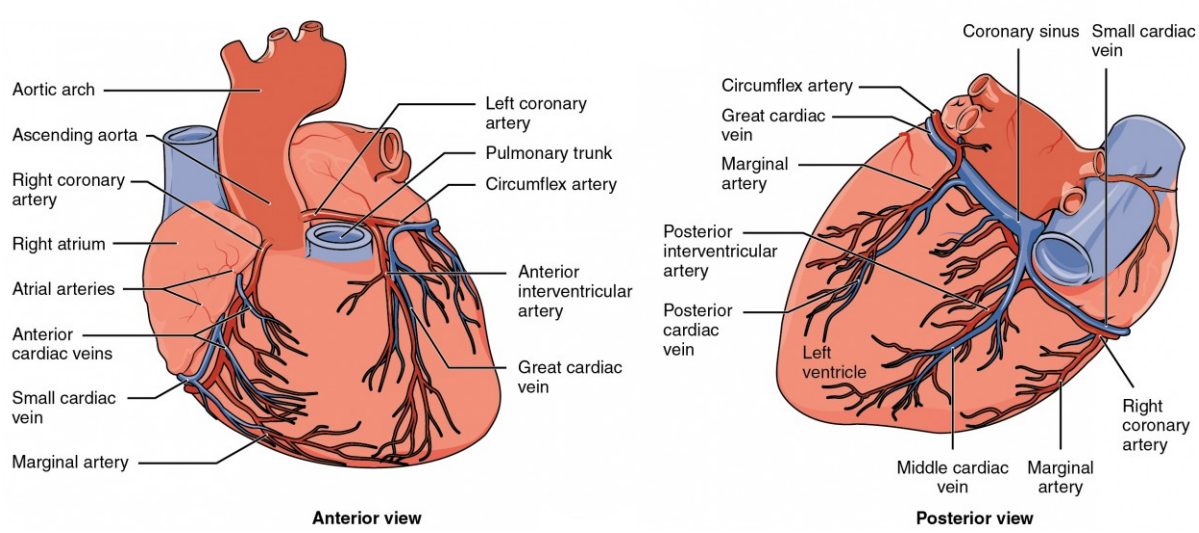

Figure 2.7: Coronary Circulation. Left: Anterior view. Right: Posterior view(Betts *et al.* 2013).

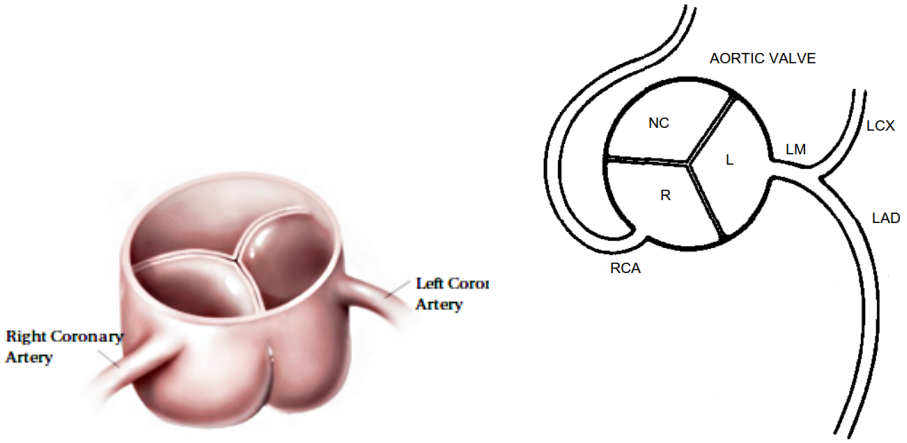

Figure 2.8: Aortic origin of Left and Right coronary arteries:L= left, R= right, NC= noncoronary, LCA= Left Circumflex Artery, RCA= Right Coronary Artery, LAD= Left Anterior Descending Artery, LM= Left Main. (Waller *et al.* 1992).

The dimensions for coronary arteries are very patient-specific as they vary with left and right dominant heart, age, gender, physical activity and body surface area (Pavone *et al.* 2009). The length of the left main coronary artery may range from 1-25 mm before bifurcation into LAD and LCX (Fox *et al.* 1973; Waller *et al.* 1992). According to Waller *et al.* (1992), the right artery can be 12-14cm long, the LAD length ranges from 10-30cm and LCX length may vary from 6-8cm. Though arteries taper in diameters, the lumen diameters of arteries are listed in table 2.2. The coronary artery dimensions of average Indian population, male and female are listed in table 2.3 from studies of Raut *et al.* (2017) and Saikrishna *et al.* (2006). For ease of reference, the arteries are divided into the proximal segment, middle segment, and distal segment, the proximal part being closer to the aorta (figure 2.9).

During systole, the blood flow in coronary arteries is very small due to ventricular contraction (figure 2.10). A significant part of coronary flow happens during diastole when heart muscles are relaxed and the artery lumen is completely open. The rate of blood flow in coronary arteries is determined by myocardial oxygen demand. Myocardium perfusion relies on aortic pressure.

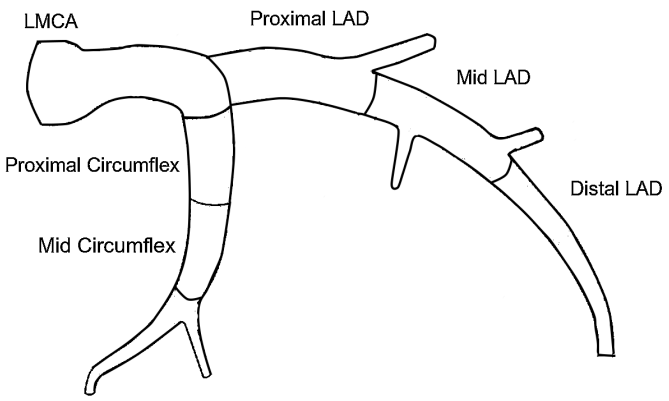

Figure 2.9: Proximal, Mid and Distal part of artery.

Artery	**Lumen Diameter (mm)**	**Mean Diameter (mm)**
Left Main	4.5 ± 0.5	4
Left Anterior Descending	2.0-5.0	3.6
LAD proximal	3.7 ± 0.4	
LAD distal	1.9 ± 0.4	
Left Circumflex	1.5-5.5	3.0
LCX proximal	3.4 ± 0.5 to 4.2 ± 0.6 *	
Right Coronary Artery	1.5-5.5	3.2
RCA proximal	2.8 ± 0.5 to 3.9 ± 0.6 *	

* Depending on right or left dominance

Table 2.2: Lumen diameter of Coronary Arteries (Dodge *et al.* 1992; Waller *et al.* 1992).

In resting conditions, coronary blood flow is 225ml/min, which corresponds to 0.8ml/min/g of the heart muscle which increases 4-10 times during exercise conditions (Hall & Guyton 2011; Chandran *et al.* 2007). Lack of adequate oxygen to myocardium results in chest pain or angina pectoris. High metabolic activity of heart reduces coronary vascular resistance and increase flow through the arteries(Hall & Guyton 2011).

Artery	**Mean diameter in mm (Male)**	**Mean diameter in mm (Female)**
Left Main	3.72 ± 0.65	3.40 ± 0.58
Proximal LAD	2.85 ± 0.59	2.72 ± 0.48
Mid LAD	2.24 ± 0.49	2.17 ± 0.50
Distal LAD	1.63 ± 0.38	1.51 ± 0.31
Proximal LCX	2.82 ± 0.63	$3\ 2.68 \pm 0.59$
Distal LCX	2.10 ± 0.68	1.77 ± 0.6
Proximal RCA	2.75 ± 0.6	2.55 ± 0.57
Mid RCA	2.47 ± 0.66	2.31 ± 0.13
Distal RCA	2.14 ± 0.61	2.01 ± 0.40

Table 2.3: Male and Female coronary artery dimensions comparison for Indian patients (Saikrishna *et al.* 2006).

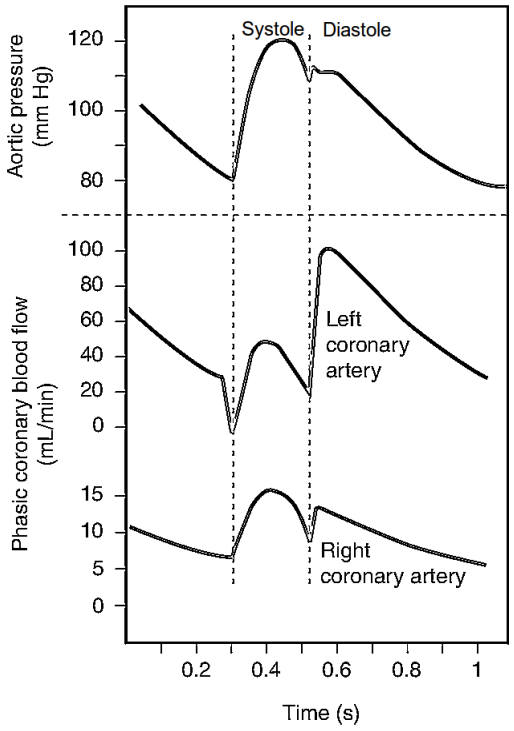

Figure 2.10: Phasic coronary blood flow in Left and right coronary arteries (Pappano *et al.* 2013).

2.2 Coronary Artery Disease

Coronary artery disease is the narrowing of coronary arteries due to the build-up of fatty deposits on the arterial wall (figure 2.11). This build-up is termed as plaque. Plaque is accumulation of cholesterol, calcium and fatty substances. The build-up of plaque is called 'atherosclerosis' (Hoskins *et al.* 2016*b*). The plaque builds up over time and hardens. The hardened plaque narrows the artery and blood flow is reduced to the heart muscle. The narrowing of blood vessel(arterial lumen) is called stenosis (Hoskins *et al.* 2016*b*). Stenoses are measured as percentage

of blockage in diameter of the artery lumen.

$$Stenosis(\%) = \frac{(D1 - D2)}{D1} \times 100\% \tag{2.16}$$

where, D1 is upstream diameter and D2 is minimum diameter with stenosis.

Stenosis is functionally significant only if it causes ischaemia (lack of oxygenated blood to heart muscle) (Hoskins *et al.* 2016*b*). Ischaemia can lead to damage or death of heart muscles. A ruptured plaque can cause the formation of blood clots on its surface (thrombosis), which again blocks the blood flow through the vessel. Reduction of blood flow to heart muscle impairs heart's mechanical function(Hall & Guyton 2011). It results in chest pain and discomfort or heaviness in the jaw, shoulder, back or arm(Cassar *et al.* 2009), which is called angina pectoris (Hall & Guyton 2011). Complete obstruction of coronary arteries leads to stroke and heart attack (Myocardial Infarction). Non-functioning cardiac muscles also lead to irregularity of heartbeat (arrhythmia) and heart-failure (Ashley & Niebauer 2004).

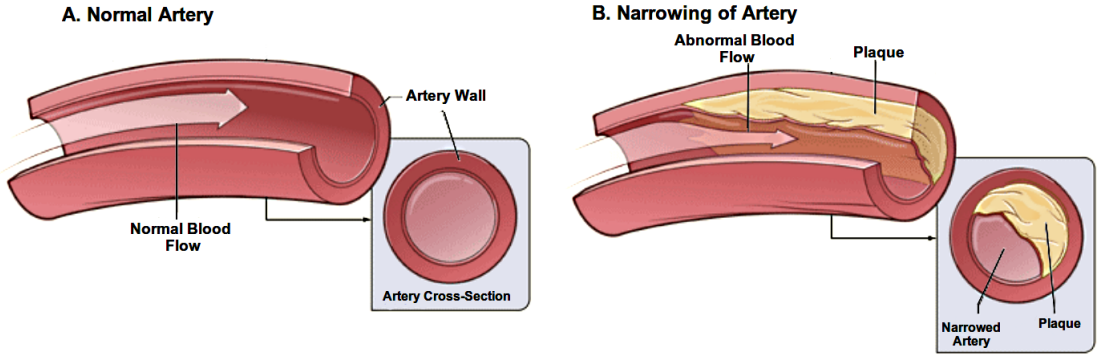

Figure 2.11: Blood flow in Healthy artery(A) and Blocked Artery(B). Image sourced from National Heart, Lung, and Blood Institute, U.S. website (National Heart, Lung, and Blood Institute 2018).

The chest pain experienced intermittently due to physical exertion or stress is called stable angina (Hall & Guyton 2011; Kern *et al.* 2018). It lasts for a short time and disappears during rest. Unstable angina is the chest pain that occurs during rest or with very little physical exertion (Hall & Guyton 2011; Kern *et al.* 2018). Patients with stable angina are diagnosed based on medical history, physical exams and other diagnostic procedures while unstable angina is a medical emergency condition and requires immediate treatment. Coronary artery disease may be asymptomatic or present with the complications such as an acute coronary syndrome (MI or unstable angina), congestive heart failure, cardiac arrhythmias, or sudden death (Cassar *et al.* 2009). CAD is caused by lifestyle factors and medical conditions. The risk factors that may cause the development of atherosclerosis or increase the likelihood of CAD are hypertension, obesity, diabetes, smoking, sedentary lifestyle, hyperlipidemia, and family history of the myocardial infarction(MI) before the age of 60 years (Pryor *et al.* 1991; Hall & Guyton 2011; Cassar *et al.* 2009; Klag 2012).

There are significant changes in blood flow, pressure and elastic properties of vessels due to atherosclerosis. Atherosclerotic plaque reduces distensibility of the vessel region over time (Chandran *et al.* 2007). Stenosis causes an increase in resistance in arteries which is compensated by dilation of arterioles to maintain total resistance and flow. Flow rate can be maintained up to 70% stenosis by diameter (figure 2.12) (Hoskins *et al.* 2016*b*). Thus, even if stenosis appears anatomically significant, it may not cause ischaemia. Artery narrowing due to stenosis causes a pressure drop across stenosis which is used as a quantitative measure for the functional significance of stenosis for the severity of coronary artery disease (section 2.3).

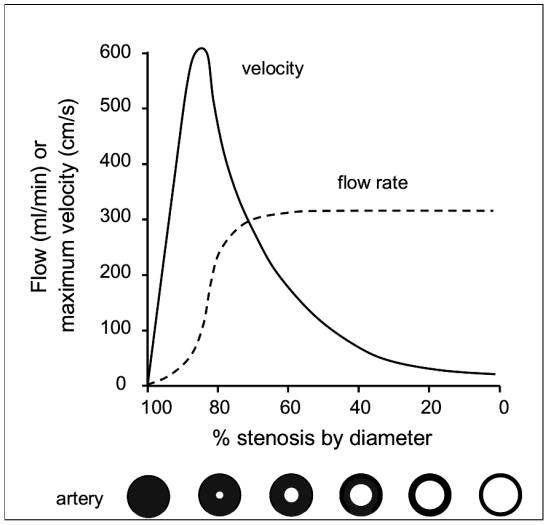

Figure 2.12: Flow rate and velocity as function of degree of stenosis for a smooth and axisymmetric stenosis (Hoskins *et al.* 2016*b*; Spencer & Reid 1979).

CCS and CAD-RADS

CCS (Canadian Cardiovascular Society) angina grading scale is a grading tool to assess patient's stable and unstable angina which may have been caused by coronary artery disease (table 2.4) (Cassar *et al.* 2009). The CAD-RADS is Coronary Artery Disease-Reporting and Data System, a standardized reporting system for the degree of coronary stenosis from Coronary CT angiography results. The table 2.5 shows the CAD-RADS classification system. CCS and CAD-RADS are designed to improve communication among medical teams for better patient management. However, the studies ((Rossmann *et al.* 2000; Moreno & Bhaganagar 2013)) have shown that morphology of plaque is more important when it comes to effects on the blood flow characteristics, thus the percentage based method can prove fairly inaccurate to quantify the severity of the disease.

Grade	**Description**
Grade I	Angina due to strenuous, rapid or prolonged exertion at activity
Grade II	Angina due to moderate exertion at activity like uphill walking or stair climbing rapidly or after meals, or in cold, or in wind, or under emotional stress, or during first few hours after waking up
Grade III	Angina even when walking or climbing stairs in normal conditions at normal pace
Grade IV	Angina at rest and during all physical activities

Table 2.4: Canadian cardiovascular Society grading of angina pectoris (Canadian Cardiovascular Society 2006).

Burden of Coronary Artery Disease

Cardiovascular diseases caused over 17 million deaths in 2016 of which over 9 million deaths were caused by coronary artery disease, the majority of them being in low and middle-income countries (World Health Organization 2016; Kaptoge *et al.* 2019). Ischaemic heart disease was

CAD-RADS Classification	**Degree of Maximal Coronary Stenosis**	**Interpretation**	**Further Cardiac Investigation**
CAD-RADS 0	0% (No plaque or stenosis)	Absence of CAD	None
CAD-RADS 1	1-24% (Minimal stenosis or plaque with no stenosis)	Minimal non-obstructive CAD	None
CAD-RADS 2	25-49%(Mild Stenosis)	Mild Non-Obstructive CAD	None
CAD-RADS 3	50-69% (Stenosis)	Moderate Stenosis	Consider functional assessment
CAD-RADS 4	**a.**70-90% Stenosis or **b.**Left Main >50% or 3-vessel obstructive($\geq$70%) disease	Severe Stenosis	**a.**Consider ICA or functional assessment **b.**ICA is recommended
CAD-RADS 5	100%(total occlusion)	Total Coronary Occlusion	Consider ICA and/or viability assessment
CAD-RADS N	Non-diagnostic study	Obstructive CAD can't be excluded	Additional or alternative evaluation may be needed

* CAD-RADS does not apply to smaller vessels (<1.5mm in diameter)

Table 2.5: Coronary Artery Disease -Reporting and Data System (CAD-RADS) for patients with stable chest pain. Table content reproduced from (Cury *et al.* 2016).

the chief individual cause of death in India in 2016 (ICMR 2017). In India, all cardiovascular diseases caused 2.8 million deaths which is 28.1% of total deaths in the year 2016 (Prabhakaran *et al.* 2018). Ischaemic heart disease caused 61.4% of all the deaths due to cardiovascular diseases (17.1% of total deaths) (Prabhakaran *et al.* 2018). The economic burden for complete treatment coverage of disease in India is estimated at around 800 billion INR (almost 13 billion USD) (Basu *et al.* 2015).

2.3 Fractional Flow Reserve(FFR)

Fractional flow reserve is the ratio of pressure distal(downstream) of stenotic lesion to the pressure proximal(upstream) of the lesion (aortic pressure) (figure 2.13). FFR is based on the assumption of proportional and linear relationship between flow and pressure-change with minimal resistance during vasodilation. FFR compares the maximum achievable blood flow through a blocked artery to the maximum achievable blood flow in the same vessel in absence of blockage.

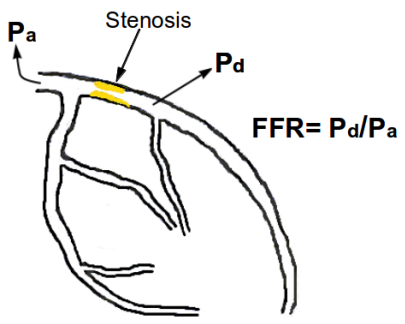

Figure 2.13: Proximal and Distal Pressures in a stenosed coronary artery.

$$FFR = \frac{p_d}{p_a} \tag{2.17}$$

where, p_d= distal pressure, p_a= proximal pressure. For a healthy vessel, FFR value is 1.0 (Tonino *et al.* 2009).

Changes in micro-circulation and haemodynamic conditions do not affect FFR (Johnson *et al.* 2015; Elgendy *et al.* 2014). FFR is a tool to assist in decision process to intervene for revascularization (restoring the blood flow) for a stenosed artery, especially in cases of intermediate blockage (table 2.5). The FFR value less than 0.75 is considered to indicate significant stenosis and stenosis with FFR > 0.8 is considered non-ischaemic (Adjedj *et al.* 2016). FFR value between 0.75 and 0.8 falls in grey zone and treatment is decided based on patient's medical history and results of other tests (Achenbach *et al.* 2017).

2.4 Diagnosis and Treatment of Coronary Artery Disease

Diagnosis and treatment of CAD are based on the identification of lesion in arteries and its subsequent management. Currently, patients suffering from stable chest-pain are diagnosed based on physical examination, medical history, and associated risk factors. Patients are subjected to exercise/stress test. They also undergo one or more of the following non-invasive tests like electrocardiogram (ECG), echocardiography(ECHO), imaging tests like CCTA, MRI, PET, etc., and/or invasive tests like coronary angiography (cardiac catheterization).

Exercise test or stress test is conducted to evaluate the effect of exertion on the heart and identify symptoms of CAD. This test is generally paired with an electrocardiogram. Electrocardiogram(ECG) is used to check the electrical function of the heart and it can reveal abnormalities of heart rhythm due to CAD (Hall & Guyton 2011). Echocardiography(ECHO) is a non-invasive imaging technique that makes use of short pulse high-frequency sound waves (ultrasound) to diagnose heart (Pappano *et al.* 2013). Different types of ECHO techniques like 2-D ECHO, M-mode ECHO and pulsed and continuous Doppler ECHO are used to assess anatomical and haemodynamic information like heart chamber size, flow velocity, ventricular wall motion, movement of valves, pressure gradients, etc. (Armstrong & Ryan 2010). Magnetic resonance imaging (MRI) utilizes radio frequency and magnetic field to visualize anatomy and flow patterns and to measure flow velocity (Hoskins *et al.* 2016*b*). Positron emission tomography (PET) utilizes radioactive tracers to assess blood flow through small arteries and perfusion in tissues. Coronary computed tomography angiography(CCTA) is an established diagnostic method to identify coronary stenosis as it has higher spatial resolution than MRI, PET and echocardiography (Hoskins *et al.* 2016*b*).

When non-invasive tests like ECG and CCTA indicate medium to high risk of ischaemia, the Invasive Coronary Angiography (ICA) is prescribed. ICA provides the most detailed visual information about the coronary circulation. ICA is considered the best diagnostic method for CAD. It helps in determining the need for further surgical intervention or revascularization. Patients benefit from revascularization only if there is functionally significant stenosis (Pijls *et al.* 2010). During ICA, while for certain cases of high risk or significant ischaemia, the anatomical correction is immediately proceeded with, for cases with intermediate stenosis, functional assessment becomes necessary to decide further action (Tonino *et al.* 2009). Functional significance of lesions is assessed using invasive (pressure-wire derived) FFR in catheterization laboratory along with ICA. The invasive FFR has been recommended for intermediate stenosis (30-70%) as its ischaemic effect is hard to determine. Addition of Invasive FFR in treatment plan provides better assessment of lesion not only for intermediate stenosis (50-70%) but also for severe category (70-90%) (Tonino *et al.* 2010).

Diagnostic procedures and techniques to identify the presence of a lesion in order to make

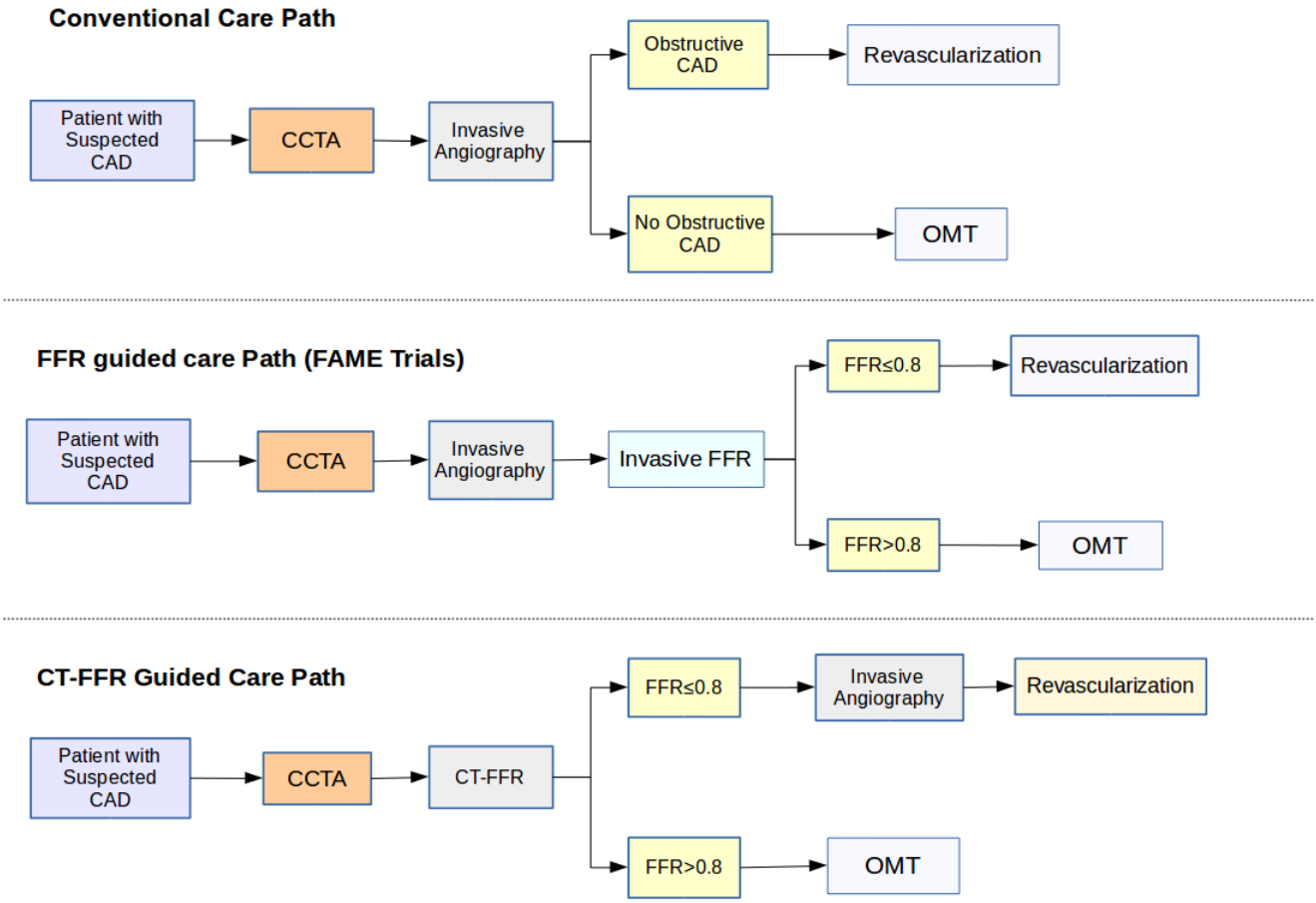

Figure 2.14: Change in CAD care-paths with inclusion of invasive FFR and CT-FFR. OMT stands for optimal medical therapy.

re-vascularization decisions have evolved over time. Coronary CT-scan has become main modality for detection of stenosis due to its diagnostic accuracy (Min *et al.* 2010). While CT-scan can localize the lesion, ICA remained technique to guide interventional decisions. However, visual assessment through ICA could overestimate the functional severity of lesion (Pijls *et al.* 2010; Tonino *et al.* 2009), leading to unnecessary re-vascularization of non-ischaemic lesions. The clinical utility and benefits of FFR to measure the physiological significance of stenosis and guide re-vascularization was established by FAME trial (Pijls *et al.* 2010; Agasthi *et al.* 2018; Zimmermann *et al.* 2019). A randomised trial FAME (Fractional Flow Reserve versus Angiography for Multi-vessel Evaluation) which included 1005 patients showed that FFR guided intervention reduced the stent placement by 30% compared to only ICA guided interventions (Tonino *et al.* 2009). Invasively measured FFR became standard of care for guiding revascularizations with European society of Cardiology (Class IA) and American Heart Association (Class II A) practice recommendations (Zarins *et al.* 2013; Achenbach *et al.* 2017). Recent developments have shown that FFR can be computed from CCTA images and it has led to the development of CT-FFR method (Min *et al.* 2012; Douglas *et al.* 2015; Agasthi *et al.* 2018). Figure 2.14 shows the change in patient management strategy with invasive FFR and CT-FFR methods. Coronary CT-scan procedure, invasive coronary angiography procedure and invasive FFR procedures are described in the following sections. CT-FFR method is discussed in detail in Chapter 3.

2.4.1 Coronary CT-Scan

Coronary computed tomography angiography (CCTA) is CT-scan to visualize coronary arteries. CCTA is known for its high negative predictive value for CAD (Budoff *et al.* 2008; Budoff & Nakansihi 2016). CT-scan works by taking static images at various phases of cardiac cycle (Pavone *et al.* 2009). During CT-scan, an X-ray tube rotates around the patient on a circular track. Coronary CT can not quantify the haemodynamic significance of stenosis and often overestimates the severity of (Zarins *et al.* 2013). It has a very high negative predictive value(it means that patietns with negative test results don't have the disease) but very moderate positive predictive value (the probability that patients with positive test results truly have the disease).

CT-Scan Procedure

For CT-scan, the patient lies on an examination table that slides and a tube and detector are continuously rotated 360° around the patient. The rotating tube sends X-ray beams simultaneously towards the patient from different angles which are received by the detectors or sensors (figure 2.15) on the other side. The detector creates an electrical signal based on the amount of X-rays absorbed by the patient's body part being scanned (Pavone *et al.* 2009).

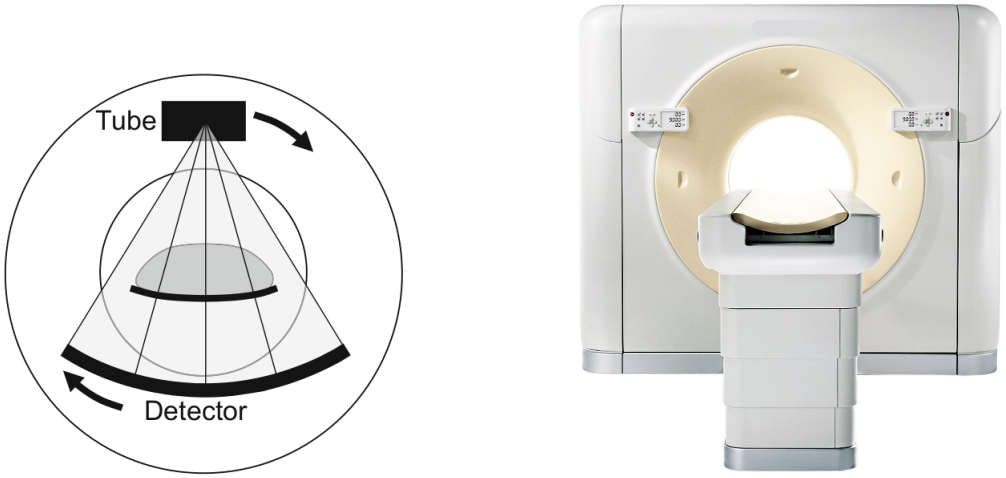

Figure 2.15: Left: CT-scanning tube and detector rotate around patient (Hoskins *et al.* 2016*a*); RightCT-Scan Equipment (Image source: `https://www.philips.co.in/healthcare/product/HC889407/brilliance-ct-64-channel---ds-refurbished-ct-scanner`, Retrieved on 17 Feb 2020).

Current CT-scans are multi-slice CT-scan which can collect 64, 128, 256 or 320 slices (number of detector rows) continuously and can be the single source or multi-source scanners. Scanners with a gantry rotation time of 420 milliseconds or less are recommended for coronary CTA (Abbara *et al.* 2009). The temporal resolution of a CT-scan image is half the rotation time (temporal resolution of 150ms for 0.3s of rotation time) of the scanner, thus faster rotation time means high-quality images (Hoskins *et al.* 2016*a*). During CTA image reconstruction, clear visualization is possible only for very high-density structures, therefore contrast is injected to increase the density of lumen. This density is measured in Hounsfield Units (HU).

Hounsfield Unit (HU) is a measure of radiodensity of a material in a CT scan. As the physical density of tissue is proportional to the absorption of X-ray beam, HU provides density of a tissue by measuring X-ray attenuation (Kalra 2018). It is defined as (Kalra 2018),

$$HU = 1000 \times \frac{\mu_{tissue} - \mu_{water}}{\mu_{water} - \mu_{air}} \tag{2.18}$$

where, μ_{tissue} is linear attenuation coefficient of tissue, μ_{water} is linear attenuation coefficient of the water and μ_{water} is linear attenuation coefficient of the air.

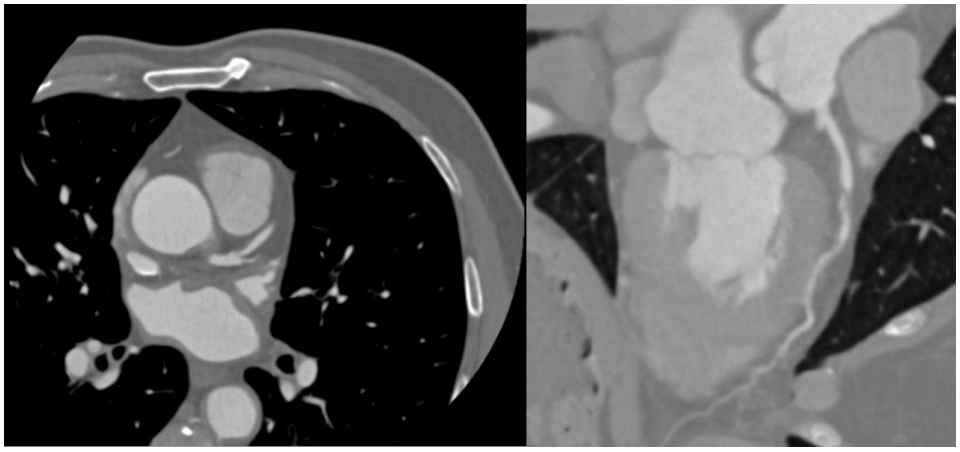

Figure 2.16: Coronary CT-scan Axial view (left) and Curved MPR view for Artery visualization.

Typical values of the Hounsfield unit for different bio-matter are listed in table 2.6. Iodine contrast increases the density of blood from 40HU to 300-500HU (Pavone *et al.* 2009), which provides a clearer image. Medical images are generated in greyscale. Each pixel in an image is assigned a numerical value for its grey-scale intensity which is expressed in Hounsfield(HU) units. Denser objects are represented by lighter (whiter) shades (high HU value) and less dense material is represented by a darker shade.

Material	**HU**
Bone	400 and above
Blood	40
Air	-1000 or less
Water	0
Muscle	20-40
Fat	-50 to -100
Contrast Agent	100-300

Table 2.6: Hounsfield Values for different substances (Pavone *et al.* 2009; Kalra 2018).

Three-dimensional reconstruction and visualization is done using either planimetric technique (using two dimensional image slices of coronary arteries) or volumetric technique (using three dimensional model of anatomy) (Pavone *et al.* 2009) using Medical image processing tools (figure 2.17). The factors that affect the quality of images are obesity, body-movement, difficulty in holding breath, and heart rate variability. Spatial resolution limits the diameter of the coronary artery to be visualized. Other problems that occur are calcification, motion-artefacts and image noise etc. Radiation dose after each CTA is recorded for each patient in the dose-length product (in mGy.cm).

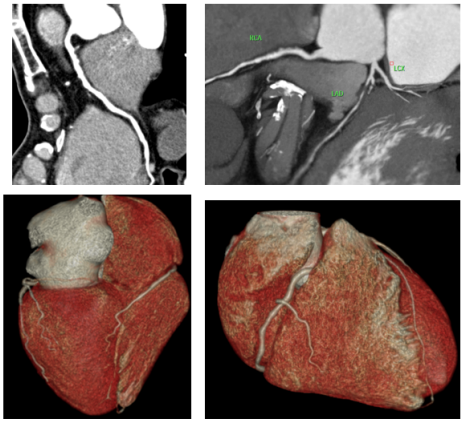

Figure 2.17: CT-Scan Images and 3D View after Image reconstruction.

Before CT-scan, patients are screened for contraindications to contrast agent and health conditions like renal insufficiency, previous heart-failure and breath-holding problems. Blood pressure and heart-rate of the patient is also monitored.

2.4.2 Invasive Coronary Angiography(ICA)

Invasive coronary angiography is performed in the cardiac catheterization laboratory (Cath-lab). A typical Cath-Lab consists of a fixed or portable cine-angiography system (figure 2.18). The main part is floor-mounted or ceiling suspended gantry and a flat-top table with adjustable height. The X-ray beam passes through the patient in rotation(from left to right anterior oblique) and skew (cranial to caudal) and captured by the image intensifier. Image intensifier transmits the data to monitor. Gantry aligns the x-ray tube and image intensifier (Baim & Grossman 2006). It produces silhouette of vascular lumen (the 2nd image in figure 2.19). The other equipment includes in-lab display system, real-time ECG and blood pressure monitors, defibrillators, catheters., etc. Nitroglycerin (NTG) and adenosine are vasodilating agents which are administered to maximize blood flow and prevent wire induced artery spasm during the procedure. The patient may be administered a local anaesthetic. The catheter is inserted either through the femoral or radial approach. The catheter is guided through main blood vessels in the body until it reaches the area of interest and vessels are visualized using contrast. ICA allows the immediate shift to treatment procedure when needed.

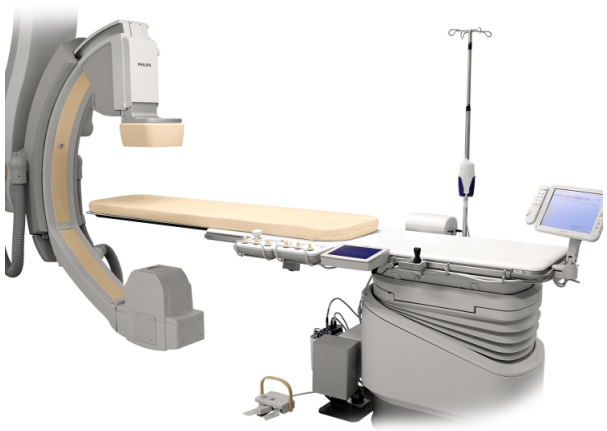

Figure 2.18: Cath-Lab Equipment (Image source:`https://avantehs.com/p/philips-allura-xper-fd10-cathangio-system/13789`, Retrieved on Feb 17, 2020).

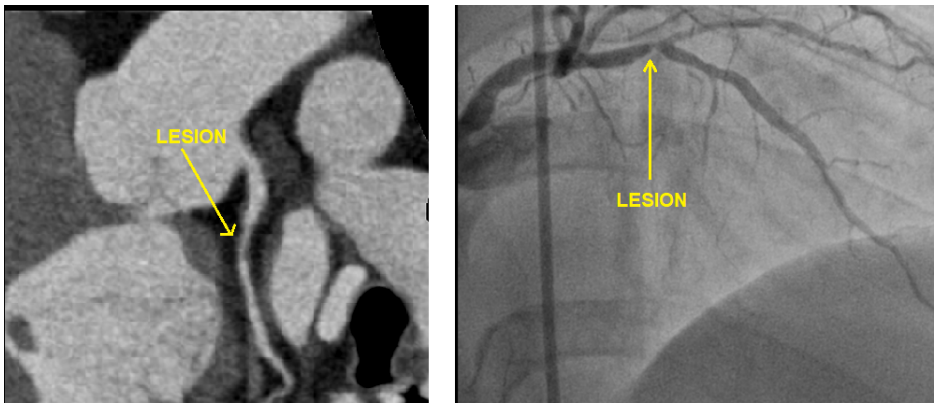

Figure 2.19: Plaque visualization in CT-Scan(left) and in Invasive Coronary Angiography(right) in Cath-Lab.

2.4.3 Invasive FFR

Invasive FFR is measured during a period of coronary hyperaemia (maximal blood flow). In hyperaemic condition, peripheral resistance becomes minimum and can be considered constant. Then, for equation 2.3, $\Delta p = QR$, where, Δp= pressure drop, and R= vascular resistance, high pressure drop directly corresponds to the reduction in blood flow for high resistance.

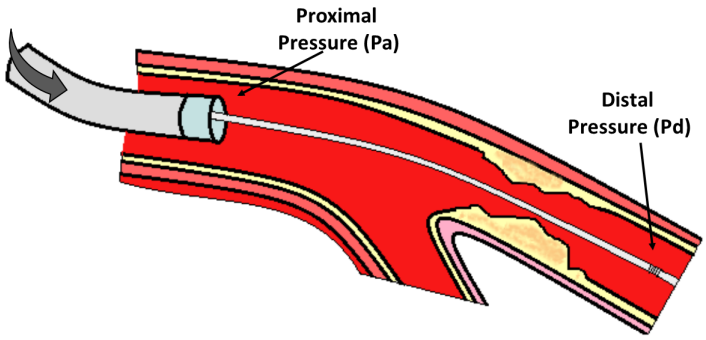

Figure 2.20: Invasive FFR measurement using Pressure wire through Catheter.

Invasive FFR is a pressure-wire based procedure which is done in cath-lab during ICA. Hyperaemia is induced using either intracoronary adenosine or intravenous adenosine infusion (Kern *et al.* 2018). A pressure sensing guidewire is passed across stenosis using a guide catheter to a coronary artery using either femoral or radial approach (2.20). The distal and proximal pressure to stenosis is measured and fractional flow reserve (FFR) is calculated (figure 2.21). A normal artery has FFR value of 1.0 (Tonino *et al.* 2009). An FFR lower than 0.80 is generally considered to represent significant ischaemia. FFR $\leq$ 0.75 is always associated with ischaemia and FFR>0.80 means absence of ischaemia. FFR zone of 0.75 to 0.80 is called grey zone and it is classified as haemodynamically relevant (Adjedj *et al.* 2016). The clinical judgement is made based on patient condition, medical history and results of other tests.

A retrospective study on patients with single-vessel disease and grey zone FFR values (0.76-0.80) showed that the patients treated with medical therapy alone had a higher rate of major adverse cardiovascular events compared with the patient treated with revascularization and medical therapy both (Adjedj *et al.* 2016). DEFER, FAME and FAME 2 are three large randomized trials that established the FFR threshold value of 0.80 and showed that for stenosis greater than 50%, FFR guided vascularization leads to better outcomes than that based on angiography alone. Even though the FFR measurement has gained prevalence, the use of invasive FFR is still not prevalent in low-income countries due to large cost of wires, extra procedural time and use of

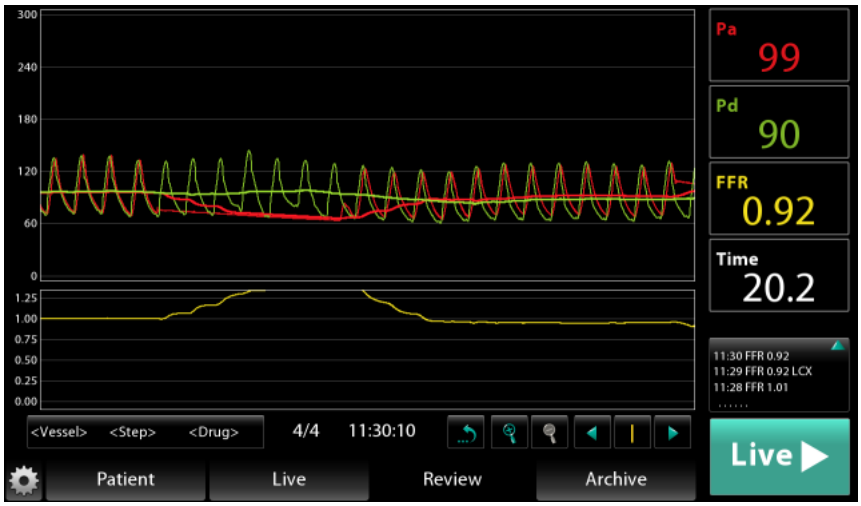

Figure 2.21: Invasive FFR values in using St. Jude Medical FFR measurement System.

adenosine agent which can cause discomfort to patients (DAC Feature 2018; Achenbach *et al.* 2017).

Coronary artery disease is treated with medical therapy and surgical procedures. Medicines are provided to control CAD risk factors and relieve symptoms. The procedures used for re-vascularization are angioplasty or percutaneous coronary intervention(PCI) and Coronary Artery Bypass Grafting (CABG). Percutaneous coronary intervention (PCI) involves balloon angioplasty and stenting (Kern *et al.* 2018). It is performed in a cardiac catheterization laboratory along with ICA or separately. The balloon is inserted into the diseased artery using a catheter and inflated to dilate the blocked part of a vessel. Sometimes stents are placed to keep the artery open. Coronary artery bypass grafting is a surgical procedure where the blood flow is redirected around the blockage in the coronary artery using a graft taken from other parts of the body. Traditionally, the factors that predict survival for a patient with CAD are left ventricular function, the anatomic extent of coronary atherosclerosis, the severity of ischaemia and angina, presence of ruptured plaque, and patient's general health conditions (Cassar *et al.* 2009).

2.4.4 Clinical Trials related to invasive FFR

In this subsection we list a number of trials which established the importance of invasive FFR and its relevace in clinical decision making.

DEFER Trial(2001)

It was a multicentre randomised study which compared deferral versus performance of PCI in non-ischaemia producing stenoses using invasive FFR as guide (Achenbach *et al.* 2017). It included 325 patients with intermediate coronary stenosis. PCI was performed for patients with FFR $\leq$ 0.75. Patients with FFR greater than 0.75 were categorized into PCI group and DEFER group based on the treatment being PCI and medical therapy respectively. There was no difference between the PCI group and DEFER group for MACE (massive adverse cardiovascular events), mortality and re-vascularization events after 1 and 5 years. It concluded that FFR$>$0.75 can be treated with a conservative approach. The 15 years of follow up for patients showed that there was no increase in event rate for patients in the DEFER group compared to PCI.

FAME Trial (2009)

Fractional flow reserve versus angiography for multivessel evaluation(FAME) trial was a randomised trial which included 1005 patient with multi-vessel coronary artery disease and compared treatment method of PCI for all stenoses $\geq 50\%$ from ICA with the treatment method of FFR guided re-vascularization for all stenoses $\geq 50\%$ (Fearon *et al.* 2007). For patients in the FFR-guided revascularization category, PCI was only performed for patients with FFR ≤ 0.80 while in the other category PCI was performed for all patients with stenoses $\geq 50\%$ stenosis. In FFR guided branch, a mean of 1.9 ± 1.3 stents per patients were implanted and in PCI only group 2.7 ± 1.2 stents per patients were implanted (Tonino *et al.* 2009; Achenbach *et al.* 2017). After 2 years of follow up, the rate of MACE was lower in FFR guided group (8.4%) compared to PCI only group (12.4%). ICA was found to be inadequate in assessing the functional significance of stenosis not only in intermediate but also for severe stenosis (Tonino *et al.* 2010).

FAME-2 Trial (2012)

This trial included patients with single and multi-vessel coronary artery disease and investigated if FFR guided treatment benefited patients (i.e. if re-vascularization based on FFR ≤ 0.80 was beneficial for patients) (Achenbach *et al.* 2017). The study showed sustained benefits for people treated with PCI compared with medicine alone for FFR ≤ 0.80.

The RIPCORD Study

The RIPCORD study assessed the impact of the availability of FFR data on the patient management plan compared to the availability of CCTA data alone (Whittaker & Curzen 2013). In the 200 patients studied, there was a change in management plane in 26% of the study population (32% of vessels) after the availability of FFR data in addition to angiographic data. These changes included cases where further data was requested and the cases where OMT only treatment was changed to re-vascularization.

Limitations of Invasive FFR

Invasive FFR requires to induce hyperaemia. For individuals with microvascular dysfunction, hyperaemia can not be achieved to its full extent, which can lead to false-negative FFR values (Achenbach *et al.* 2017). Also, the FFR measurement also results in incorrectly high values for patients with severe hypotension (Achenbach *et al.* 2017).

Invasive coronary angiography was the primary tool to assess the extent of coronary artery disease until the development in imaging techniques allowed CT-scan resolution to visualize coronary arteries. ICA still remains the same for patients with very unstable angina. Failure of ICA to correctly identify ischaemia causing lesions led to invasive FFR. The use of invasive FFR resulted in fewer stenting procedures (Achenbach *et al.* 2017). It also reduced the overall procedural cost and subsequent complications associated with stents and duration of hospital stay (Tonino *et al.* 2009; Tanaka *et al.* 2019; Sengottuvelu *et al.* 2016). However, it has been observed that only 40% of cases after ICA require consequent percutaneous interventions (Gorenoi *et al.* 2012). To reduce the burden of unnecessary invasive procedure, there has always been a search to find non-invasive mean to calculate FFR. Recent methods of non-invasive diagnosis of CAD involve estimation of FFR from CCTA data. The method is labelled as CT-FFR or FFR_{CT}. CT-FFR method is discussed in the next chapter.

Chapter 3
CT-FFR

Computed tomography derived fractional flow reserve (CT-FFR) is a method to calculate FFR from CCTA data-sets. About 50% the lesions considered severe by visual assessment in coronary CTA are found to be non-ischaemic (Meijboom *et al.* 2008), thus visual interpretation overestimates the severity of CAD. Invasive angiography (ICA) with FFR assessment is the standard for the combined anatomical and functional test which also allows ad-hoc revascularization of ischaemic lesions. However, it was found that nearly 60% of patients undergoing ICA do not have obstructive CAD (Patel *et al.* 2014; Gorenoi *et al.* 2012). These cases require no further interventional procedure. Such patients would benefit from non-invasive functional diagnosis of stenosis severity. This approach resulted in computational FFR from CT-images or CT-FFR method. The section 3.1 discusses the CT-FFR procedure and the section 3.2 presents the research studies which evaluated CT-FFR. The section 3.3 presents limitations of CT-FFR method.

3.1 CT-FFR Procedure

CT-FFR is a single test method to quantify the anatomical and functional severity of stenosis in the coronary arteries. It does the non-invasive evaluation of FFR from coronary computed tomography angiography (CCTA) images. The process involves the construction of a digital model of coronary anatomy (aortic root with epicardial arteries) from CCTA and calculating FFR across the entire vascular tree using computational fluid dynamics simulation (figure 1.8). The methodology of CT-FFR computation,

- Acquisition of CCTA image data set
- Modelling of coronary artery bed which includes aortic root and coronary arteries
- Meshing of the 3D model
- Defining boundary conditions of the arterial tree using the physiological model of circulation
- Numerical solution of Navier-Stokes equations for blood flow
- Computing fractional flow reserve from the pressure distribution in coronary artery tree

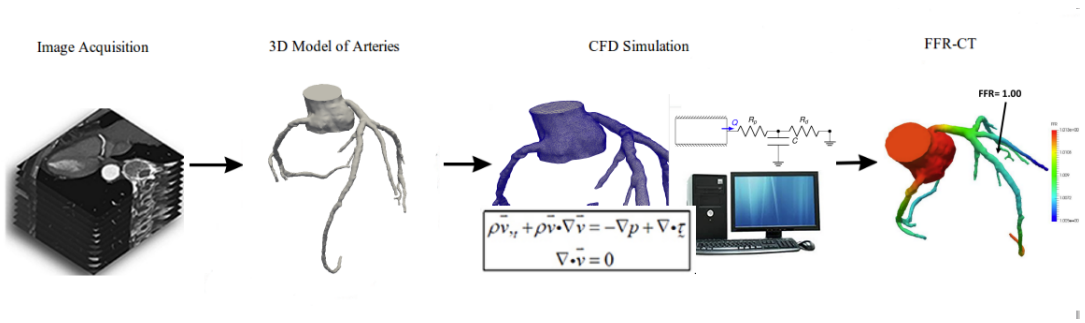

Figure 1.8: CT-FFR Method.

The steps in CT-FFR methodology are explored in subsequent chapters. The use of patient-specific models has become possible due to improvements in medical imaging (for the anatomy

of coronary arteries from 64-detector row CT scanner) and advances in modelling along with reducing cost of computer hardware (Zarins *et al.* 2013). This method can also be used for 'virtual stenting', in which one simulates how stent placement would improve blood flow in the vessel. CT-FFR is shown to have higher accuracy and predictive value compared to CCTA alone (Zarins *et al.* 2013). FFR calculated using coronary computed tomography angiography(CCTA) images may help rule out the invasive coronary angiography for patients with intermediate coronary stenosis that do not require consequent percutaneous intervention after ICA (Gorenoi *et al.* 2012). Thus, CT-FFR is one of the measures being taken to minimize invasive procedures before patients undergo revascularization.

Two companies HeartFlow Inc. and Siemens have developed CT-FFR software called FFR_{CT} and cFFR respectively. The HeartFlow FFR_{CT} software by HeartFlow, Inc., has been cleared by the U.S. Food and Drug Administration (FDA) for clinical use in prediction of FFR and it is being regularly used in USA, Japan and in European Union (Cohen 2014; HeartFlow Inc. 2019*a*).

3.1.1 HeartFlow FFR_{CT} Software

HeartFlow, Inc., is a U.S.A. based medical technology company which developed non-invasive cardiac vascular modelling tools. The FFR_{CT} by the HeartFlow®is the first commercial technology that allows non-invasive functional assessment for the extent of coronary artery disease (CAD) based on patient anatomy and physiology (DAC 2017). It was awarded CE mark (EuropeanUnions(EU) mandatory conformity marking for meeting standards for health, safety, and environmental protection) in 2011 and cleared by FDA in 2014 (Cohen 2014; HeartFlow Inc. 2019*a*). It provides its services in the United States, Canada, Europe and Japan. The reported cost of CT-FFR procedure by HeartFlow is around 1500USD compared to the 9000USD charged for standard Invasive FFR in United States (HeartFlow Cost 2019; Kincaid 2018).

HeartFlow Process

The process requires the patient to undergo CCTA at a local hospital. The patient data is anonymized and then transmitted to HeartFlow for analysis via the Cloud. A three-dimensional model of patient′s coronary arteries is created. HeartFlow FFR_{CT} is simulation (HeartFlow Inc. 2019*a*) software for Navier-Stokes equations which simulates blood flow in 3D model of arteries and calculates FFR value for the entire coronary tree. The results are delivered in 5 hours or less via Cloud computing (Budoff & Nakansihi 2016; Kincaid 2018; Koo *et al.* 2011).

CT-scan data-sets are quantitatively tested for image quality such that the artery lumen and myocardium can be segmented (requiring complete coronary tree and myocardium to be estimated in single cardiac phase) (Lu *et al.* 2017). FFR_{CT} software requires at least 64-slice CCTA and FFR cannot be calculated when images lack sufficient quality e.g. excess calcification (BlueCross NC 2017). In HeartFlow FFR_{CT}, blood is modelled as Newtonian fluid and a parallel supercomputer solves incompressible Navier-Stokes equations (Koo *et al.* 2011). FFR is computed from pressure distribution in the artery. It produces a colour-coded analysis of FFR values at all points for each vessel (figure 3.2). The results are intended to aid clinicians to assess the impact of blockage on blood flow, especially for stable symptomatic angina patients.

HearFlow analysis assessment does not include cases of recent myocardial infarction, complex congenital heart disease, prior CABG surgery, pacemaker or defibrillator or prosthetic heart valves. It is also not evaluated for patients with body mass index $> 35 kg/m^2$, coronary arteries with excess calcification, patients under suspicion of an acute coronary syndrome, patients with significant arrhythmias or tachycardia or patients who require emergency procedures (Kincaid 2018; HeartFlow Inc. 2019*a*).

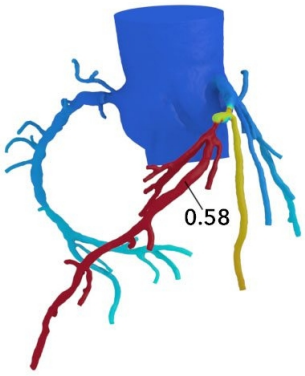

Figure 3.2: Coronary Artery model colormapped with indicated FFR value from HeartFlow. Image retrieved from https://www.heartflow.com/ on Oct 2019.

3.1.2 Siemens cFFR Software

Siemens cFFR is the product of Siemens AG Healthcare, Forchheim. Germany. The coronary tree lumen and myocardium data are extracted from CT-images and myocardial mass and vascular resistance is calculated (Kruk *et al.* 2016; Coenen *et al.* 2015). A 3-dimensional model of the coronary model is semiautomatically created in software, and with coronary blood flow simulation, the software calculates virtual FFR values throughout the coronary tree. The CT-FFR study by Kruk *et al.* (2016) on 96 lesions in 90 patients using cFFR showed that software can differentiate between ischaemic and non-ischaemic stenoses for intermediate stenosis cases. Another study by Coenen *et al.* (2015) on 106 patients, showed a diagnostic accuracy of 75% for cFFR software.

While the HeartFlow FFR_{CT} uses three-dimensional analysis and gives results in a few hours from central location, Siemens cFFR can also be used for one-dimensional analysis on on-site software available on dedicated workstations (Budoff & Nakansihi 2016). A single study by cFFR for can take 10 to 50 min (Kruk *et al.* 2016), but the software is not commercially available.

3.2 Research Studies evaluating CT-FFR

FDA approval of HeartFlow was based on the data from three prospective multicentre trials DISCOVER-FLOW study ((Koo *et al.* 2011)), DeFACTO study (Kruk *et al.* (2016); Min *et al.* (2012)) and, HeartFlow NXT study (Nørgaard (2014)). The FFR_{CT} evaluation through these trials are listed in table 3.1. There have been other clinical studies like PLATFORM, etc. to evaluate the safety and accuracy of CT-FFR method.

DISCOVER FLOW Study (completed 2011)

DISCOVER-FLOW (diagnosis of ischaemia-causing stenosis obtained via non-invasive fractional flow reserve)(Koo *et al.* 2011) was the first of its kind of studies to evaluate CT-FFR. The study comprised 103 patients suspected of coronary artery disease. The patients underwent clinically indicated CCTA, invasive coronary angiography and invasive FFR, and FFR_{CT} procedure. The patients included were adults with an indication of $\geq$50% of stenosis in the major coronary artery ($\geq$2.0mm diameter) from CCTA ((Koo *et al.* 2011)). The patients with prior CABG were excluded ((Koo *et al.* 2011)). FFR_{CT} analysis was performed at Heartflow Inc. The value of FFR $\leq$0.80 was taken as lesion-specific ischaemia. For the vessels with 50 to 69% stenosis predicted by CCTA, FFR_{CT} showed the diagnostic accuracy, sensitivity, specificity, positive predictive value,

and negative predictive value of 83.0%, 66.7%, 88.6%, 66.7%, and 88.6% per vessel respectively ((Koo *et al.* 2011)). The correlation value(0.68) between FFR_{CT} and invasive FFR values was deemed good with slight underestimation of FFR_{CT} with measured FFR.

The study concluded that FFR-CT increased the adeptness to detect lesions that cause ischaemia by reducing false positives and provided superior diagnostic performance as an additive to CCTA.

DeFACTO Study (completed 2012)

DeFACTO (Determination of Fractional flow reserve by Anatomic Computed TOmographic angiography) study included 252 patients from 17 centres in 5 countries ((Min *et al.* 2012; Kruk *et al.* 2016)). These patients underwent CCTA, invasive coronary angiography (ICA), invasive FFR and FFR_{CT} procedure. The study aimed to gauge the accuracy of FFR_{CT} by comparison with standard invasive FFR measurement for intermediate stenosis in arteries. The included patients had $\geq$50% of stenosis in a major coronary artery from CCTA. The value of FFR $\leq$0.80 was taken as lesion-specific ischaemia. Patients with conditions like prior CABG surgery, pacemaker or defibrillator or prosthetic heart valve, prior percutaneous coronary intervention (PCI), acute coronary syndrome, significant arrhythmia, adenosine or contrast allergy were excluded ((Min *et al.* 2012; Kruk *et al.* 2016)). The analysis was conducted for ICA, CCTA and FFR_{CT} by independent laboratories on per vessel basis and per-patient basis. The FFR_{CT} showed accuracy, sensitivity, specificity, positive predictive value (PPV), and negative predictive value (NPV) of 71%, 74%, 67%, 41%, and 90% compared to CCTA alone values of 63%, 34%, 72%, 27%, and 78% respectively ((Min *et al.* 2012; Kruk *et al.* 2016)). The study did not achieve its primary goal of lower 95% confidence interval(CI) limit for diagnostic accuracy of >70% for FFR_{CT} with CCTA using invasive FFR as reference (73% diagnostic accuracy for FFR_{CT}). The study determined that FFR_{CT} would reduce false-positive cases while the specificity and positive predictive value from this method remained low.

	DISCOVER-FLOW (2011)	**DEFACTO (2012)**	**HEARTFLOW NXT (2013)**
No. of Patients	103	252	254
CT-FFR sensitivity against Invasive FFR per vessel	88%	80%	84%
CT-FFR specificity against Invasive FFR per vessel	82%	61%	86%
CT-FFR accuracy against Invasive FFR per vessel	84%	-	86%
CT-FFR sensitivity against Invasive FFR per patient	93%	90%	86%
CT-FFR specificity against Invasive FFR per patient	82%	54%	79%
CT-FFR accuracy against Invasive FFR per patient	87%	73%	81%

Table 3.1: Comparison of results from FFR_{CT} Evaluation Studies.

HeartFlow NXT Study (completed 2013)

HeartFlowNXT (HeartFlow analysis of coronary blood flow using CT angiography: NeXT steps) ((Nørgaard 2014)) was similar to previous studies that were designed o determine the diagnostic accuracy of FFR_{CT} using standard invasive FFR as reference. The prospective multicentre study used a refined version of FFR_{CT} technology with better image segmentation and physiological

models. For study 254 patients with suspected coronary artery disease were analyzed at 11 centres in 8 countries ((Nørgaard 2014)). Patients with previous CABG or PCI or with an acute coronary syndrome, previous myocardial infarction <30 days before coronary CTA, patients with reactions to beta-blockers, adenosine or nitro-glycerine and with body mass index $>35kg/m^2$ were excluded ((Nørgaard 2014)). The study showed that the diagnostic accuracy of FFR_{CT} was 81% per-patient basis. The sensitivity, specificity, PPV, and NPV for FFR 86%, 79%, 65%, and 93%, respectively on per-patient basis for 95% confidence-interval which is much better than earlier evaluations((Nørgaard 2014)). Per vessel correlation of FFR_{CT} to FFR (Pearson′s correlation co-efficient 0.82; p <0.001) was also deemed good . Better results were attributed to improvements in FFR_{CT} technology (addition of micro-circulatory resistance models) and to better CT image quality ensuring the acquisition being controlled and adherence to SCCT CTA acquisition guidelines ((Nørgaard 2014)).

PROMISE FFR CT Sub-study (completed 2014)

This sub-study of PROMISE (PROspective Multicenter Imaging Study for Evaluation of Chest Pain) trial was a retrospective observational study designed to assess the impact of CT-FFR in improvement in the efficiency of patient treatment strategy (Min *et al.* (2015)). A subgroup of patients that underwent CCTA and ICA under PROMISE trial was included. CT-FFR analysis was conducted at HeartFlow Inc. for the study population of 181 patients. There was agreement of 71% between FFR_{CT} and ICA for severe stenosis (Min *et al.* (2015)). In the study 91% of coronary revascularizations had positive FFR_{CT} (Min *et al.* (2015)). The study observed that ICA decreased by 44% for patients with ≤50% stenosis when it was done based on CT-FFR.

PLATFORM TRIAL (completed 2015)

PLATFORM (Prospective Longitudinal Trial of FFR-CT: Outcome and Resource Impacts) study was designed to evaluate the clinical effectiveness of CT-FFR guided patient management (Douglas (2016)). It was a 1-year prospective study which enrolled adults (≥18 years) with intermediate obstructive CAD in 11 countries. Out of 584 patient, 204 followed CT-FFR guided strategy (CCTA followed by FFR_{CT}) and 380 followed usual care strategy (ICA). One year follow up was obtained for 581 patients. The study showed that FFR_{CT} led to the cancellation of 60% planned ICA procedures. For 29 patients which underwent both FFR_{CT} and invasively measure FFR, the comparison showed that for FFR_{CT}, the overall accuracy of 84.0% (95% confidence interval: 70.9% to 92.8%), similar to that of NXT trial (Douglas (2016)).

THE FFR-CT RIPCORD STUDY (RIPCORD 2: completed 2015)

This multicentre sub-study of NXT trial was designed to determine the effect of adding CT-FFR to CTCA to evaluate legion severity (Curzen *et al.* (2016)). The difference inpatient treatment plans with and without the inclusion of FFR_{CT} was assessed. Total of 200 patients with chest pain who underwent computed tomographic angiography (CTA) and FFR_{CT} procedure from NXT trial were selected for a confidence level of 95% with a 0% margin of error and a response distribution of 50% (Curzen *et al.* (2016)). The availability of CT-FFR data made the treatment plan change in 36% of study cases that were initially based on CCTA data alone. There was 18% reduction in PCI. The study showed as a proof of concept that CT-FFR method had a substantial effect on decision making in patient management.

Cost Effectiveness of CT-FFR

The DISCOVER-FLOW trial showed the 30% reduction in project cost for FFR_{CT} guided strategy compared to visual assessment strategy at 1 year (USD 7,674 vs. USD 10,702) (Koo *et al.*

2011). PLATFORM trial showed that mean 1-year per-patient cost of care, quality of life and utilization of resources for FFR_{CT} guided strategy was lower compared to ICA (Douglas 2016).

3.3 Limitations of CT-FFR

As CT-FFR depends on the CT-scan images, the quality of CCTA raw images affects the FFR prediction. In PLATFORM trial, 13% of CCTA images and in NXT trial, 12% of CCTA images were found to be low quality and deemed not suitable for analysis (Koo *et al.* 2011; Nørgaard 2014). While CT-FFR requires no additional imaging procedure, the extra procedural cost gets added for a group of patients. Current FFR calculation by HeartFlow is off-site data analysis process which requires data transfer and results in delay. Other than the limitations of HeartFlow FFR_{CT}, the validation studies and practical use of CT-FFR method has been limited to patients with stable angina. CT-FFR is not concerned with the microvascular diseases which can still cause ischaemia and require other diagnostic procedures.

As the invasive FFR has been deemed most suitable for intermediate stenosis, the use of CT-FFR for the same can benefit the assessment of intermediate lesions (Budoff & Nakansihi 2016). All the above studies showed that CT-FFR improves the ability to discriminate patients compared to CCTA only evaluation. CT-FFR can reduce the number of high false-positives by CCTA as shown in NXT trial where 68% of patients with false-positive results based on coronary CT angiography were reclassified by FFR_{CT} to true-negatives (Nørgaard 2014).

Chapter 4
Data Collection and Medical Imaging

The study framework of CT-FFR method requires CCTA images to create three-dimensional models of coronary artery bed. Invasive FFR value for the same CT-data set is needed to substantiate the FFR computed from simulations. But there are no publicly available datasets for the study to the best of our knowledge. One of the objectives of the project was to create a high-quality repository which could be used for the current study and for similar studies in future. This chapter explains the process of data collection that involves clinical protocols and database creation. The database includes data anonymization of the data, data storage and the data retrieval system. We also review the medical imaging standard DICOM which is also a standard file format for most of the medical images.

4.1 Clinical Data Collection

The data collection exercise was undertaken in collaboration with Sri Jayadeva Institute of Cardiovascular Sciences and Research (SJICR), Bengaluru (Govt. of Karnataka - Regd. Autonomous Institute). The medical data of patients who show symptoms of coronary artery disease and, were required to undergo both CCTA and Invasive FFR procedure was collected with institutional approval and informed consent from all the patients (figure 4.1). The data includes the CCTA image sets, ICA image sets and invasive FFR values. The demographic information from patients which include information on age group, gender, socio-economic group, along with echocardiography and blood test results were also recorded. Cardiovascular risk factors like diabetes, hypertension, dyslipidemia were also documented.

Patient Selection

This study population includes adults(>18 years old) with stable angina who undergo ICA after CCTA as standard medical procedures that are part of regular care for suspected CAD. Patients with 100% occlusion of arteries, with allergy or contraindication to the contrast agent, adenosine and nitroglycerine were excluded from the study.

Pre-procedure medication for CT-scan and invasive FFR

- **β-blocker:** CT-scan image quality is better for low heart rate (near to 60 beats/min). Thus β-blockers are used to reduce heart rate for small durations (Abbara *et al.* 2009). It can be administered orally or intravenous.
- **Nitroglycerine(NTG):** Nitrates are used for coronary vasodilation and administered before coronary CTA (Abbara *et al.* 2009). Nitroglycerin can dilate left main coronary artery by 5% and smaller arteries upto 50% (Nichols *et al.* 2011).
- **Adenosine:** It is a vasodilator used during cardiac catheterization.
- **Contrast agent**: Contrast agents are iodine concentrations which are injected to improve image quality by increasing arterial opacification.

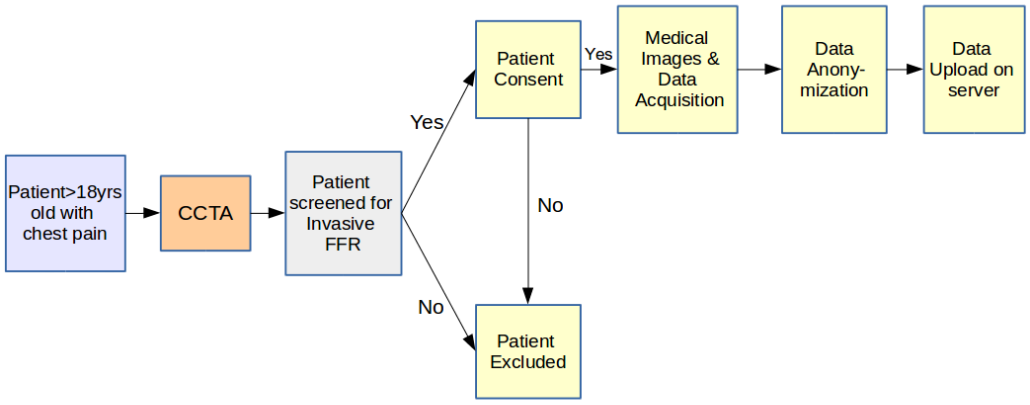

Figure 4.1: Data-collection Process.

4.1.1 Coronary CTA acquisition

The Society of Cardiovascular Computed Tomography (SCCT) provides guidelines for acquiring and reporting of CCTA data (Abbara *et al.* 2009). Based on these guidelines, in current project a standard protocol was defined for CCTA data acquisition (figure 4.2). Factors like difficulty in holding breath, obesity, body movements, increased heart rate, and contraindication to β -blocker or nitroglycerin affect the quality of CT-scan (Abbara *et al.* 2009; Cademartiri *et al.* 2008). Thus, patients were screened for such contraindications and health conditions. Patients were also screened for health conditions like renal insufficiency and previous heart failure. Blood pressure and heart-rate of the patient was monitored. Heart rate $<$ 70bpm and ability to hold the breath for comparable time are required to avoid motion artefacts in CT-scan (Cademartiri *et al.* 2008).

Inclusion Criteria

- Heart rate $<$ 65bpm (spontaneous or β-blocker induced)
- Ability to hold breath

Exclusion criteria

- High heart rate
- Allergic to contrast, nitroglycerin, iodine contrast media
- Renal insufficiency (serum creatinine >120 mmol/L)
- Pregnancy

Coronary CTA was performed with Philips Brilliance 64-slice scanner, 3^{rd} generation scanner with an aperture of 70cm (the specifications of the scanner are listed in Appendix A). CT-scan was done on patients with creatinine <1.5 and heart rate <65bpm. Creatinine level ensures that the patient's kidneys are healthy enough for contrast injection. As CT-scan is based on freezing cardiac motion, lower heart rate provides a larger imaging window and better quality images. Oral and/or the intravenous beta-blocker metoprolol was administered targeting a heart rate of <65 beats/min for patients with higher heart rate. Immediately before image acquisitions, nitroglycerin(NTG) was administered on the table to ensure coronary vasodilation. During acquisition, iodine contrast was injected which was followed by a saline flush. CT-scans were

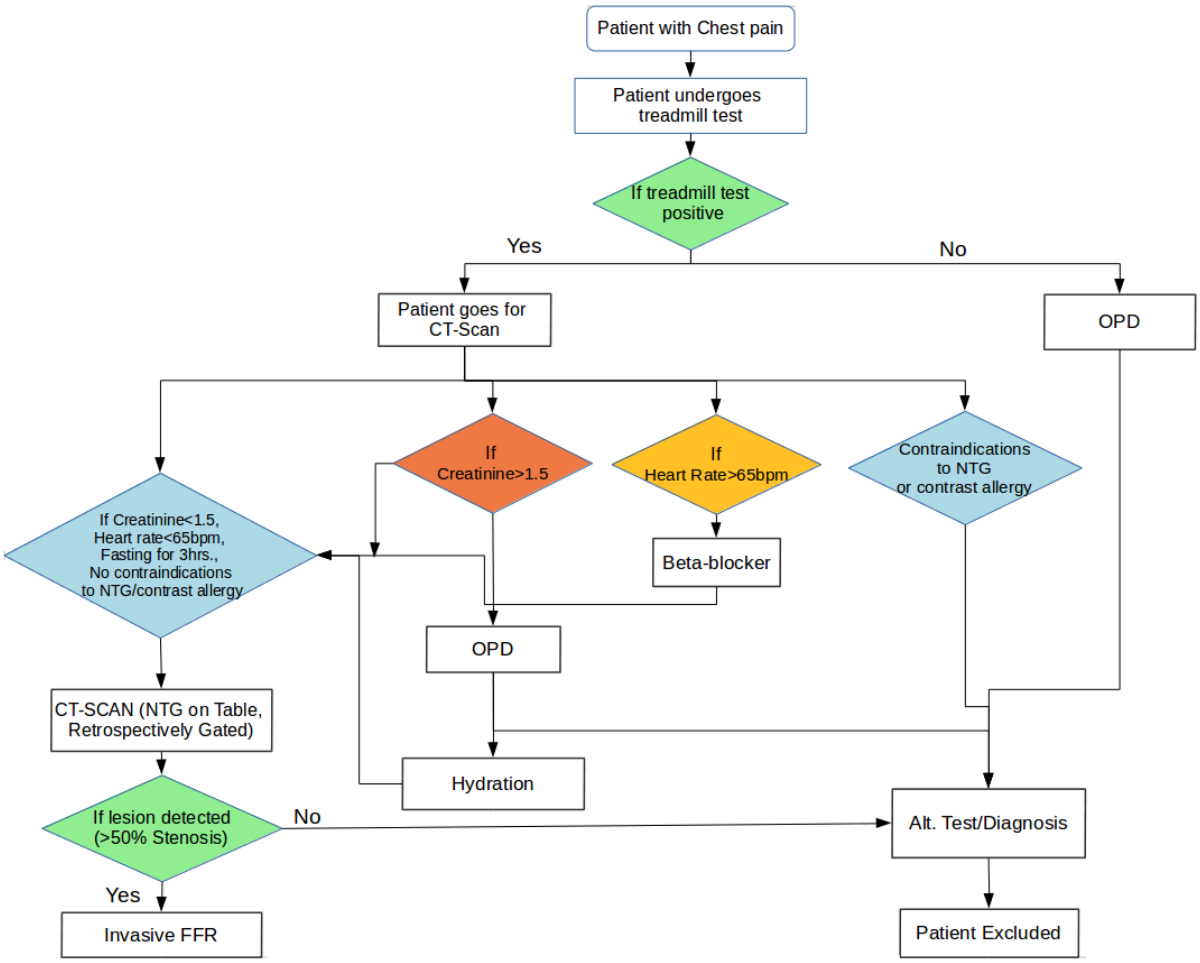

Figure 4.2: Coronary CTA Acquisition Process. OPD (Outpatient Department).

obtained in helical or spiral mode with retrospective electrocardiographic gating. The spatial resolution of a CT image acquired at SJICR (Sri Jayadeva Institute of Cardiovascular Sciences and Research) is 24 line pairs/cm and 512x512 pixels with 0.5 mm slice spacing and 0.4x0.4mm pixel spacing.

4.1.2 ICA Images and FFR data acquisition

ICA procedure was performed in Cath-lab with Philips Allura Xper FD10 Cath/Angio System (Appendix A) (figure 4.3). It is floor mounted cardiovascular imaging system with two LCD monitors in the examination room and two LCD monitors in the control room. Invasive FFR was performed at the time of ICA using PressureWire Aeris with Agile Tip (St. Jude Medical Systems AB (Abbott)) (Appendix A)(figure 4.4). It is a wireless device with a hydrophilic coating and a guidewire diameter of 0.014 inches (0.036cm). It is used in conjunction with QUANTIEN^{TM} Integrated FFR system, a Wireless Wi-Box Unit to store and display data from pressure wire. Aortic pressure is zeroed at the beginning. The calibration and pressure equalization is performed according to guidelines. Nitroglycerin was administered to minimize vessel resistance before measuring FFR and adenosine was administered to induce hyperaemia. ICA was performed for all the patients and FFR was measured for at least one vessel of the patient.

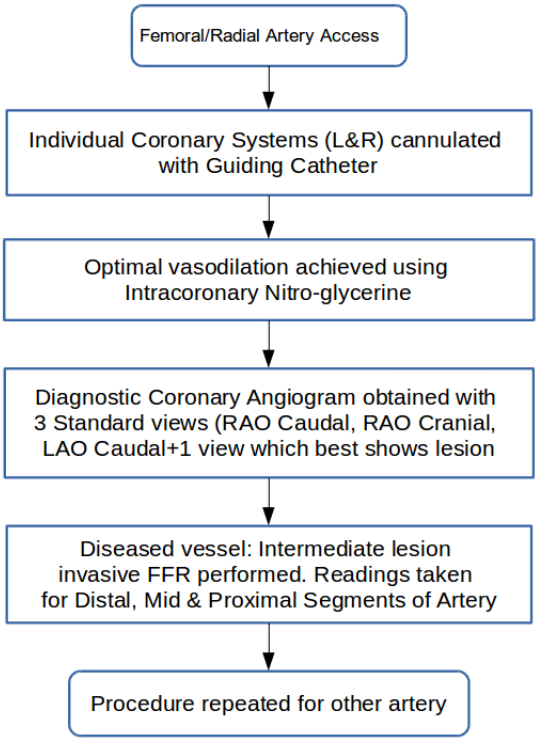

Figure 4.3: Invasive Angiography Procedure Protocol.

4.2 Medical Imaging

Medical imaging consists of technique and processes used for visualizing body interior for diagnosis, monitor and treat medical conditions. These imaging techniques include X-ray imaging (CT-scans, Fluoroscopy, Mammography, etc.), ultrasound imaging and MRI (Magnetic Resonance Imaging) and PET. The imaging techniques like CT and ultrasound provide geometry (shape and volume of the organ) and motion (flow pattern and blood velocity) information and they are called structural imaging techniques (Hoskins *et al.* 2016*b*). Contrast agents, PET and nuclear medicine provide information like chemical and biological function and blood perfusion, etc. and these are categorised as functional imaging techniques (Margolis *et al.* 2007). Most of the imaging modalities can be used to generate functional information. Medical images are stored in file formats of Analyze, DICOM (Digital Imaging and Communications in Medicine), Nifti(Neuroimaging Informatics Technology Initiative) and Minc (Larobina & Murino 2014). DICOM is the most common and successful format used today. The coronary CTA images and invasive coronary angiography images are saved in DICOM format.

Digital Imaging and Communications in Medicine (DICOM) standard is a globally accepted mode of communication and management in the medical field. It is an extension of ACR-NEMA standard (Dicom NEMA 2019*c*), a standard developed to interconnect different medical imaging devices (OTpedia 2019). The standard is a multi-part document and published as NEMA standard PS3 (Dicom NEMA 2019*a*). It is also recognized as ISO 12052 standard (Dicom NEMA 2019*d*). The standard was designed to standardize the medical image and data communication between different medical equipment and systems. It also provides protocols for network communication and file format structure and facilitates online and offline image management, transfer, storage, retrieval, processing, display, security profiling, archiving and printing of medical images (Bidgood *et al.* 1997; Dicom NEMA 2019*d*).

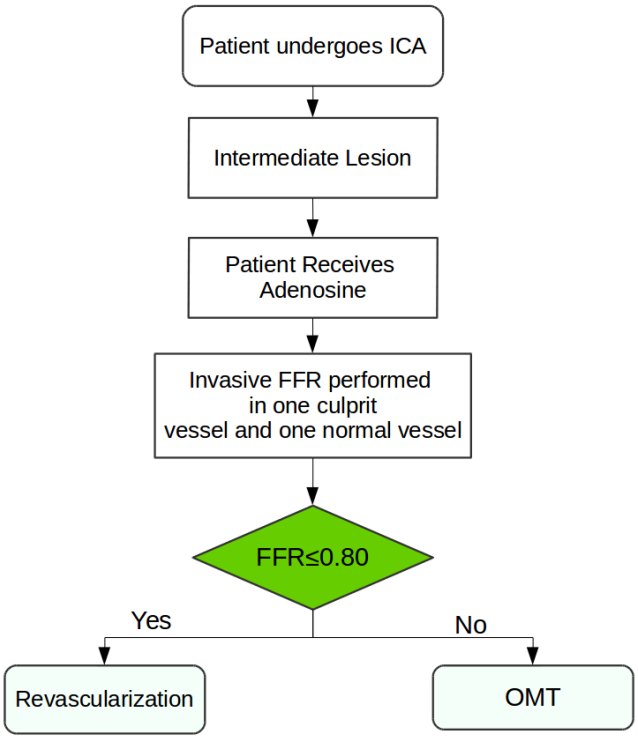

Figure 4.4: Invasive FFR Procedure Protocol.

DICOM Images

DICOM image file is a series or stack of 2-dimensional cross-sectional image slices. A complete set of image slices creates volume (figure 4.5). The file is DICOM standard-compliant image file (Standard part 3.10 (DICOM format files or *.dcm*)) which provides a DICOM file and storage format for the image. The DICOM file contains image information and metadata. A metadata is medical information and it includes patient demographic data, data acquisition date, place and time, equipment details, diagnostic procedure details, physician′s name etc. The information stored by DICOM file is categorized into modules like Patient Module, General Study and Series Module, Equipment Module, Image Module, SOP Module etc. from image information object definitions (figure 4.6) of DICOM standard PS 3.3 (Parisot 2003; Innolitics 2016). There are other modules like frame of reference module, contrast/bolus module, overlay plane module, and modality-specific information modules like CT-image module, MR image-module, etc. along with clinical trial or research modules.

Structure of a DICOM Image

A DICOM object is made of Data elements or attributes. A series of data-elements makes a Data-set. This information is stored as data-set in DICOM file which is segregated as header and image data-set. The header contains file metadata. It contains 128 byte fixed field file preamble and 4 byte size DICOM prefix with 'DICM' character string. A data-set is composed of a series of data elements. It includes a tag (label) and length of data-elements. Data-sets also contain the information of SOP COMMON module. A data-element comprises of object attribute values with a unique tag, value representation(VR) and, length and range of value. The complete DICOM image data contains information in three dimensions, consisting of multiple slices that form 3D image stack. It consists of a number of rows and columns that define the image size, samples per pixel to define the number of separate planes or colour channel. For greyscale images, samples per pixel is set to 1 and for RGB the value is 3 (Dicom NEMA 2019*b*).

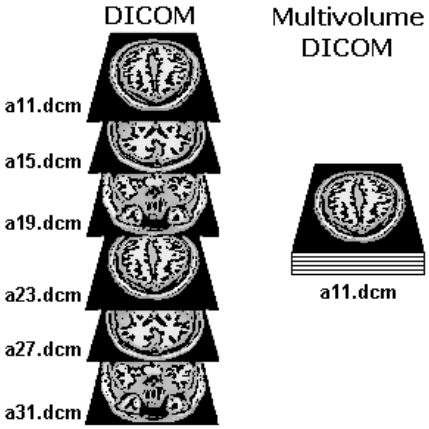

Figure 4.5: DICOM Image Set, 2D images and 3D volume.(Image retrieved from "`http://people.cas.sc.edu/rorden/ezdicom/activex/index.html`" on Sept 7, 2018).

Transfer syntax is used for encoding Data Set include a unique identifier. The DICOM file header with metadata contains transfer syntax.

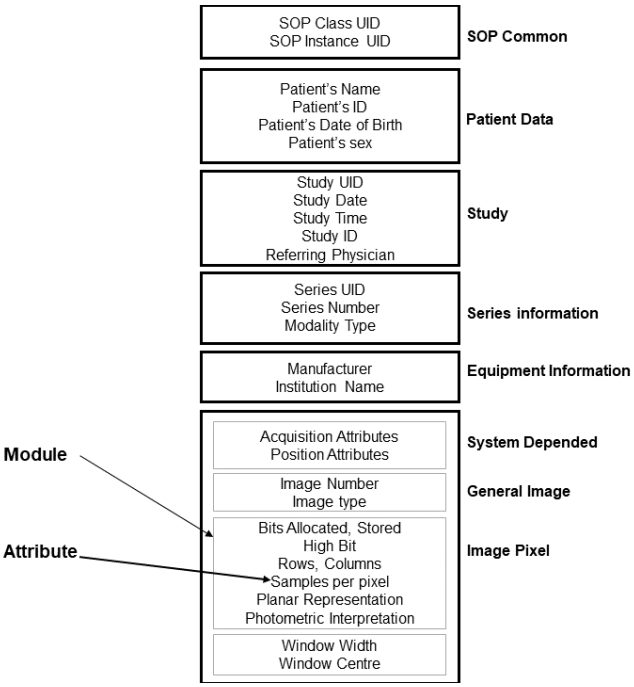

Figure 4.6: DICOM Data Model Structure (Damien 2015).

DICOM Image Processing

Due to the complex format of DICOM files, the visualization and processing of DICOM image require special browser/programs. Medical imaging solution provider companies like GE, Philips, Siemens, etc. provide such software along with their equipment. There are other commercial and free (open-source) browser/software too, that allow viewing, processing and editing of DICOM files. These software programs differ based on their ease of use, speed and accuracy of operations. These software are of two types: DICOM image viewer with limited features only for viewing DICOM images and the other with photo editing type interface to edit, convert anonymize, register Dicom file. A DICOM file viewer typically deals with a variety of images as they come from different sources. The size of these images may range from 512x512pixels to 1024x1024

pixels or even larger. DICOM images for CT have three views: axial, sagittal and coronal. The images for a particular disease are viewed in particular contrast range (also called window). It gives details like the image acquisition time, image no., slice location, magnification, measurements, and 3D volume rendering and few other features. The free (open source) software are only intended for educational and research purposes and not used for medical diagnosis. VTK (Visualization Toolkit, (VTK 2019)) and ITK (Insight Segmentation and Registration Toolkit, (ITK 2019)) are highly used image analysis open-source libraries to develop DICOM processing programs like Osirix, 3D Slicer, ITK snap, InVesalius etc. VTK and ITK are implemented using C++ with classes accessible from Python and Java. Both of these libraries provide basic image-processing tools, segmentation, surface processing and volumetric mesh features. Most of the programs allow viewing of DICOM header information to varying degrees. There are other features like annotations (ability to add text or labels), anonymizing (ability to save DICOM images anonymously), ROI (Ability to create a region of interest) etc. are available in different programs. General features of DICOM software:

- Import/Export, Read and Open all or some slices from the image along with Metadata),
- 2D and 3D Viewing Option,
- Contrast adjustment and windowing an image,
- Image cropping to select a region of Interest, resizing and rotate,
- Volume Rendering,
- Convert and Save the images to different file formats (like jpeg, bmp, tiff, png, etc.),
- GUI features for creating multiplanar reformation (MPR) or maximum intensity projection (MIP) images,
- Controlling the level of compression in images,
- Segmentation features
  - Automatic, Semi-automatic, Manual Segmentation
  - Threshold, Region growing, markup methods
  - Slice by slice segmentation or group segmentation
- 3D Model Generation
  - Removing and adding surface
  - Surface smoothing
  - Scaling of Model
  - Slice
- Documentation files.

4.3 Database and Data storage

The objective of the data-collection process is to build a research dataset relevant for CT-FFR study which can be incremented over time with further data acquisition. In the year 2018 and 2019, data of 24 subjects was collected for the project. The baseline demographics and clinical characteristics are listed in table 4.1 for this study population.

Characteristics	**Number**
Total patients	24
Demographics	
Age, years	47.2 ± 9.16
Male	20
Female	4
Clinical Risk Factors	
Hypertension	10
Diabetes	7
Dyslipidaemia	1
Smokers	7
Family history of pre-mature CAD	1
Previous history of heart disease	1
Stenotic Vessel identified by CCTA	
LMCA	2
LAD	22
LCX	17
RCA	12

Table 4.1: Baseline characteristics of participants in collected-data for current study.

Data Anonymization

The DICOM image datasets for all participants are de-identified and anonymized. De-identification involves removing all patient identifiers like name, address and hospital identification number from the header or replacing them with false values (Noumeir *et al.* 2007). For the current study, the subjects are provided with a unique study-id. The patient name, address and hospital id are removed while the patient's age and sex are kept as the information can be relevant for future studies. The demographic and relevant clinical information is documented using portable document format (PDF) files with study-id. Attributes related to physician and hospital are also removed. For DICOM anonymization, DicomBrowser and DicomCleaner tools are used with customized settings (figure 4.7). The data acquisition date and time were replaced with dummy date and time values. The study description, series description and acquisition protocol which can be used for image processing are not removed. The images where the patient and institutional information is burned in pixel data were modified manually using DicomCleaner tool. Using the blackout feature, the information blocks were removed.

Data Records

All the data from the study is stored in the local server at JNCASR. The complete data sets are also recorded in web-database. The website for the database was created with PHP and MySQL. The web-page can be accessed at "`http://www.jncasr.ac.in/dicon/`". The figure 4.8, 4.9 and 4.10 show the screenshots from website which allows the uploading of data-sets and viewing of database. Data-set for a single patient includes demographic information stored in case-file, CT-scan and blood test reports, CCTA and ICA images, FFR data and echocardiogram report.

The database is far from complete as the data-collection process continues. While we only

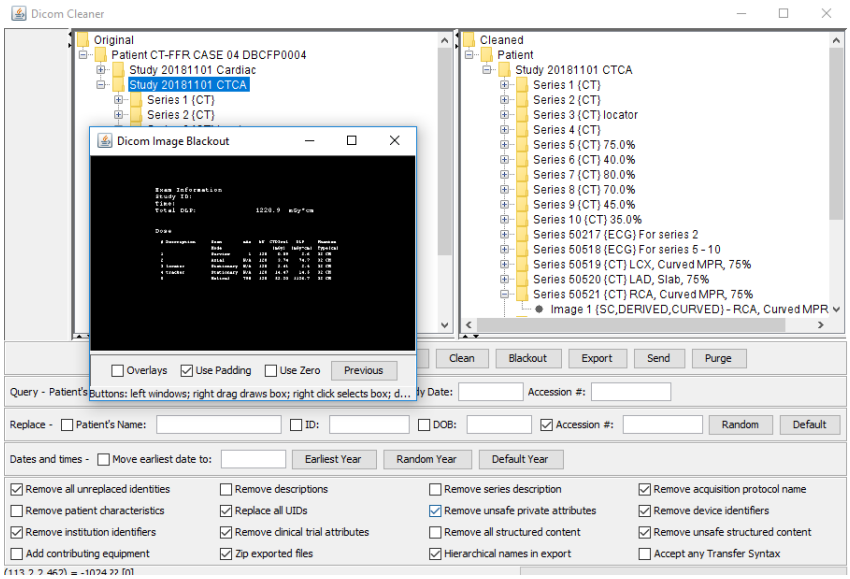

Figure 4.7: Anonymization in DicomCleaner.

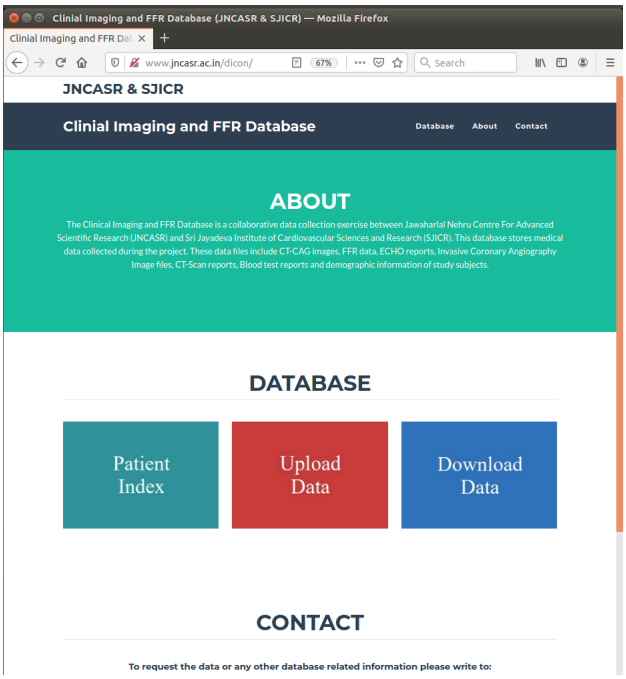

Figure 4.8: Screenshot of database main web-page. The database is accessible at "`http://www.jncasr.ac.in/dicon/`".

use the CCTA and invasive FFR data for current-study of CT-FFR framework, the other information is recorded to include the different aspects of CAD diagnosis. Even though small in scale, collection process intends to create a reference data-set that can be used for investigation, evaluation, development and testing of either conventional or commercial tools including but not limited to CT-FFR analysis.

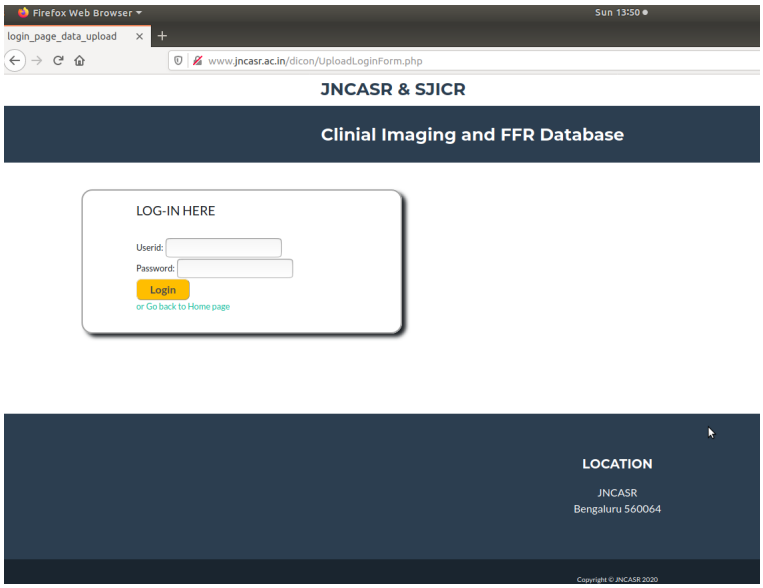

Figure 4.9: Screenshot of Login-page to upload data in database.

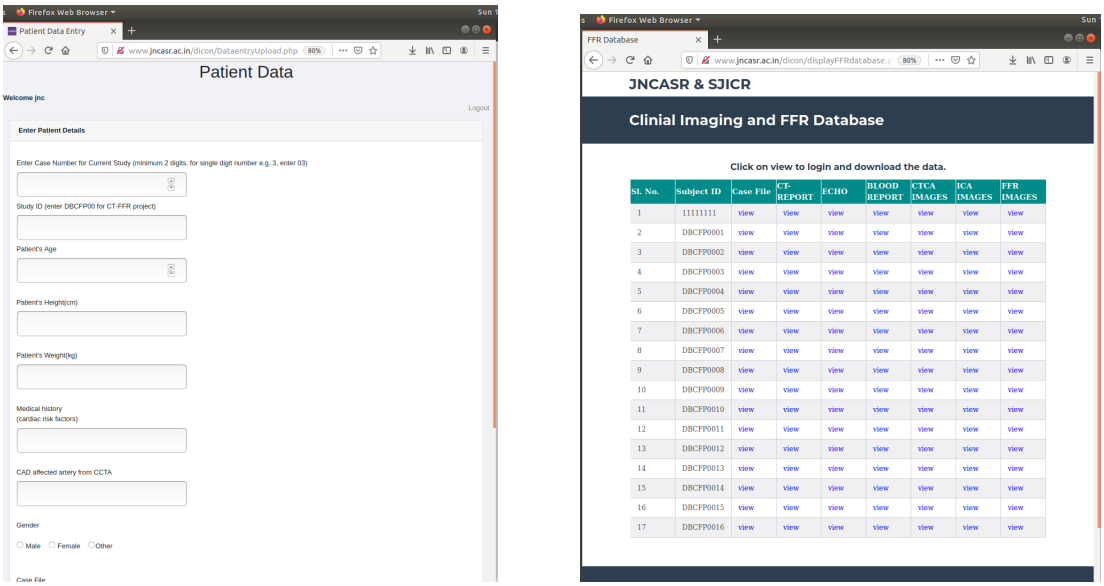

Figure 4.10: Screenshot of Upload data form (left) and the data download page (right).

Chapter 5
3D Modelling of Vascular Structures

This chapter describes the process of modelling coronary artery tree from CCTA images. The 3D model creates patient-specific computational domain for blood-flow simulation. The three-dimensional model of an organ can be constructed from a set of medical images obtained from modalities like CT-scans and MRI. In medical applications, these anatomical models are more commonly used for surgical planning and training. The model generation from images consists of segmentation, surface creation and volumetric mesh-generation (Bekkers & Taylor 2008). To create models from DICOM images, multiple image-processing software packages commercial (e.g. Mimics, AMIRA-AVIZO, slicOmatic, 3D-Doctor) and open source (e.g. ITK, VTK, ITK-SNAP, 3D slicer, ANALYZE, MITK, SimVascular, CRIMSON) are available.

The three-dimensional arterial model of coronary bed represents the lumen of the arteries. Coronary CT-scan images are a series of 2D slices of the heart. The geometry of the coronary arterial tree is extracted using segmentation of lumen of LAD, LCX and RCA with aorta from these slices. The spatial resolution of a CT image in the collected CCTA data is 512x512 pixels with 0.4mm slice spacing and $0.4mm \times 0.4mm$ pixel spacing.

5.1 Image Segmentation

The first step of creating a geometry is to segment the region of interest from the images. Segmentation is defined as the process of dividing an image into regions. Pixels in a region share a common property (i.e. intensity). Segmentation allows separation of lighter and darker regions in greyscale images. Segmentation can be manual, automated or semi-automated process. Currently, automated methods are used with high-quality images. Isolated regions of low-quality images are segmented manually. However, manual segmentation is time-consuming. Some of the challenges in segmentation are faced due to noise in images, non-uniform contrast, different vessel sizes (Basit *et al.* 2014). Segmentation methods can be classified in various ways as different methods tend to overlap. Most common methods used today are threshold, edge detection, region growing, deformable models, and level-set. Most of the segmentation methods use either or both of the following approaches:

- **Edge based segmentation**

  The edges in an image are the regions where there is a significant change in grey value from one pixel to another. The edge can be labelled manually by drawing boundary lines by the cursor. The edge and non-edge are also classified based on gradient method which looks for maxima and minima in first derivative of the image, or by Laplacian method which looks for the zero crossings in the second derivative of the image (Alazzawi *et al.* 2015). Once the edges are detected, the closed object boundaries are selected and filled in.

- **Region based segmentation**

  In region-based segmentation, the segment starts from the centre of a region and grows till the boundary (Huang & Tsechpenakis 2009). Seeds can be placed manually at the region of interest or automatically by using local minima from the variance filter. The selection expands from a single pixel to the neighbourhood by choosing pixels with a given set of qualities and grouping them together. Pixels falling in a different range of pixel values than the one defined are put in another group, forming the different spatial cluster.

5.1.1 Threshold Technique

A typical image has different intensity in different regions. The objects in an images can be categorized based on the proximity to a threshold intensity. In threshold segmentation, an image is divided into two categories. By defining a single value of threshold T, if a pixel is located at lattice position (x,y), then threshold value point $p(x, y)$ are put in one category such that $p(x, y) \leq T$ and remaining pixels are put in category two. Otherwise, user defines minimum and maximum range of pixel intensity and the pixel within the range are put in one category and the others in second category. It is called image binarization (figure 5.1). The pixels in a category may or may not form a single connected component. For, $T = T[x, y, p(x, y)]$, where x and y are the coordinates of $p(x, y)$, threshold image $g(x, y)$ is defined as:

$$g(x,y) = \begin{cases} 1, & \text{if} p(x,y) > 1 \\ 0, & \text{if} p(x,y) \leq 0 \end{cases} \tag{5.1}$$

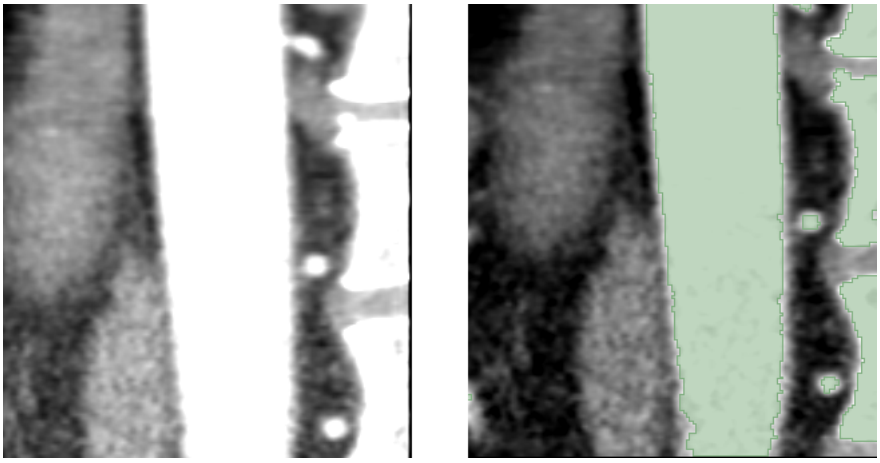

Figure 5.1: Left: Raw grey scale image; Right: Segmented region based on pixel intensity.

5.1.2 Contour Models (Deformable models)

In this method, a connected set of points (called snake), grows towards boundary or edge and changes location or shape until it meets the predefined constraints which are based on global energy minimization process (Huang & Tsechpenakis 2009) (figure 5.2). Contour models are of two types: parametric and geometric. Parametric models (explicit models) are called active contours where parametric curves represent the shape (Huang & Tsechpenakis 2009).

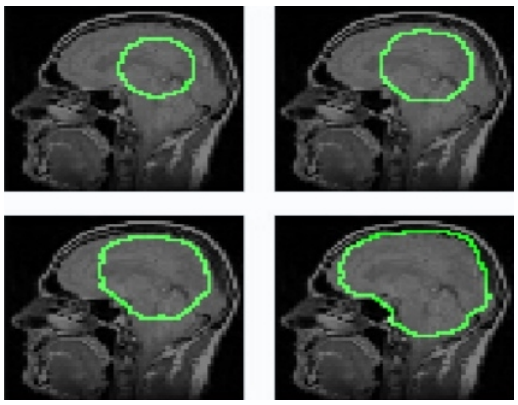

Figure 5.2: Active Contour Model(evolution of contour).

The Level Set Method

This method is the contour model method based on moving curves. These curves represent continuously evolving two dimensional curve in a three dimensional surface (Jiang *et al.* 2012) (figure 5.3). Segmentation boundary is defined as part of the surface where contour level is zero and it is called zero level set. If a function, given by $\phi(x, y, t)$, represents an implicit surface such that $\phi(x, y, t = 0) = \pm d$. Here, d is the distance between position (x, y) and zero level set. Curve of interest is defined as $\phi(x, y, t) = 0$ and Movement formula for level set

$$\phi_t + F\,|\bigtriangledown\phi| = 0 \tag{5.2}$$

where, F= speed function, related to evolving surface characteristics like curvature or normal direction, etc. and image characteristics like gradient (Jiang *et al.* 2012). The equation 5.2 describes the contour movement.

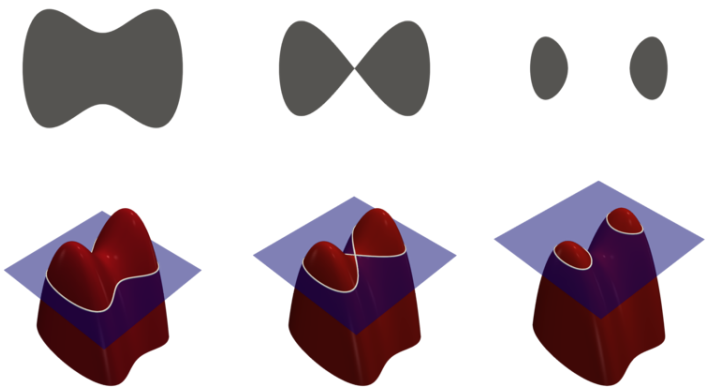

Figure 5.3: Level Set Method (Nicoguaro,Wikipedia 2018).

5.2 Segmentation tools and reconstruction of coronary arteries

In this section, the process of creating a model of coronary artery bed is explained using two tools, 3D Slicer and SimVascular. Both of these tools incorporate Visualization toolkit (VTK 2019) and Insight Segmentation and Registration toolkit (ITK 2019) with GUI (Graphical User Interface). Models are created from the coronary CTA-images of participants in the study. The CT dataset consisted of 512×512 transaxial CT images of the entire heart taken at a 0.4mm slice thickness and a pixel size of 0.32mm. Two different approaches have been used to create a 3D model for subjects: thresholding method and level set method. From the large set of CT-scan images, segmentation is done for the set that provides the most information. For coronary CTA, the phase that provides most information is mid-to-end diastole phase (Pavone *et al.* 2009; Cademartiri *et al.* 2008). The segmentation by threshold method in 3D slicer was semi-automatic while the level-set segmentation in SimVascular was done manually.

5.2.1 About 3D Slicer

The 3D slicer is an open-source extensible software application used for medical image processing and visualization. It is available on various operating systems such as Linux, Windows and MacOSX. It incorporates many libraries like VTK, MRML(Medical Relay Markup Language) and Qt. Slicer provides both generic and specialized tools and also works as a platform for the development of imaging applications (Fedorov *et al.* 2012). 3D Slicer visualization can be used

for 2D, 3D and 4-dimensional data sets. 3D slicer shows 2D views in axial, coronal and sagittal planes along with 3D volume rendering of the object if selected. Slicer modular structure includes filtering, registration, segmentation and surface module to manipulate triangulated surface models. 3D slicer has segmentation tools like thresholding, edge detection, fast marching method, level tracing method, region growing method, etc. It supports markups like fiducials and rulers and annotations. It also allows for Dicom image registration. 3D slicer platform includes specific components like OpenGL to support accelerate rendering, portable libraries, core application framework and plugins(modules) as shown in figure 5.4

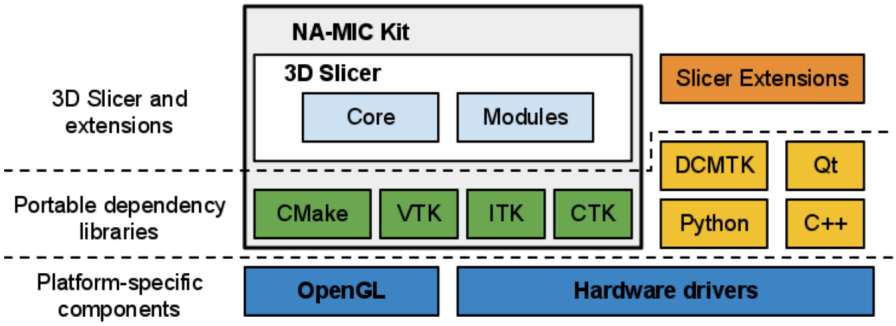

Figure 5.4: 3D Slicer Ecosystem (Fedorov *et al.* 2012).

Model Creation in 3D Slicer

3D Slicer ver. 4.8.1 was used to create a model of the patient using the threshold method. The threshold method is used to create a model in the 3D slicer. The threshold for coronary arteries ranges from 200 to 400 HU. This large variation requires manual input during the segmentation process. To create segments, paint effect was used to highlight the region of the aorta and coronary arteries in slices. The level-tracing, grow from seeds and fill between slices effects were used to cover the entire region of interest. After segmentation the extracted lumen was converted to surface mesh(figure 5.7).

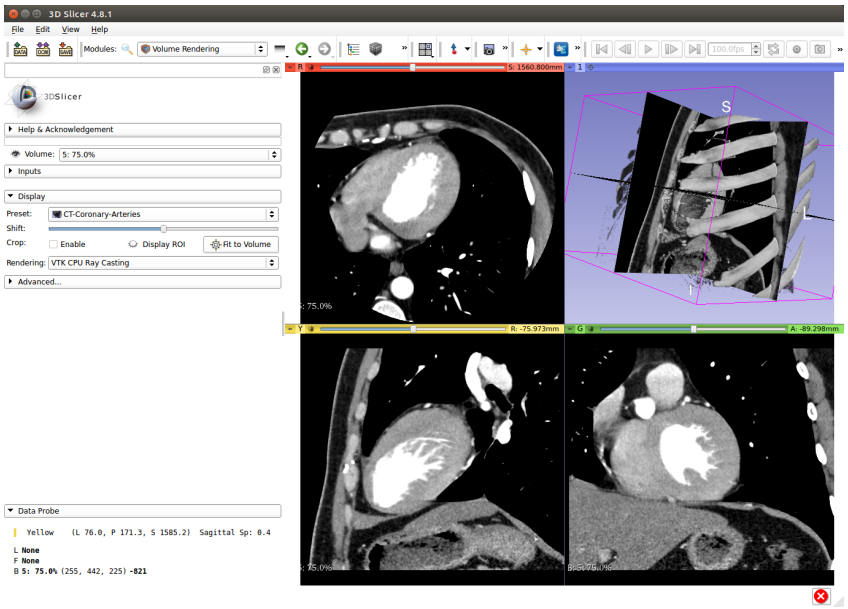

Figure 5.5: CT-Scan images in 3D Slicer GUI with Volume Rendering.

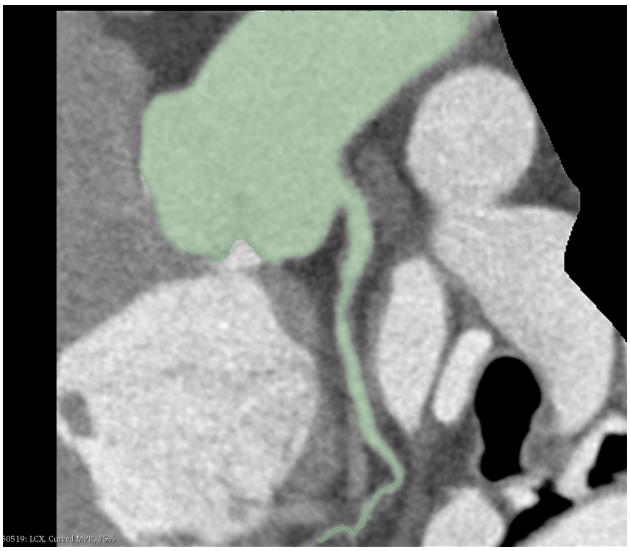

Figure 5.6: Threshold method in Slicer.

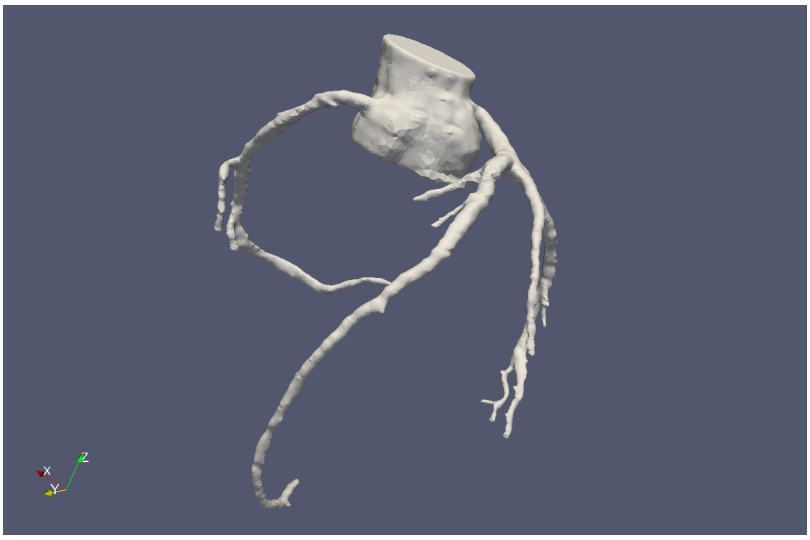

Figure 5.7: Model Generated in slicer using Threshold method.

5.2.2 About Simvascular

SimVascular, released in 2007, is open-source software for image-based patient-specific cardiovascular modelling and blood flow simulation (Updegrove *et al.* 2017). While 3D Slicer is only an image processing package, SimVascular also integrates CFD package for mesh generation and flow simulation. It enables 2-D and 3-D image segmentation and geometric operations for anatomic modelling and includes an integrated flow solver (Updegrove *et al.* 2017). SimVascular incorporates VTK, ITK and MITK libraries. SimVascular pipeline shown in figure 5.8 starts with image processing. Both threshold and level-set techniques can be used to create geometry. SimVascular creates a triangulated surface model from the segmented region. The model can be exported or meshed in SimVascular using packages like TetGen or MeshSim. SimVascular also includes fluid-structure interaction and closed loop modelling for lumped parameter network (Updegrove *et al.* 2017).

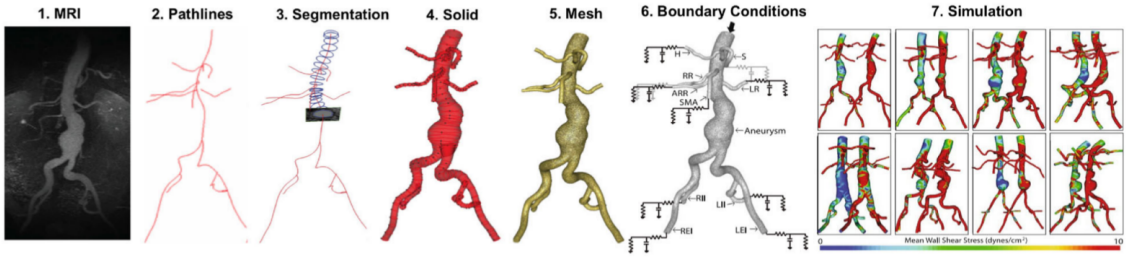

Figure 5.8: SimVascular Pipeline (Updegrove *et al.* 2017).

Model Creation in SimVascular

The coronary arteries are segmented using level set method manually. The method is based on edge detection. Pathlines (centre vessel paths) are created for coronary arteries and aorta (figure 5.9). Along the pathlines, lumen boundary of each vessel is segmented in 2D slices. The set of curves is set at the boundary of coronary arteries where there is a significant change in brightness (figure 5.10). SimVascular delineates vessel boundaries in a cross-sectional imaging window which are lofted together with splines and then the solid model is generated (figure 5.11). While the geometry created in 3D slicer was truncated just below the origin of the arteries, for the model created in SimVascular we tried to extend the geometry below aortic root and accommodate the opened aortic valve which caused slight distortion from the intended curve of the aortic annulus. The volumetric mesh of the model can be created in meshing tab. The manual segmentation process with level-set was more time-consuming than the threshold segmentation with the 3D slicer, especially to resolve the connectivity between slices during bifurcations.

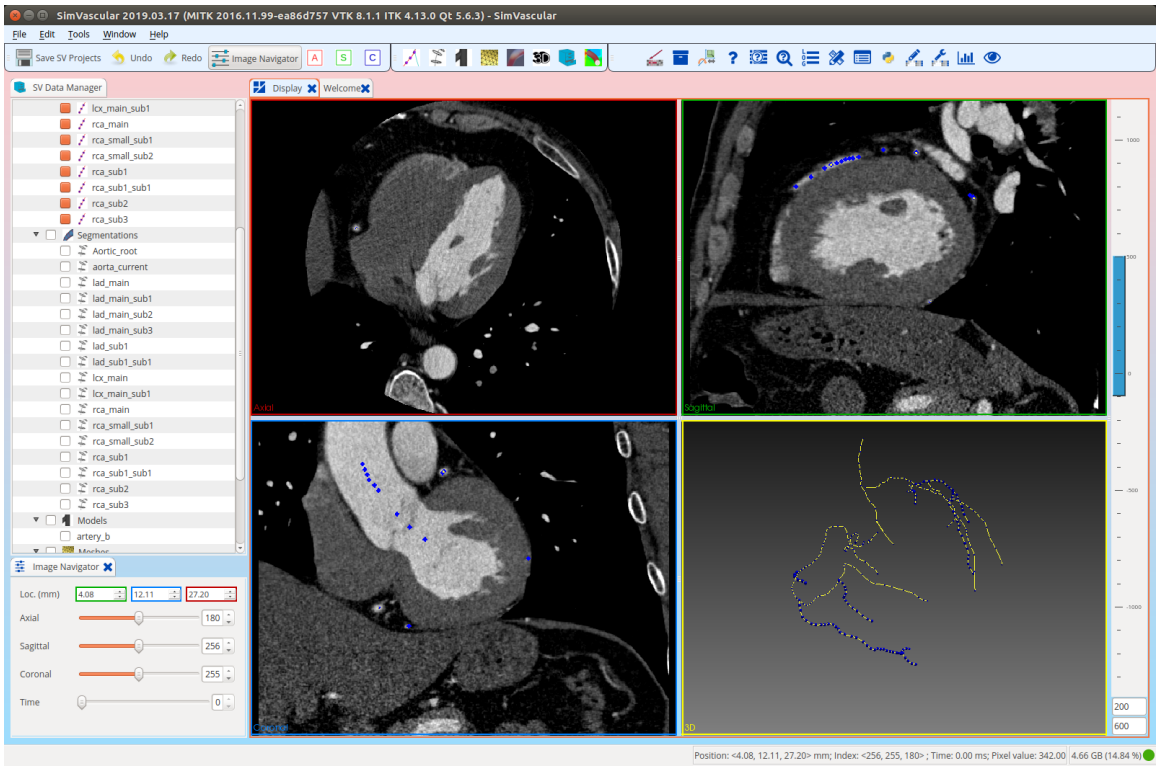

Figure 5.9: Creating pathlines along the centreline of coronary arteries in SimVascular display window.

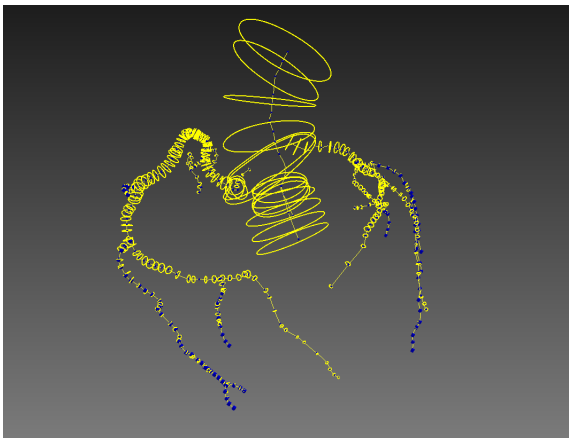

Figure 5.10: 2D contour segmentation in SimVascular.

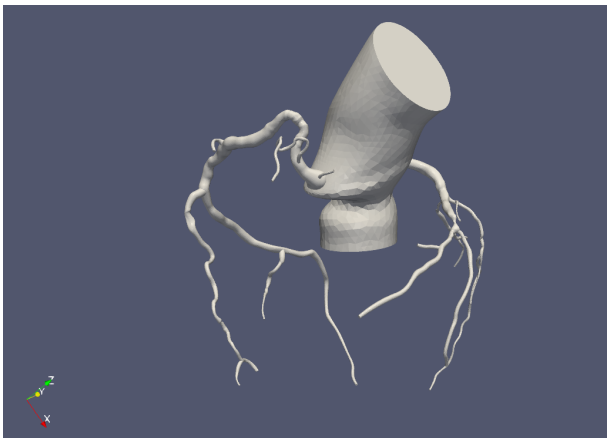

Figure 5.11: Model Generated in SimVascular.

Mesh Refinement

As SimVascular is used for flow-simulation for the current study, the volumetric mesh for models is done in SimVascular. The geometry created in 3D slicer was imported to SimVascular and remeshed using TetGen in SimVascular. SimVascular uses two kernels TetGen and MeshSim (optional) to generate unstructured tetrahedral meshes. Unstructured meshes are commonly used for 3d coronary models, these meshes are built on the node coordinates and the connection between the nodes to form elements. The mesh refinement of the model includes repairing errors and discontinuities and smoothing the model. The reconstructed model geometries are refined to improve its topology which also includes triangulate optimization. The two models created using SimVascular and 3D slicer have been used for blood flow simulation(Chapter 6).

Chapter 6
Coronary Blood Flow Simulation

This chapter describes the process of blood flow simulation in the vascular models. Modelling of the entire cardiovascular system includes modelling heart chambers, arteries, systemic and pulmonary circulation and micro-circulation. All of these models can be individually simulated or integrated based on prediction requirement of the patient-specific analysis. Different levels of numerical models include lumped parameter (termed as 0D models) and distributed models (termed as 1D, 2D or 3D models). In the cardiovascular system, 0D models are often used for heart chambers, large arteries and veins, 1D models have been used for larger system arteries, and 3D models have been used for specific vessels ((Blanco & Feijóo 2009)). To understand local behaviour of flow, two or three-dimensional models are used while lumped parameter models are used for finding global characteristics. (Mantero *et al.* 1992). The current simulation process involves multiscale simulation (3D-0D coupling). It consists of the lumped parameter model being used as boundary conditions to the geometric model. We explain the reduced model of the cardiovascular system, in particular the zero-dimensional (0D) models that are used for rapid analysis of system characteristics. The 0D models are framed using the hydraulic-electrical analogy. The flow is simulated in the patient-specific models for two individuals whose data has been collected during data collection process at Sri Jayadeva Institute of Cardiovascular Sciences and Research (SJICR). The pressure and flow rate are extracted and fraction flow reserve (FFR) value is derived from these results which is compared against invasive FFR.

6.1 Analogy of the cardiovascular system with electrical circuit

The blood flow is driven through the cardiovascular system by pressure difference which is similar to current flow through the electrical circuit due to potential difference. Thus, the pressure difference is analogous to potential difference or 'voltage drop' and the blood flow rate is analogous to current in a circuit. Poiseuille′s law for flow in a tube is analogous to Ohm′s law for the flow of current in an electrical circuit.

Hagen-Poiseuille flow relationship is given by equation

$$Q = \Delta P / R \tag{2.3}$$

where, Q is the volumetric flow rate and ΔP is pressure difference between two ends and the resistance R is given as,

$$R = \frac{8\eta L}{\pi r^4} \tag{2.5}$$

where,η is the dynamic viscosity,L is the length of pipe and r is radius of the pipe. The equation 2.3 can be re-written in the following form,

$$Q = \frac{\pi r^4 \Delta P}{8\eta L} \tag{6.1}$$

Resistors dissipate energy similar to viscosity and, the capacitor in an electrical circuit stores charge which is analogous to arterial walls storing energy during pulsatile flow due to compliance. Fluid inertia is equivalent to inductors in an electrical circuit. The pulsatile flow through the arterial system is analogous to alternating current. Analogous of Kirchoff's law also exists in the circulatory system. The charge conservation in an electrical circuit is similar to the conservation

of matter(blood) in the circulatory system. Total pressure drop in the cardiovascular loop is equivalent to the pressure of the left ventricle which is similar to the voltage drop in the electrical circuit being equal to the voltage of the source in a loop. Thus, the blood pressure, blood flow, volume, resistance and compliance of cardiovascular system correspond to voltage, current, charge, resistance and capacitance of an electronic circuit respectively (table 6.1).

Electrical Circuit	**Electrical Circuit Symbols**	**Cardiovascular System**
Electrical Resistance $R_e = \frac{V}{I}$		Electrical Resistance $R_c = \frac{P}{Q}$
Capacitance(C_e) $I = C_e \frac{dV}{dt}$		Vessel Compliance(C_c) $Q = C_c \frac{dP}{dt}$
Inductance(L_e) $V = L_e \frac{dI}{dt}$		Blood Inertia(L_c) $P = L_c \frac{dQ}{dt}$
Diode $I = \begin{cases} 0, & \text{if} V < 0 \\ \frac{V}{R_e}, & \text{if} V \geq 0 \end{cases}$		Valve $Q = \begin{cases} 0, & \text{if} P < 0 \\ \frac{P}{R_c}, & \text{if} P \geq 0 \end{cases}$

Table 6.1: Analogy of Electrical Circuit and Cardiovascular System.

The arteries, arterioles, capillaries, venules and veins are arranged in a series in the cardiovascular system. If each of these segments is considered as a single component, then the total resistance based on electrical analogues system (figure 6.1a) is given by

$$R_{total} = R_{arteries} + R_{arterioles} + R_{capillaries} + R_{veins} + R_{venules} \tag{6.2}$$

When blood vessels divide to form branches similar to parallel circuit (figure 6.1b),

$$\frac{1}{R_{total}} = \frac{1}{R_1} + \frac{1}{R_2} + \frac{1}{R_3} \tag{6.3}$$

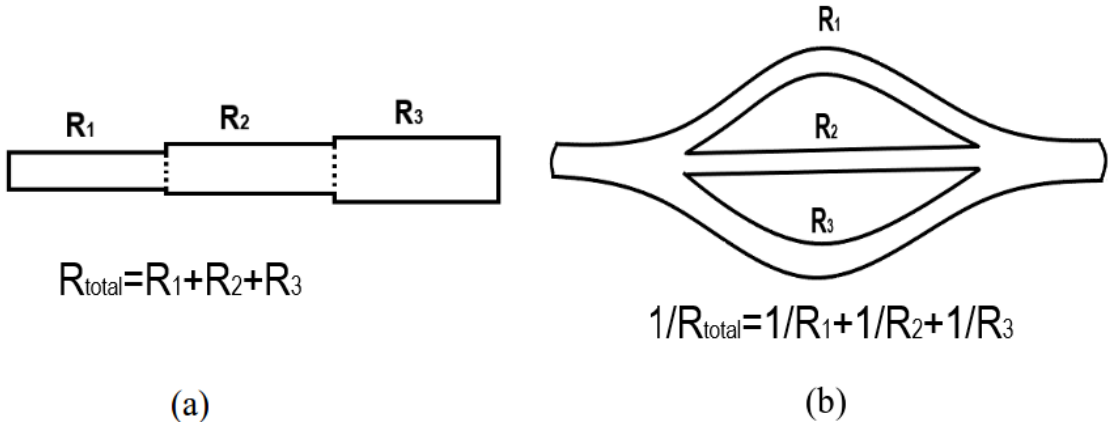

Figure 6.1: Total resistance in series and parallel configuration (Chandran *et al.* 2007).

6.1.1 Cardiovascular system as lumped parameter model

Lumped parameter or zero dimensional models use the analogous nature of fluid flow in vascular system and current flow in electric circuit. The fundamental variables like pressure, flow and

volume are assumed to be uniformly distributed within a section of vessel at any instant of time and give rise to the set of simultaneous ordinary differential equations(ODEs)(Shi *et al.* 2011). The correlation between fluid and electrical counterparts can be shown as (Ghasemalizadeh *et al.* 2014),

- $0.01ml/Pa = 1\mu F(compliance - capacitance)$
- $1Pas^2/ml = 1\mu H(inertia - inductor)$
- $1mmHg = 1volt(pressure - voltage)$
- $133416ml = 1A(volume - charge)$

They are used for modelling global properties of the cardiovascular system and coronary blood flow and also as boundary conditions for local 3D models. Main components of the lumped parameter model are peripheral resistance (R), arterial compliance (C) of conduit vessels. These models do not capture nonlinearities. The most common arterial flow model is the Windkessel model on which 0D models are based.

Windkessel Model

The Windkessel model consists of three elements: a pump which represents the heart, an elastic chamber which represents artery and resistance which represents flow through arterioles and capillaries. Blood vessels are assumed as elastic storage vessels which convert intermittent blood flow into steady flow (Chandran *et al.* 2007) and veins are considered as zero pressure sink (Shi *et al.* 2011). There are 2-element, 3-element and 4-element windkessel models. The increased number of elements accounts for new physiologic factors. Windkessel model is based on mass balance, i.e. Inflow - Outflow= Rate of storage. The electric circuit equivalent of pipe flow (figure 6.2(a)) is shown in figure 6.2(b). If Q_{in} is inflow, Q_{out} is flow to peripheral vessels and Q_a stored volume per time unit in a vessel,

(a) (b)

Figure 6.2: (a) Pipe flow (b) Equivalent electric circuit.

For an equivalent electric circuit figure 6.2(b), for voltage diffrence of ($E_1 - E_2 = E$),

$$\begin{aligned} I = \frac{E_1 - E_2}{R} = \frac{E}{R_{total}} \\ I_{in} = I_c + I_{out} \\ I_{in} = C_e \frac{dE}{dt} + \frac{E}{R_{total}} \end{aligned} \tag{6.4}$$

where, I_{in}= current flowing to the circuit,C_e= capacitance.

for pipe flow in figure 6.2(a),

$$\begin{aligned} Q &= \frac{P_1 - P_2}{R} \\ Q_{in} = Q_a + Q_{out} &= \frac{dV}{dt} + \frac{p}{R} \\ &= \frac{dV}{dp}\frac{dp}{dt} + \frac{p}{R} \\ &= C\frac{dp}{dt} + \frac{p}{R} \end{aligned} \tag{6.5}$$

where, C is total arterial compliance, R is total peripheral resistance and P=mean arterial pressure (p_m), assuming venous pressure (p_v) to be close to zero. As the pressure at the end point of the circulation is nearly zero, $P_1 - P_2 = p$.

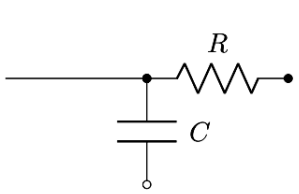

Two element windkessel model

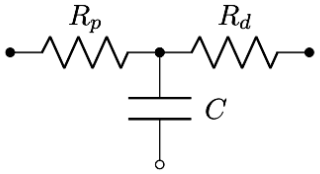

Three element windkessel (RCR) model

Figure 6.3: Windekessel models.

- **Two element Windkessel Model**
  The model includes one resistor and one capacitor. For this model , the equation 6.5 can be written as

$$\frac{dp}{dt} + \frac{1}{RC}p = \frac{Q(t)}{C} \tag{6.6}$$

- **Three element Windkessel(RCR) Model**
  Three element windkessel model adds additional impedance to two-element model. This model is called RCR model. If p is the pressure at aortic root and p_d is distal pressure.

$$p - p_d = R_p Q \tag{6.7}$$

  writing equation 6.6 for p_d,

$$\frac{dp_d}{dt} + \frac{1}{R_d C}p_d = \frac{Q(t)}{C} \tag{6.8}$$

  substituting equation 6.7 into equation 6.8,

$$\frac{dp}{dt} + \frac{1}{R_d C}p = \frac{Q(t)}{C}\left(1 + \frac{R_p}{R_d}\right) + R_p\frac{dQ}{dt} \tag{6.9}$$

These models have been further developed into RLCR, RLRC, RLRCR, RLCRCLR models by adding additional elements to improve the microcirculation model (Shi *et al.* 2011).

6.1.2 Distributed Parameter Modelling

- **1D Models**

  1D models is used to capture Wave transmission effects present in aorta and large arteries and also as boundary condition with 3D models (Shi *et al.* 2011). In the 1D model, the

flow rate is calculated by integrating the velocity over cross-sectional area of the vessel. The governing equations of 1D models are 1D form of the incompressible continuity and Navier-Stokes equations. The 1D equation can calculate flow rate and mean pressure but they can not simulate three-dimensional flow and pressure loss (Vignon-Clementel *et al.* 2006).

- **2D Models**

  2D models are used for local flow study in axisymmetric domains as the radial variation of flow velocity can be represented by 2D models and also as boundary conditions(Shi *et al.* 2011).

- **3D Models**

  3D models are used for local flow study. These models are based on 3D Navier-Stokes equations.

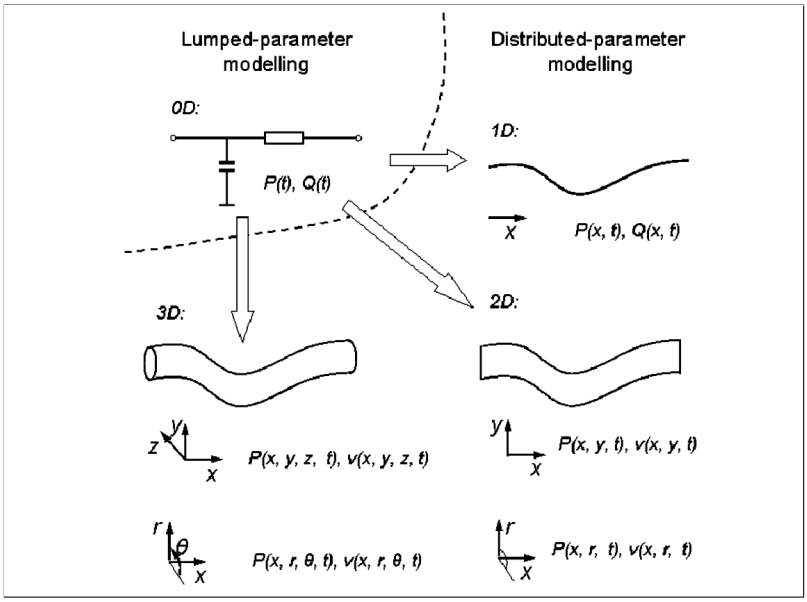

Figure 6.4: Different Modelling Scales (Shi *et al.* 2011).

Other than these models, the cardiovascular system is also subjected to frequency-domain studies. Combining flow rate boundary condition with pressure boundary condition using the reduced-order model are frequently used. Multi-scale modelling integrates 0D, 1D, 2D and 3D models. 1d methods for downstream vessels and 3D for arteries are found to be highly accurate. 3D coronary bed models are coupled to 0D models or 1D-models which represent rest of the circulation to obtain correct estimations of the pressure values.

6.2 Blood flow characteristics in circulatory System

An average adult has blood volume of roughly 5 litres with average blood density of $1060 kg/m^3$ (Hall & Guyton 2011). The dynamic viscosity of blood is $3.5 \times 10^{-3} kg/m.s$ (Hall & Guyton 2011). Blood viscosity in arteries depends on shear rates (Hoskins *et al.* 2016*b*). Blood shows non-Newtonian behaviour at shear rates less than $100 s^{-1}$ (Berger & Jou 2000). The mean and maximum shear rate in large arteries is 200-300sec^{-1} and 800-1000sec^{-1} respectively (Hoskins *et al.* 2016*b*; Wu *et al.* 2004). At high shear rate, the blood shows Newtonian behaviour, so the blood flow is considered Newtonian in heart chambers and large arteries (diameter $\geq 1mm$), assuming homogeneous distribution of red blood cells (Hoskins *et al.* 2016*b*). Blood is considered

Flow Region	**Peak Reynolds Number**	**Homogeneous distribution of Red Cells**	**Turbulence Exists**
Heart	5000-20000	Yes	Yes
Ascending Aorta	5000	Yes	Yes(post-systole)
Smallest Arteries	500	Yes	No
Microcirculation	0.0003(capillaries)-0.5(arterioles)	No	No
Smallest Veins	100	No	No
Vena Cavae	3000-4000	No	No

* Inferior and Superior vena cava length combined

Table 6.2: Blood Flow in Characteristics in Cardiovascular System (Hoskins *et al.* 2016*b*).

non-Newtonian in smaller vessels where shear rate is low (micro-circulation). Table 6.2 lists the behaviour of blood flow through cardiovascular system. The effect of non-Newtonian nature of blood are seen at Reynolds number less than 100 (Cho & Kensey 1991). As the pressure and velocity profile show periodic variation with cardiac cycle, the blood flow in heart is pulsatile. However, blood flow and pressure in arteries have been found to always not be periodic in time due to changes in heart rate, respiration, and flow transitions (Vignon-Clementel *et al.* 2010). Periodic nature of blood flow is characterized using Womersley number(α):

$$\alpha = \frac{d}{2}\sqrt{\frac{\rho\omega}{\mu}} \tag{6.10}$$

where, ω (radians/sec) is heart rate, d is diameter. The value of α in ascending aorta can be upto 20 while in capillaries it is about 10^{-3} (Chandran *et al.* 2007; Hoskins *et al.* 2016*b*). Blood flow in arteries is altered due to stenosis, making flow from laminar to turbulent (Moreno & Bhaganagar 2013). It has also been suggested to incorporate non-Newtonian characteristics for flow separation region around plaque for better estimation of wall shear stress and local pressure drop (Cho & Kensey 1991). The turbulence has been detected in regions distal to stenosis due to high-frequency pressure signals for 23%-76% lesions (Wootton & Ku 1999; Moreno & Bhaganagar 2013).

For blood flow simulation in the current study, the following assumptions are made:

- Blood is a Newtonian and viscous fluid.
- Blood flow is incompressible and laminar.
- Vessel walls are rigid(non-deformable) and there is no slip at the vascular wall.

The objective of the study is to calculate FFR. Since the coronary arteries are less elastic than larger arteries like aorta, the rigid wall assumption is considered practical for cardiac cycle averages (Uus 2016). The Navier-Stokes equations for incompressible Newtonian fluids are used for modelling blood flow.

6.3 Boundary Conditions

The 0D boundary conditions are imposed on the 3D geometrical model of three coronary artery bed such that flow and pressure are coupled at each outlet. These conditions represent the cardiovascular network upstream and downstream of the aorta and the coronary arteries.

6.3.1 Inlet flow boundary conditions

Either pressure or flow waveforms can be used as boundary conditions at aortic inlet. For current study, the inflow waveform is applied at aorta inlet (figure 6.5). The flow waveform is imposed at the inlet (aortic root). The applied waveform is based on assumptions of a cardiac cycle period of 1 second (heart rate of 60bpm).

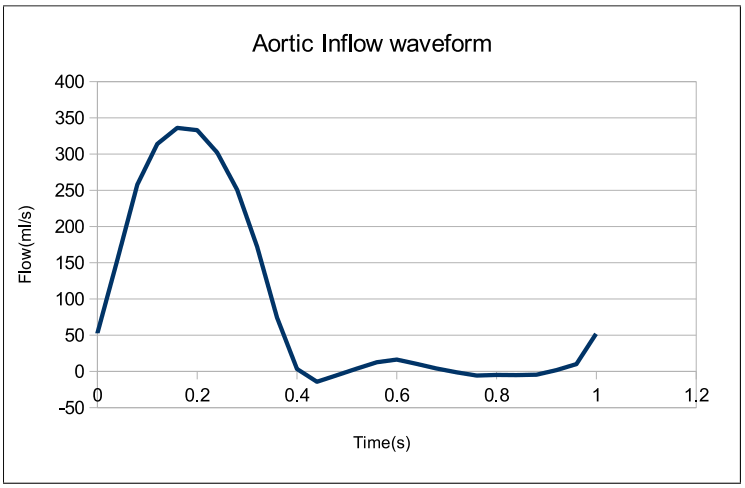

Figure 6.5: Inflow Waveform (Absi 2018; Karmonik *et al.* 2014).

6.3.2 Outlet boundary conditions

The outlet boundary conditions are imposed to represent the downstream vasculature of the aorta and coronary arteries. The 0D models are coupled to the outlet of the 3D model to simulate for peripheral resistance during the hyperaemia condition.

Aorta outlet boundary condition

As aortic outlet boundary condition, we use windkessel RCR boundary condition from equation 6.6 (figure 6.6). The p(t) and Q(t) are pressure and flow rate at the outlet. The pressure p(t) is evaluated from the flow Q(t) from the 3D model. For RCR model, R_p represent the arterial vasculature resistance, the R_d represents the resistance of microcirculation and venous circulation downstream of the aorta and C represents the downstream compliance.

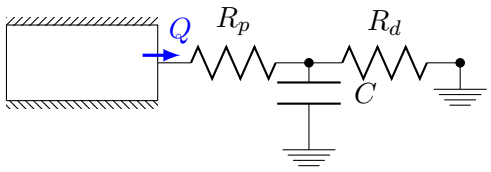

Figure 6.6: Aorta outlet boundary condition.

$$p(t) = p_d(t) + (R_p + R_d)Q(t) + R_dC(\frac{dp_d}{dt} - \frac{dp}{dt} + R_p\frac{dQ}{dt}) \tag{6.11}$$

Coronary outlet boundary condition

For each coronary outlet, boundary conditions are assigned using lumped parameter RCRCR model (figure 6.7). This model consists of downstream coronary arterial resistance (R_a), coronary

arterial compliance(C_a), arterial microcirculation resistance ($R_{a-micro}$), venous microcirculation resistance ($R_{v-micro}$ and venous resistance (R_v). It also includes myocardial compliance (C_{im}) and intra-myocardial pressure (P_{im}).The majority of the flow in coronary arteries happens during diastole. To accommodate this effect, the intra-myocardial pressure is included in the loop which represents the pressure in left and right ventricles (figure 6.8), which are assigned separately for left and right coronary outlets respectively. The pressure at the outlet is calculated from the flow rate (equation 6.12).

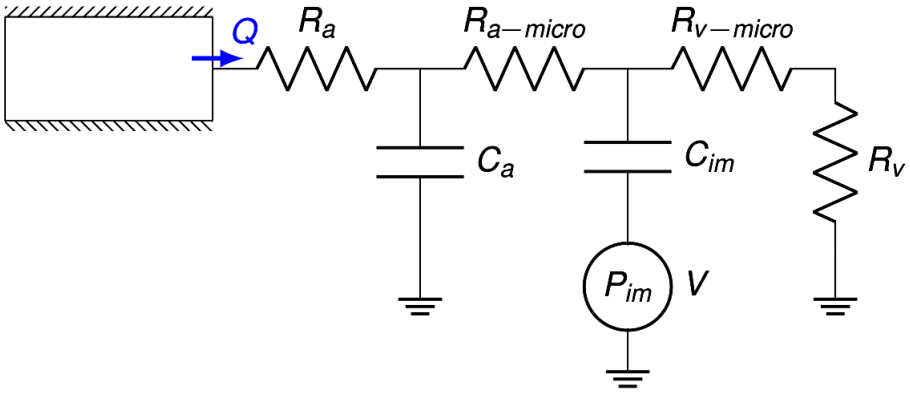

Figure 6.7: Boundary condition at coronary outlets.

$$p(t) = Q(t)(R_a + R_{a-micro} + R_c) + \frac{dQ(t)}{dt}(C_a R_a R_{a-micro} + C_a R_a R_c + C_{im} R_a R_c + C_{im} R_a R_{a-micro}) + \frac{dp(t)}{dt}(-C_a R_{a-micro} - C_a R_c - C_{im} R_v) + \frac{dp_{im}}{dt} C_{im} R_c + C_{im} C_a R_{a-micro} R_c \left(\frac{d^2(-p(t) + R_a Q(t))}{dt^2}\right) \tag{6.12}$$

where,$R_c = R_{v-micro} + R_v$.

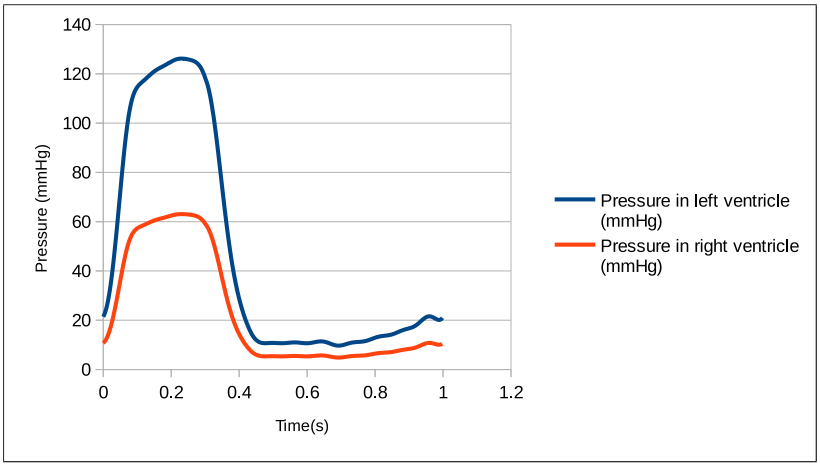

Figure 6.8: Pressure variation in left and right ventricles (Hall & Guyton 2011).

6.4 Simulation Set-up

We have carried out flow simulation for two subjects from the project. The simulation is set-up with the 3D model by assigning boundary conditions, and corresponding parameters for haemo-

dynamic characteristics. Haemodynamics is affected by vessel geometry, compliance, branching, flow waveform shape, the shape of the inlet velocity profile. The blood flow in the coronary artery bed model is simulated in SimVascular. A volume mesh is generated from ".stl" file using TetGen. Each face of the model is assigned a unique identifier (inlet, outlet, wall etc.). For the inlet boundary, the aortic flow waveform is applied using the prescribed boundary condition. At aortic and coronary outlet RCR and RCRCR boundary conditions are applied (figure 6.9). For these boundary conditions, the pressure at any outlet, p(t) is solved using outflow rate Q(t) from the 3D model.

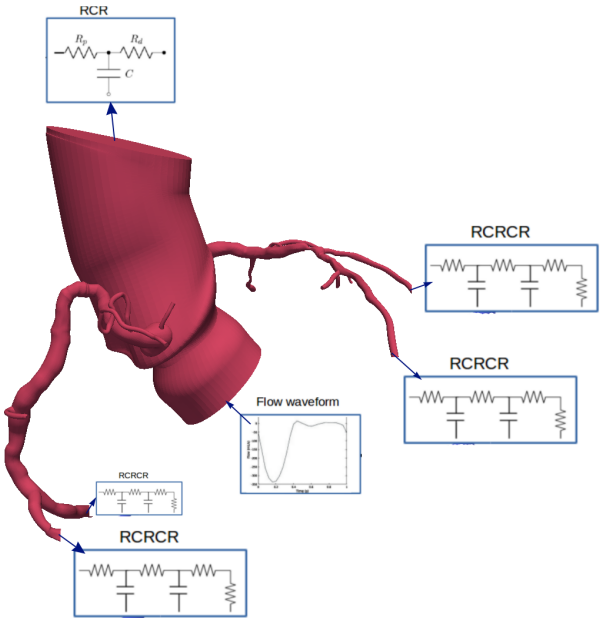

Figure 6.9: Simulation setup with inflow, RCR and RCRCR boundary conditions.

The heart rate and cardiac output are unknown for both subjects. Even though patient's heart rate and cardiac output would be different during the actual procedure of invasive FFR, for both cases studies the simulation results are generated by giving inputs of heart rate and cardiac output value for a healthy human. The boundary conditions are estimated from the rest conditions values of the systolic and the diastolic blood pressure and heart rate. Simulation is set up for a heart rate of 60bpm and cardiac output of 5l/min(83ml/sec)).

6.4.1 Calculation of Vascular Resistance

For systolic pressure of 120mmHg and the diastolic pressure of 80mmHg, Mean arterial pressure(MAP),

$$p_{mean} = 80 + \frac{120 - 80}{3} = 93.33 mmHg = 124432 dyne/cm^2$$
$$\text{Total Peripheral Resistance} R_{total} = MAP/CO \tag{6.13}$$
$$R_{total} = \frac{P_{mean}}{CO} = R_d + R_p = 124432/83 = 1499.2 dyne.sec/cm^5$$

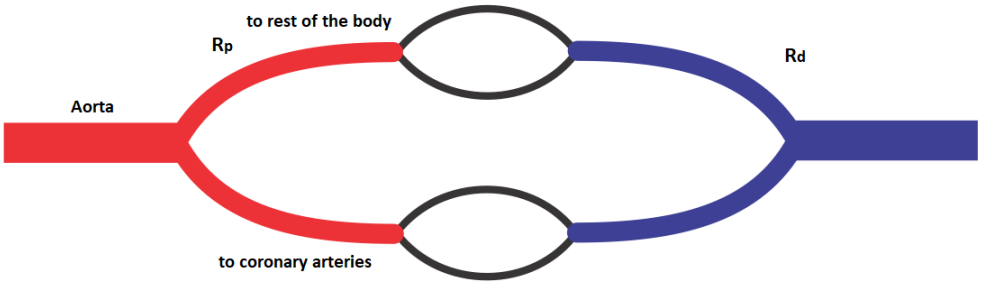

Figure 6.10: Paralled artery and body circuit.

Coronary arteries and rest of the body are in parallel circuit (figure 6.10),

$$\frac{1}{R_{total}} = \frac{1}{R_{cor,tot}} + \frac{1}{R_{restofthebody}}$$

For Coronary flow input of 4% of CO (Kim *et al.* 2010), (6.14)

$$R_{restofthebody} = 1.04 R_{total}$$

$$R_{cor,tot} = 26 R_{total}$$

For RCR boundary condition at aorta outlet from Sankaran *et al.* (2012),

$$\frac{R_d}{R_p} = 10$$

$$R_p = 0.09 * R_{restofthebody} \quad (6.15)$$

$$R_d = 0.91 * R_{restofthebody}$$

$$\text{then, } R_p = 140.3,\ R_d = 1418.8$$

For RCRCR boundary condition at the coronary outlet, the total coronary resistance is split among different outlets. The downstream resistance for each outlet is divided using Murray's morphometric law

$$Q \propto d^k \quad (6.16)$$

Here, Q is flow rate and d is the diameter of the vessel, k is empirically derived constant (Taylor *et al.* 2013). Murray suggested the value of k equal to 3 (Taylor *et al.* 2013).

Murray's Law

The arteries progressively divide into smaller vessels and as the number of branches increases the vessel diameters get smaller. Murray′s law suggests that under the assumptions of blood flow obeying Poiseuille′s law "for arterial networks with minimized pumping power, the volumetric flow rate in an arterial segment is proportional to the cube of the diameter" (Fung *et al.* 2011). Murray derived the following relation between the diameters of parent artery and branching arteries using principle of minimum work for maximum circulation efficiency (Murray 1926):

$$d_1^3 = d_2^3 + d_3^3 \quad (6.17)$$

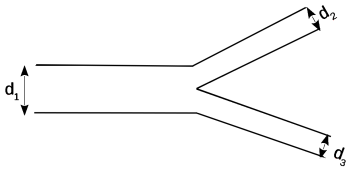

Figure 6.11: Parent Artery and bifurcation.

From equation 6.16 ($Q \propto d^k$) and equation 2.3 ($\Delta P = QR$),

$$R \propto d^{-k} \tag{6.18}$$

From equation 6.18, the smaller vessels have higher resistance to coronary branches. For current study, the value of constant k is taken as 2.6 from generalized Murray's law from Zhou *et al.* (1999). If combined total area of all coronary outlets is A_{total} and A is the area of a single coronary outlet then the resistance at specific coronary outlet is derived from equation 6.18 as,

$$\begin{gathered} R_{cor} = \left(\frac{\sqrt{A_{total}}}{\sqrt{A}}\right)^{2.6} R_{cor,tot} \\ \text{for each coronary artery}, R_{cor} = R_a + R_{a-micro} + R_{v-micro} + R_v \end{gathered} \tag{6.19}$$

the following microcirculatory resistance values are calculated as follows from Sankaran *et al.* (2012) for each artery,

$$R_a = 0.32 * R_{cor},\ R_{a,micro} = 0.52 * R_{cor},\ R_v = 0.16 * R_{cor} \tag{6.20}$$

6.4.2 Approximation of Arterial Compilance

While the values of vascular resistance can be easily approximated from cardiac output and pressure, the same is not true for the arterial compliance. The value of capacitance is tuned for aorta and coronary outlets such that pressure range fall on or closer to 120-80mmHg. As capacitance have no effect on mean flow, the capacitance of aortic outlet is calculated iteratively with trial and error to obtain the desired pressure range (high value ofcompliance cause pressure peak to shift to right) (Sankaran *et al.* 2012) . The compliance of left and right side of coronary branches are calcuated from total compliance for left coronaries and total compliance of right coronaries respectively. For each left coronary artery branch compliance (Sankaran *et al.* 2012),

$$\begin{gathered} C_{left,\,cor} = \frac{A}{A_{total}} C_{total,left} \\ C_a = 0.11 C_{left,\,cor},\ C_{im} = 0.0.89 C_{left,\,cor} \end{gathered} \tag{6.21}$$

For blood flow, a density of $1.06 g/cm^3$ and dynamic viscosity of $0.04 dynes/cm^2 s$ was assigned for the simulations. SimVascular uses stabilized FEM formulation of incompressible Navier-Stokes equations (equation 6.22) to solve the flow and pressure across coronary artery bed (Updegrove *et al.* 2017).

$$\begin{gathered} \boldsymbol{\nabla}.\boldsymbol{u} = 0 \\ \rho.\frac{\partial \boldsymbol{u}}{\partial t} + \rho \boldsymbol{u}.\boldsymbol{\nabla}\boldsymbol{u} = -\nabla P + \boldsymbol{\nabla}.(\eta \boldsymbol{\nabla}\boldsymbol{u}) \end{gathered} \tag{6.22}$$

where, u is the velocity, P is the pressure, η is viscosity and ρ is the density.

In SimVascular, simulation can be run using a single core or with multiple cores using the Message Passing Interface (MPI). The simulation needs to run for several cardiac cycles for the conversion of the solution and before pressure stabilizes. For current simulation, it takes four cardiac cycles to stabilize (figure 6.14). The simulations need to run for at least 6 cardiac cycles for both the study cases. The number of timesteps per cycle is 1000 with fixed time step size (0.01s). Decreasing the time step size further did not affect the results. For transient simulations for the duration of 6 heartbeats, depending on the volume mesh size, the simulation took about 36-60 hours on 6 cores for IntelCore i5-8400CPU with 2.80Gz 64bit model.

6.5 Simulation Results

The flow simulation results are analysed for stenosis using pressure, flow rate, and FFR in the 3D domain. The virtual FFR is calculated for mean pressure values after the pressure had stabilized.

6.5.1 Case Study 01

Clinical History and Diagnosis

This case study involves a 46-year-old male with angina on exertion and cardiovascular risk factors of hypertension and obesity. The patient underwent CCTA which showed moderate stenosis in LAD and luminal irregularity in LCX (figure 6.12). The patient was referred for ICA and PCI. From ICA, 80% of stenosis was identified in both LAD and LCX. The invasive FFR was measured and the arteries were stented.

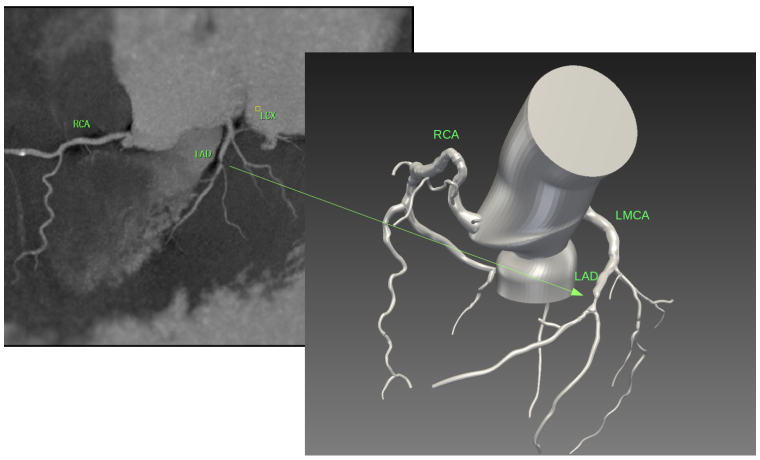

Figure 6.12: The lesion in LAD from CCTA images and in the 3D model for case study 1.

Simulation Results for case study 01

The coronary artery bed model for the case study is shown in figure 6.12. The arteries are modelled up to secondary branches. The figure 6.13 shows the flow rate at aorta inlet and aorta outlet for 10 cardiac cycles. The pressure variation is shown in figure 6.14. The slightly distorted geometry at the place of aortic annulus did not affect the flow to the arteries. The pressure values stabilize after four cycles. The coronary flow shows out of phase characteristic of flow and pressure waveform for the left coronary artery, as the majority of flow in coronaries happens during the diastolic phase. The boundary conditions reproduce this behaviour for current simulation for left and right coronary arteries as shown in figure 6.15 and figure 6.16. The aortic pressure, the pressure proximal and distal to the lesion in LAD are plotted in figure 6.17 and flow velocity before and after the lesion is plotted in figure 6.18. The figure 6.19 shows

the average pressure distribution in coronary artery bed for a single cardiac cycle. The figure 6.20 shows the streamlines for a single cardiac cycle.

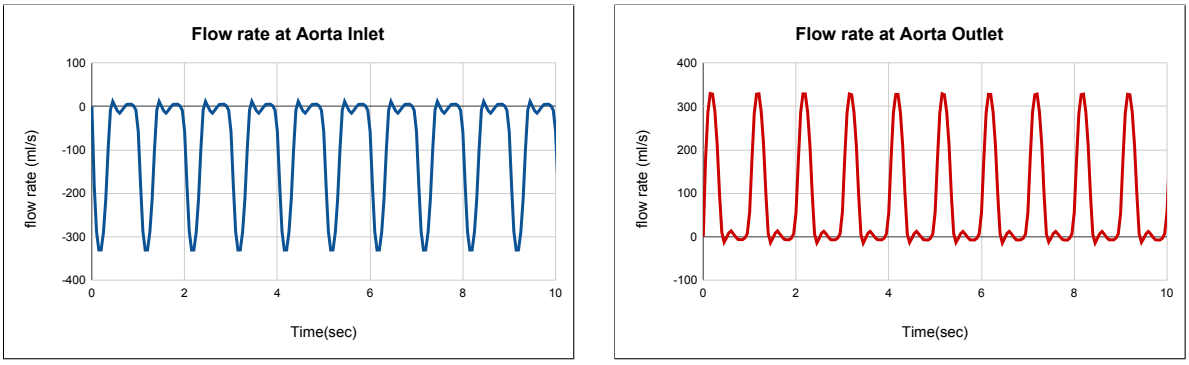

Figure 6.13: Flow rate at aorta inlet and outlet

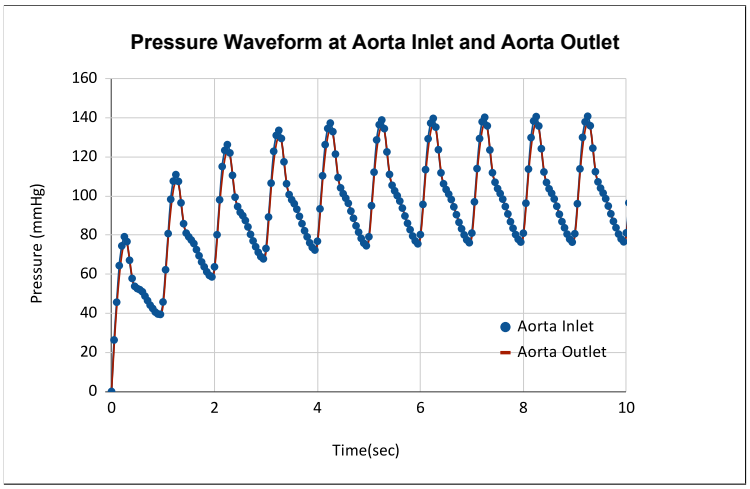

Figure 6.14: Pressure waveform at aorta inlet and outlet.

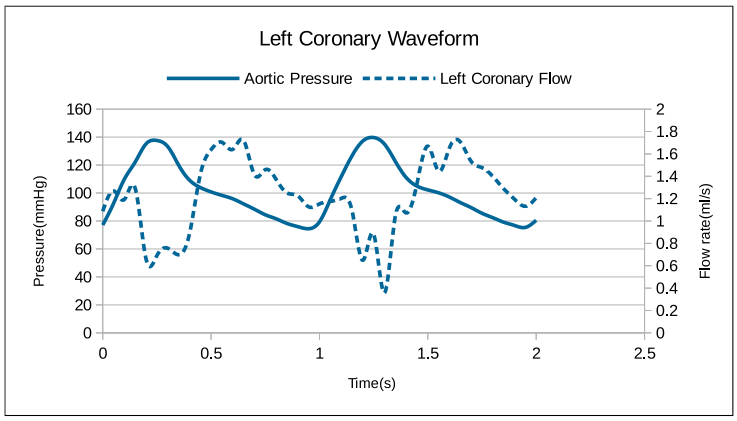

Figure 6.15: Flow and pressure waveform for Left coronary artery (proximal).

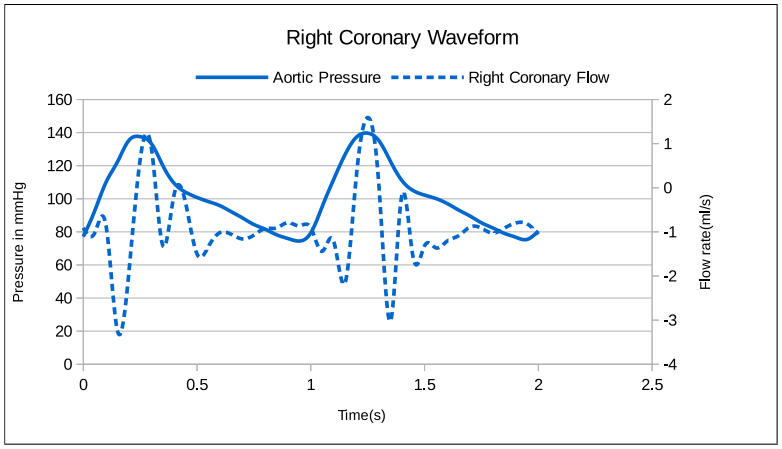

Figure 6.16: Flow and pressure waveform for Right coronary artery (proximal).

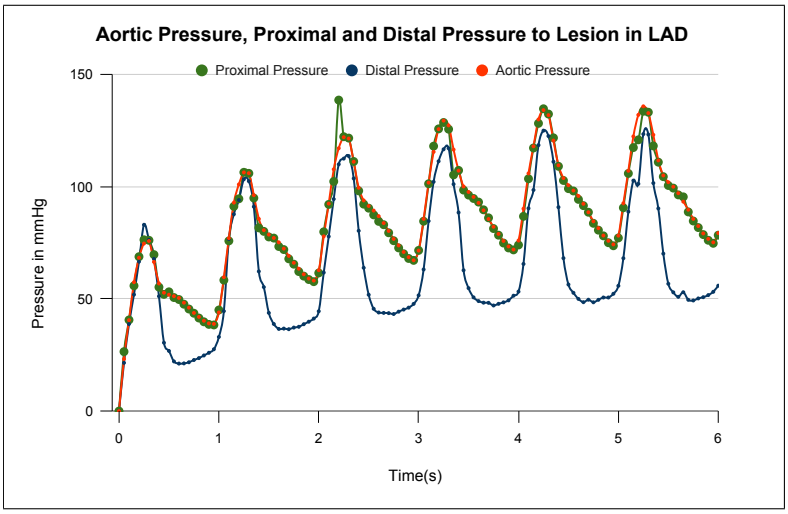

Figure 6.17: Aortic Pressure, Pressure proximal and distal to lesion in LAD.

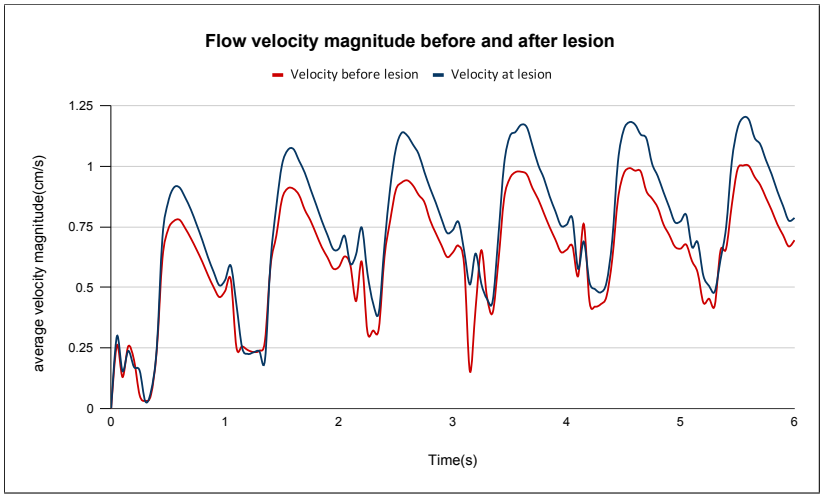

Figure 6.18: Flow velocity proximal and distal to lesion in LAD.

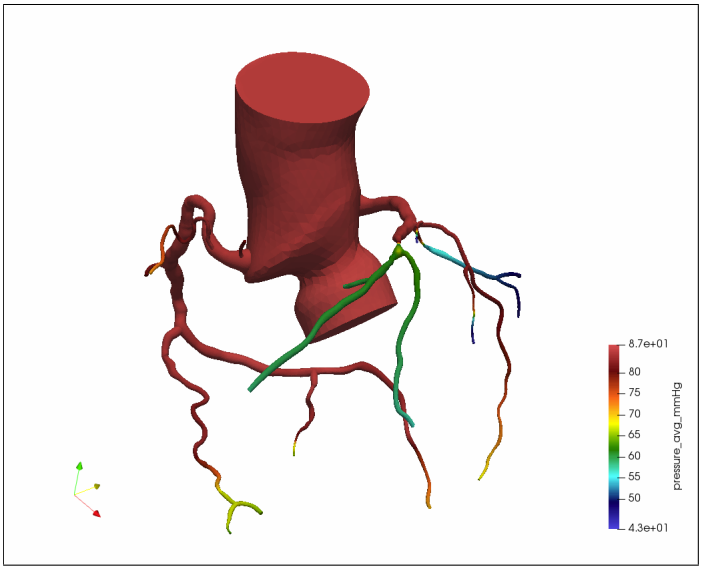

Figure 6.19: Average pressure distribution in coronary artery bed.

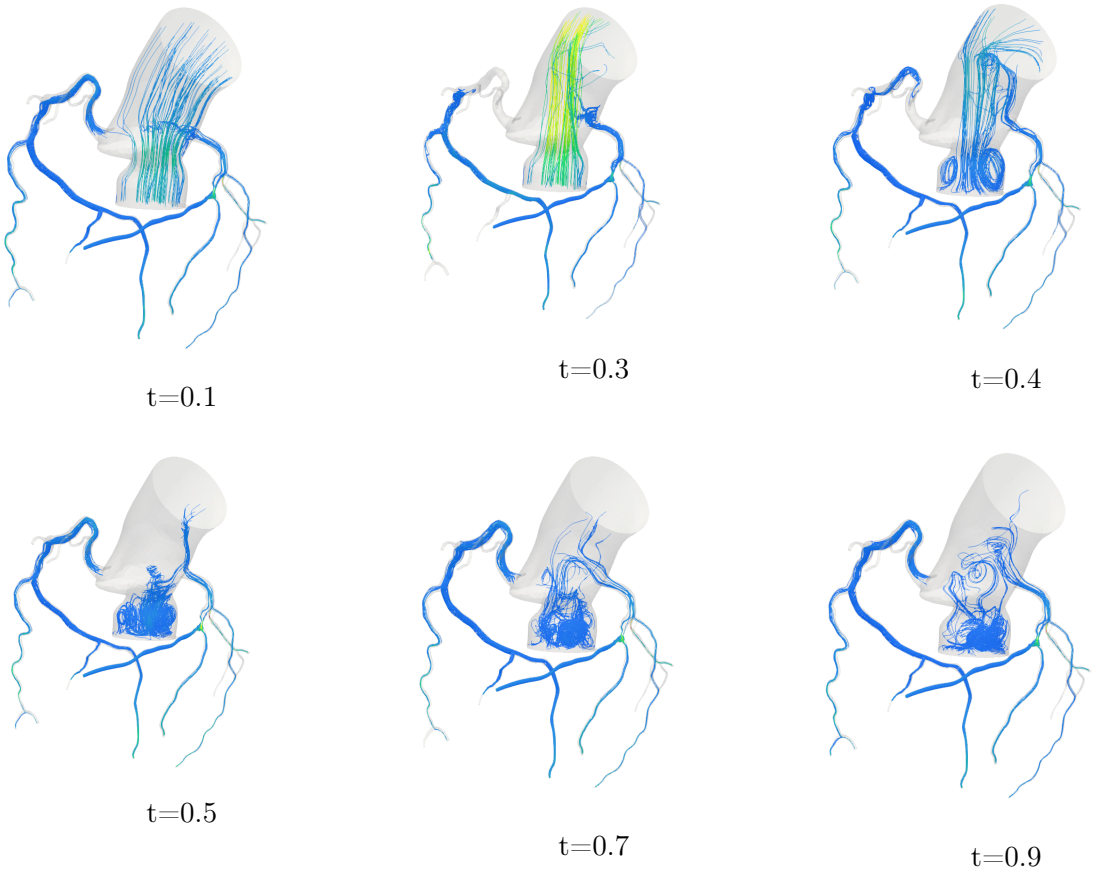

Figure 6.20: Streamlines at different instances of a cardiac cycle.t=0.1 is peak diastole phase and t=0.5 is peak systole phase.

Comparison of Invasive FFR and Computed FFR for case 01

The figure 6.21 show the invasive FFR value for stenoses LAD. The FFR values throughout the coronary tree are shown in figure 6.22. The invasive FFR for value for stenosed LAD is 0.59. The FFR value computed from simulation distal to the LAD lesion is 0.57 (figure 6.23). The simulation show FFR values for LCX in the range of 0.5 to 0.6.

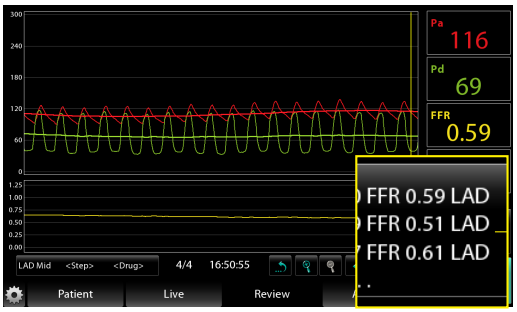

Figure 6.21: Invasive FFR for stenosed LAD for case 01.

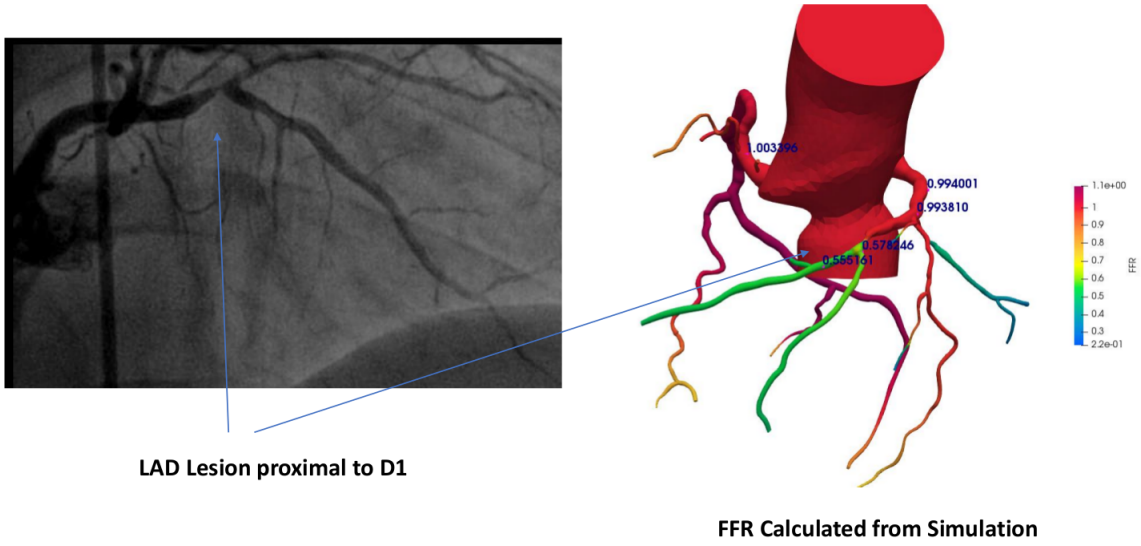

Figure 6.22: Stenosed artery fom ICA image and calculated FFR for case 01.

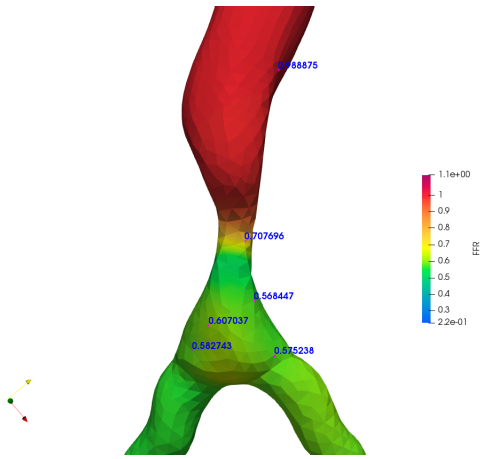

Figure 6.23: FFR values at proximal and distal points to lesion in LAD for case 01.

6.5.2 Case Study 02

Clinical History and Diagnosis

This case is a 43-year-old male with angina on exertion for the duration of 1 month and cardiovascular risk factors of hyperthyroidism and hypertension. The coronary CTA of the patient showed stenosis in LAD with eccentric calcified plaque. The calcified plaque was also visible in LCX and RCA. The LAD trifurcated and the ramus had myocardial bridging. The patient was referred for ICA.

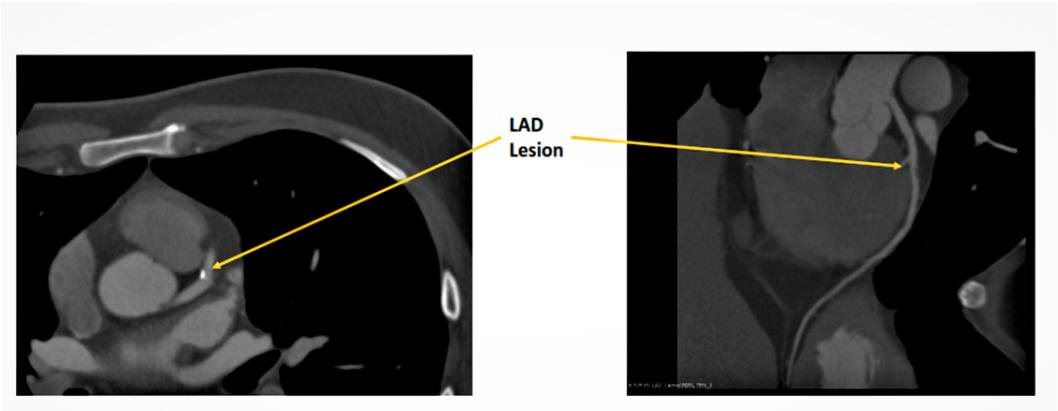

Figure 6.24: CCTA with stenosis in LAD for case 2.

Simulation results for case study 02

For this case, the simulation was run for 6 cardiac cycles. The pressure values stabilize after four cycles (figure 6.25). The FFR values are calculated from the mean pressure values for the last two cardiac cycles.

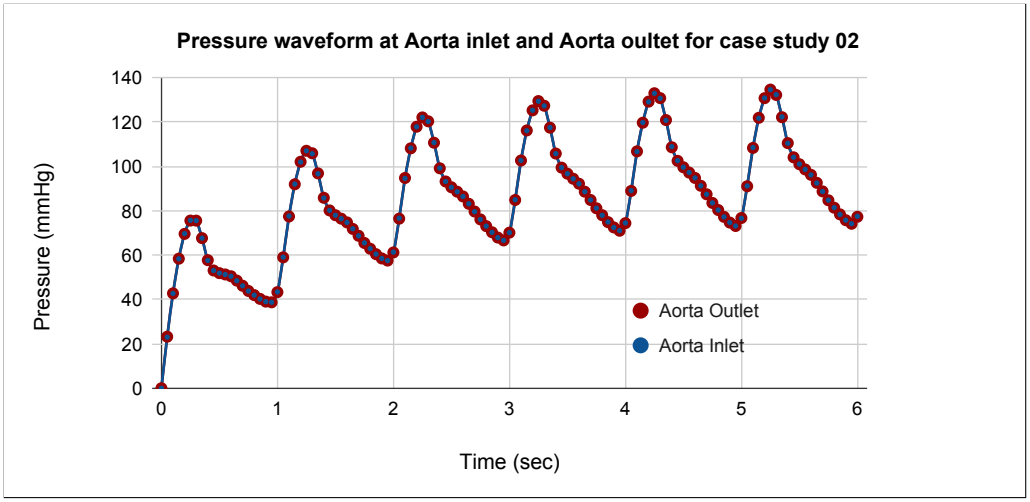

Figure 6.25: Pressure waveform at aorta inlet and outlet for case 2.

Comparison of Invasive FFR and Computed FFR for case 02

The invasive FFR for all the arteries of the patient was greater than 0.9. Thus, there was no PCI. The simulation results also show the FFR for 1.0 for the stenosed region in LAD as shown in figure 6.26.

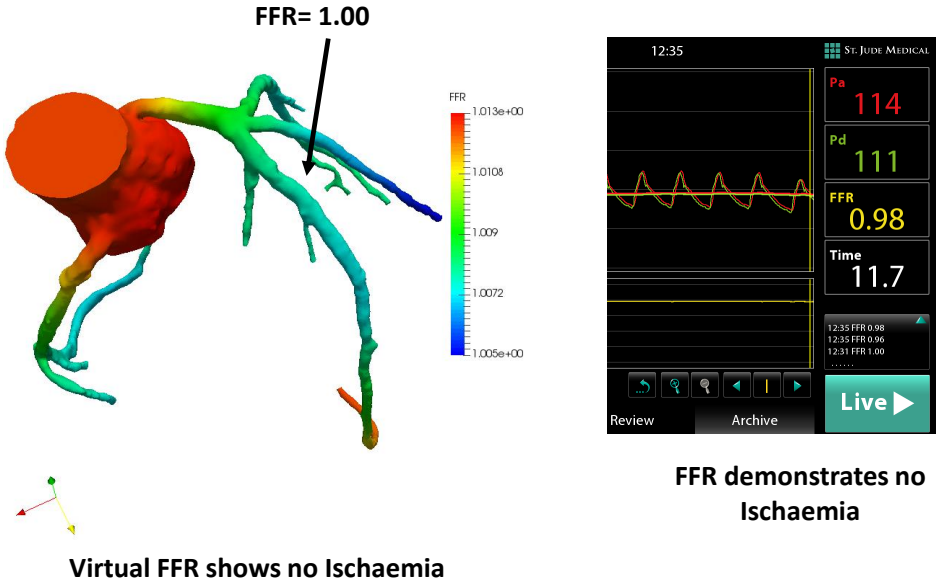

Figure 6.26: Comparison of Invasive FFR with Computed FFR for case 2.

We demonstrated the CT-FFR calculation for two cases of stenosed coronary arteries. Case 01 had an obstructive coronary artery disease while case 02 had non-obstructive stenosis in the arteries. For both the cases, there is good concordance between invasive FFR and computed FFR values. The current framework showed that the physiologically realistic simulation results can be obtained with the modelling assumptions and implemented boundary conditions.

Chapter 7
Outlook

With the increasing prevalence of the coronary artery disease and among the multitude of diagnostic procedures available, there is always a search for an ideal diagnostic test which can hasten the process and reduce the cost in overall patient management. CT-FFR method is a diagnostic method which is being utilized to provide further diagnostic certainty using CCTA datasets. The goal of this project has been to present the methodology of CT-FFR method with open source tools. We reviewed the systematic framework of CT-FFR method relevant to the non-invasive diagnosis of coronary artery disease along with conventional diagnostic strategies and its impact on patient treatment. The process involves the segmentation of coronary arteries from CCTA images, the implementation of reduced-order boundary conditions for 3D models, tuning of boundary condition parameters, and blood flow simulation.

We created a small repository of clinical data through data collection at a local tertiary care hospital. The CCTA and invasive FFR are required data sets for study and validation for CT-FFR tools. Other than these, the data repository also includes invasive coronary angiography data, ECHO reports, blood test reports and patient demographic data. The database is the first Indian database for CT-FFR process. The database for data storage and retrieval was also created. While the data collection to increment our current database continues, we expect that the reference data-set can be used for further research and investigation and the development and testing of clinical tools including but not limited to CT-FFR analysis.

The patient-specific 3D geometric models were created using open-source software (3D Slicer and SimVascular) with the collected CCTA data sets. The model is created by segmentation of arterial lumen from CCTA volume. The blood flow was simulated in two of these models in SimVascular. The blood flow modelling assumptions and flow boundary conditions are specified at the inlet and the outlets of arterial geometry. The lumped parameters models (0D models) implicitly coupled at the boundary of the 3D domain represent the peripheral vasculature. The flow simulation was set up using average values for healthy human at normal conditions as input. The pressure distribution and flow rates were obtained from flow simulation results and the virtual FFR was computed along the arterial branches. The first case study included the patient with obstructive coronary artery disease and the second case-study included the patient with non-obstructive coronary artery disease. For both the cases, the computed FFR showed correlation with clinically measured invasive FFR results. It confirms the general applicability of the implemented assumptions and boundary conditions for the patient-specific blood flow modelling and simulation.

While accurate mathematical modelling of human circulatory system remains a challenge and notable topic of research because of its complexity, the basic tools necessary for evaluation of coronary artery disease are available and already in use. However, the FFR calculated from the models can only be as accurate as the quality of CT-image allows. The modelling of coronary arteries from CT images remains a challenging aspect as the segmentation of coronary artery lumen requires a lot of manual intervention which makes it a time-consuming process. The setup and preparation of computational domain for simulation in CFD solvers also needs a lot of user input which includes tuning of the compliance and resistance values for the arteries. The automation techniques for segmentation, specifications of optimal parameters for patient-specific modelling and simulation along with setup for blood flow simulation need further investigation.

A patient-specific commercial tool for FFR calculation would require much more precision, reproducibility, accuracy and speed along with the optimization of existing mathematical setup. Currently, the HeartFlow is the only available commercial tool for non-invasive FFR evaluation. As the recent studies (Ischemia trial(Lopes *et al.* 2020) and ORBITA trial (Al-Lamee *et al.* 2018)) put further emphasis on the non-invasive treatment of coronary artery disease and minimizing the invasive procedures, a method like CT-FFR gets more relevant for future research in terms of clinical context despite its current limitations. Other than FFR calculation, the same framework can be utilized for evaluation of stenting, the CABG procedure and in the study of other cardiovascular conditions such as peripheral vascular disease, etc. The development and adaptation of such a tool for Indian population in a cost-effective manner would require a larger-scale effort from both the academia and the industry.

Appendix A

A.1 Philips Brilliance 64-Slice CT-Scanner

It is 3^{rd} generation scanner with an aperture of 70cm and MRC (Maximum Rotalic Ceramic) X-Ray Tube. It is paired with CT user environment Philips Extended Brilliance^{TM} Workspace. Specifications of scanner are listed in table A.1.

Parameters	**Values**
Detector	40mm z-axis coverage, solid state GOS
Rows	64
Elements/Row	672
Slice thickness	0.5-10mm
Spatial Resolution	24 line pairs/centimeter
Pitch	0 to 1.5 (user selectable)
Range of CT numbers	-1000 to +3095
Scan FOV	up to 50cm
Image Reconstruction Matrices	256x256, 512x512 , optional 768x768 and 1024x1024
Image Reconstruction time per slice	up to 40 images/sec wiht 3-D cone beam

Table A.1: Philips Brilliance 64-Slice CT-Scanner Specifications (Medwow 2018; Philips CT website 2018)

A.2 Philips Allura Xper FD10 Cath Lab System

It is floor mounted cardiovascular imaging system with two LCD monitors in examination room and features like auto-adjustable copper filteration, virtual collimation, and dose monitoring. It includes 100kW high frequency converter X-ray generator and 4-way floating Xper table. Specifications are listed in table A.2.

A.3 FFR Measurement System

FFR is measured using a mobile unit which includes a touchscreen display, wireless Wi-Box Unit, pressure wire, connection cable, adapter cable, and monitor cable. The product is designed, developed and manufactured by St. Jude Medical Systems AB (abbott).

Wi-box unit is AO transmitter, installed between the AO-transducer and hemodynamic recording system. The system uses frequency hopping spread spectrum (FHSS). FFR is measured using PressureWire Aeris with Agile tip (figure A.1). It is a device with hyrophilic coating. Pressure sensor is located at 3cm length from the tip (length of the radioplaque tip). System specifications are listed in table A.3 and A.4.

Parameters	**Values**
Gantry cranial-to-caudal angulation	45deg/45deg
Motorized rotation rate	25deg /sec
X-ray density	<1mm Al
Radiographic mA	1-1250
Radiographic kV	40-125
Radiographic Timer	2ms-4sec
Fluoroscopic mA	60mA nominal for pulsed fluoro
Fluoroscopic kV	40-125
Number of X-ray tube	1
Focal spot size for X-ray tube	0.5/0.8mm
Imaging features	15 and 30 fps (1024x1024), and 0.5 to 6 fps with vascular option
Detector dimensions	19cm x 18cm
Pixel size	184 μm x 184 μm
Bit depth	14

Table A.2: Philips Allura Xper FD10 Cath Lab System Specifications, (Phillips Medwow 2018)

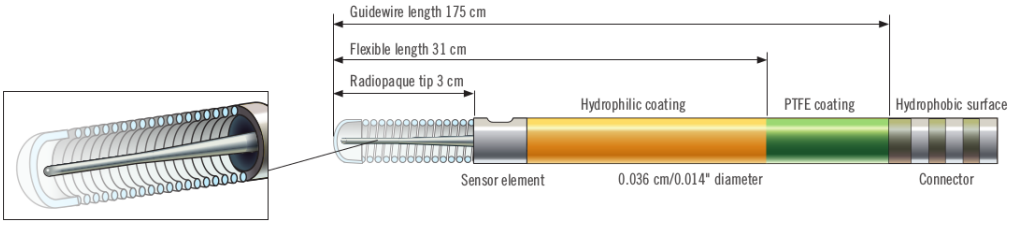

Figure A.1: Pressure wire Aeris with Agile Tip from St. Jude MedicalSystems AB (abbott) (St. Jude global 2018)

Guidewire Length	: 175 cm
Flexible length	: 31cm
Pressure guidwire diameter	: 0.036cm (0.014”)
Radioplaque tip	: 3cm
Operating pressure range	: -30 to +300 mmHg
Accuracy	: $\pm$1mmHg
Zero drift	: <7mmHg/h
Resolution	: $\leq$0.2mmHg
Frequency response	: 0 to 25 Hz

Table A.3: Pressure measurement Specifications (SJM manual 2020)

Wireless Transmission	
Radio Range	: 2m (15-20m in free line of sight)
Battery time transmitter	: 3 hours
Frequency range	: 2.4000-2.4835 GHz (ISM Band)
Radio Type	: Frequency-hopping spread spectrum (FHSS)
Radio Power	: 1mW peak, 7μW average
Total Signal time delay	: <10 ms

Table A.4: Specifications of Wireless transmission(FCCID user manual 2019)

References

Abbara, S., Arbab-Zadeh, A., Callister, T. Q., Desai, M. Y., Mamuya, W. & Thomson, L. 2009 SCCT guidelines for performance of coronary computed tomographic angiography: A report of the Society of Cardiovascular Computed Tomography Guidelines Committee. *Journal of Cardiovascular Computed Tomography* **3** (3), 15.

Absi, R. 2018 Oscillatory and pulsatile flows in environmental, biological and industrial applications.

Achenbach, S., Rudolph, T., Rieber, J., Eggebrecht, H., Richardt, G., Schmitz, T., Werner, N., Boenner, F. & Möllmann, H. 2017 Performing and Interpreting Fractional Flow Reserve Measurements in Clinical Practice: An Expert Consensus Document. *Interventional Cardiology Review* **12** (02), 97.

Adjedj, J., De Bruyne, B., Floré, V., Di Gioia, G., Ferrara, A., Pellicano, M., Toth, G. G., Bartunek, J., Vanderheyden, M., Heyndrickx, G. R., Wijns, W. & Barbato, E. 2016 Significance of Intermediate Values of Fractional Flow Reserve in Patients With Coronary Artery Disease. *Circulation* **133** (5), 502–508.

Agasthi, P., Kanmantharedy, A., Khalil, C., Egbuche, O., Yarlagadda, V., Sachdeva, R. & Arsanjani, R. 2018 Comparison of Computed Tomography derived Fractional Flow Reserve to invasive Fractional Flow Reserve in Diagnosis of Functional Coronary Stenosis: A Meta-Analysis. *Scientific Reports* **8** (1), 11535.

Al-Lamee, R., Thompson, D., Dehbi, H.-M., Sen, S., Tang, K., Davies, J., Keeble, T., Mielewczik, M., Kaprielian, R., Malik, I. S., Nijjer, S. S., Petraco, R., Cook, C., Ahmad, Y., Howard, J., Baker, C., Sharp, A., Gerber, R., Talwar, S., Assomull, R., Mayet, J., Wensel, R., Collier, D., Shun-Shin, M., Thom, S. A., Davies, J. E., Francis, D. P., Al-Lamee, R., Thompson, D., Sen, S., Tang, K., Davies, J., Keeble, T., Kaprielian, R., Malik, I. S., Nijjer, S. S., Petraco, R., Cook, C., Ahmad, Y., Howard, J., Shun-Shin, M., Sethi, A., Baker, C., Sharp, A., Ramrakha, P., Gerber, R., Talwar, S., Assomull, R., Foale, R., Mayet, J., Wensel, R., Thom, S. A., Davies, J. E., Francis, D. P., Khamis, R., Hadjiloizou, N., Khan, M., Kooner, J., Bellamy, M., Mikhail, G., Clifford, P., O'Kane, P., Levy, T. & Swallow, R. 2018 Percutaneous coronary intervention in stable angina (orbita): a double-blind, randomised controlled trial. *The Lancet* **391** (10115), 31 – 40.

Alazzawi, A., Alsaadi, H., Shallal, A. & Albawi, S. 2015 Edge detection-application of (first and second) order derivative in image processing.

Alfakih, K., Byrne, J. & Monaghan, M. 2018 CT coronary angiography: A paradigm shift for functional imaging tests. *Open Heart* **5** (1), e000754.

Armstrong, W. F. & Ryan, T. 2010 *Feigenbaum's Echocardiography 7th 2010*. Lippincott Williams and Wilkins.

Ashley, E. & Niebauer, J. 2004 Coronary artery disease. *In:Cardiology Explained. London: Remedica; 2004 . Available from: "https://www.ncbi.nlm.nih.gov/books/NBK2216/"* .

Baim, D. S. & Grossman, W., ed. 2006 *Grossman's Cardiac Catheterization, Angiography, and Intervention*, 7th edn. Philadelphia: Lippincott Williams & Wilkins.

Basit, S., Khan, S. A. & Akram, M. U. 2014 Segmentation of coronary arteries. In *2014 IEEE Symposium on Industrial Electronics & Applications (ISIEA)*, pp. 66–70. Kota Kinabalu, Malaysia: IEEE.

Basu, S., Bendavid, E. & Sood, N. 2015 Health and Economic Implications of National Treatment Coverage for Cardiovascular Disease in India: Cost-Effectiveness Analysis. *Circulation: Cardiovascular Quality and Outcomes* **8** (6), 541–551.

Bekkers, E. & Taylor, C. 2008 Multiscale Vascular Surface Model Generation From Medical Imaging Data Using Hierarchical Features. *IEEE Transactions on Medical Imaging* **27** (3), 331–341.

Berger, S. A. & Jou, L.-D. 2000 Flows in Stenotic Vessels. *Annual Review of Fluid Mechanics* **32** (1), 347–382.

Betts, J. G., Young, K. A., Wise, J. A., Johnson, E., Poe, B., Kruse, D. H., Korol, O., Johnson, J. E., Womble, M. & DeSaix, P. 2013 Anatomy and physiology, chapter 19 the cardiovascular system: The heart, figure 19.15 coronary circulation. `https://openstax.org/books/anatomy-and-physiology/pages/19-1-heart-anatomy`, [Online: accessed 10-April-2019].

Bidgood, W. D., Horii, S. C., Prior, F. W. & Syckle, D. E. V. 1997 Understanding and Using DICOM, the Data Interchange Standard for Biomedical Imaging. *Journal of the American Medical Informatics Association* **4** (3), 14.

Blanco, P. J. & Feijóo, R. A. 2009 A 3D-1D-0D COMPUTATIONAL MODEL FOR THE ENTIRE CARDIOVASCULAR SYSTEM p. 26.

Blausen,Wikipedia 2013 Illustration depicting coronary artery disease, Under Wikimedia Commons Licence. `https://en.wikiversity.org/wiki/WikiJournal_of_Medicine/Medical_gallery_of_Blausen_Medical_2014#/media/File:Blausen_0259_CoronaryArteryDisease_02.png`, [accessed on 20-April-2020].

BlueCross NC 2017 Corporate medical policy: Computed tomography angiography for coronary artery evaluation, bluecross blueshield of north carolina. https://www.bluecrossnc.com/sites/default/files/document/attachment/services/public/pdfs/medicalpolicy/computed_tomography_angiography_for_coronary_artery_evaluation.pdf, [Online; accessed 22-April-2019].

Budoff, M. & Nakansihi, R. 2016 Noninvasive FFR derived from coronary CT angiography in the management of coronary artery disease: Technology and clinical update. *Vascular Health and Risk Management* p. 269.

Budoff, M. J., Dowe, D., Jollis, J. G., Gitter, M., Sutherland, J., Halamert, E., Scherer, M., Bellinger, R., Martin, A., Benton, R., Delago, A. & Min, J. K. 2008 Diagnostic performance of 64-multidetector row coronary computed tomographic angiography for evaluation of coronary artery stenosis in individuals without known coronary artery disease: Results from the prospective multicenter accuracy (assessment by coronary computed tomographic angiography of individuals undergoing invasive coronary angiography) trial. *Journal of the American College of Cardiology* **52** (21), 1724 – 1732.

Cademartiri, F., Palumbo, A., Maffei, E., Fusaro, M., Vignali, L., Menozzi, A., Brambilla, V., Reverberi, C., Ardissino, D., Zompatori, M. & Crisi, G. 2008 Tips and tricks in Multislice CT coronary angiography. *Researchgate* p. 9.

Canadian Cardiovascular Society 2006 Canadian Cardiovascular Society Grading of Angina Pectoris. http://www.ccs.ca/images/Guidelines/Guidelines_POS_Library/Ang_Gui_1976.pdf, [Online; accessed 22-April-2019].

Cassar, A., Holmes, D. R., Rihal, C. S. & Gersh, B. J. 2009 Chronic Coronary Artery Disease: Diagnosis and Management. *Mayo Clinic Proceedings* **84** (12), 1130–1146.

Chandran, K. B., Rittgers, S. E. & Yoganathan, A. P. 2007 *Biofluid Mechanics: The Human Circulation*. Boca Raton: CRC/Taylor & Francis.

Cho, Y. I. & Kensey, K. R. 1991 Effects of the non-Newtonian viscosity of blood on flows in a diseased arterial vessel. Part 1: Steady flows. *Biorheology* **28** (3-4), 241–262.

Coenen, A., Lubbers, M. M., Kurata, A., Kono, A., Dedic, A., Chelu, R. G., Dijkshoorn, M. L., Gijsen, F. J., Ouhlous, M., van Geuns, R.-J. M. & Nieman, K. 2015 Fractional flow reserve computed from noninvasive ct angiography data: Diagnostic performance of an on-site clinician-operated computational fluid dynamics algorithm. *Radiology* **274** (3), 674–683, pMID: 25322342.

Cohen, B. 2014 Fda approves heartflow ffrct: Non-invasive method for determining coronary ischemia. http://www.ptca.org/news/2014/1126_HEARTFLOW.html, [Online; accessed 10-Jan-2019].

Colleran, R., Douglas, P. S., Hadamitzky, M., Gutberlet, M., Lehmkuhl, L., Foldyna, B., Woinke, M., Hink, U., Nadjiri, J., Wilk, A., Wang, F., Pontone, G.,

Hlatky, M. A., Rogers, C. & Byrne, R. A. 2017 An FFR $_{CT}$ diagnostic strategy versus usual care in patients with suspected coronary artery disease planned for invasive coronary angiography at German sites: One-year results of a subgroup analysis of the PLATFORM (Prospective Longitudinal Trial of FFR $_{CT}$: Outcome and Resource Impacts) study. *Open Heart* **4** (1), e000526.

Cury, R. C., Abbara, S., Achenbach, S., Agatston, A., Berman, D. S., Budoff, M. J., Dill, K. E., Jacobs, J. E., Maroules, C. D., Rubin, G. D., Rybicki, F. J., Schoepf, U. J., Shaw, L. J., Stillman, A. E., White, C. S., Woodard, P. K. & Leipsic, J. A. 2016 CAD-RADSTM Coronary Artery Disease – Reporting and Data System. An expert consensus document of the Society of Cardiovascular Computed Tomography (SCCT), the American College of Radiology (ACR) and the North American Society for Cardiovascular Imaging (NASCI). Endorsed by the American College of Cardiology. *Journal of Cardiovascular Computed Tomography* **10** (4), 269–281.

Curzen, N. P., Nolan, J., Zaman, A. G., Nørgaard, B. L. & Rajani, R. 2016 Does the Routine Availability of CT–Derived FFR Influence Management of Patients With Stable Chest Pain Compared to CT Angiography Alone? *JACC: Cardiovascular Imaging* **9** (10), 1188–1194.

DAC 2017 Ge healthcare, heartflow announce cardiovascular ct collaboration for ffr-ct, 2017. `https://www.dicardiology.com/product/ge-healthcare-heartflow-announce-cardiovascular-ct-collaboration-ffr-ct`, [Online; accessed 10-Jan-2019].

DAC Feature 2018 Diagnostic and interventional cardiology feature-ffr technologies:new technology directions in fractional flow reserve (ffr), 2018. `https://www.dicardiology.com/article/new-technology-directions-fractional-flow-reserve-ffr`, [Online; accessed 12-Feb-2019].

Damien, D. 2015 A very basic dicom introduction. `https://dcm4che.atlassian.net/wiki/spaces/d2/pages/1835038/A+Very+Basic+DICOM+Introduction`, [accessed 20-Sep-2018].

Dawson, T. H. 2005 Modeling of vascular networks. *Journal of Experimental Biology* **208** (9), 1687–1694.

Dicom NEMA 2019*a* Dicom ps3.1 2019b - introduction and overview. `http://dicom.nema.org/medical/dicom/current/output/html/part01.html`, [Online: accessed 2-Feb-2019].

Dicom NEMA 2019*b* Dicom ps3.3 2019b - information object definitions. `http://dicom.nema.org/medical/dicom/current/output/html/part03.html#PS3.3`, [Online: accessed 2-Feb-2019].

Dicom NEMA 2019*c* Dicom:dicom faq (excerpt from http://www.dclunie.com/medical-image-faq/html/part1.html). `https://www.dicomstandard.org/faq/`, [Online: accessed 2-Feb-2019].

Dicom NEMA 2019*d* Dicom:overview. `https://www.dicomstandard.org/`, [Online: accessed 2-Feb-2019].

Dodge, J. T., Brown, B. G., Bolson, E. L. & Dodge, H. T. 1992 Lumen diameter of normal human coronary arteries. Influence of age, sex, anatomic variation, and left ventricular hypertrophy or dilation. *Circulation* **86** (1), 232–246.

Douglas, P. S. 2016 1-Year Outcomes of FFRCT-Guided Care in Patients With Suspected Coronary Disease. *Journal of the American College of Cardiology* **68** (5), 11.

Douglas, P. S., Pontone, G., Hlatky, M. A., Patel, M. R., Norgaard, B. L., Byrne, R. A., Curzen, N., Purcell, I., Gutberlet, M., Rioufol, G., Hink, U., Schuchlenz, H. W., Feuchtner, G., Gilard, M., Andreini, D., Jensen, J. M., Hadamitzky, M., Chiswell, K., Cyr, D., Wilk, A., Wang, F., Rogers, C. & De Bruyne, B. 2015 Clinical outcomes of fractional flow reserve by computed tomographic angiography-guided diagnostic strategies vs. usual care in patients with suspected coronary artery disease: The prospective longitudinal trial of FFR $_{CT}$: Outcome and resource impacts study. *European Heart Journal* **36** (47), 3359–3367.

Elgendy, I. Y., Conti, C. R. & Bavry, A. A. 2014 Fractional Flow Reserve: An Updated Review: Fractional flow reserve review. *Clinical Cardiology* **37** (6), 371–380.

FCCID user manual 2019 Wireless transmission. `https://manuals.sjm.com/~/media/manuals/product-manual-pdfs/0/2/0249b90f-f4b4-409d-8dcf-5a1ab899478a.pdf`, [accessed Aug-2019].

Fearon, W. F., Tonino, P. A., De Bruyne, B., Siebert, U. & Pijls, N. H. 2007 Rationale and design of the fractional flow reserve versus angiography for multivessel evaluation (FAME) study. *American Heart Journal* **154** (4), 632–636.

Fedorov, A., Beichel, R., Kalpathy-Cramer, J., Finet, J., Fillion-Robin, J.-C., Pujol, S., Bauer, C., Jennings, D., Fennessy, F., Sonka, M., Buatti, J., Aylward, S., Miller, J. V., Pieper, S. & Kikinis, R. 2012 3D Slicer as an image computing platform for the Quantitative Imaging Network. *Magnetic Resonance Imaging* **30** (9), 1323–1341.

Fox, C., Davies, M. J. & Webb-Peploe, M. M. 1973 Length of left main coronary artery. *Heart* **35** (8), 796–798.

Fung, G. S. K., Segars, W. P., Gullberg, G. T. & Tsui, B. M. W. 2011 Development of a model of the coronary arterial tree for the 4D XCAT phantom. *Physics in Medicine and Biology* **56** (17), 5651–5663.

Ghasemalizadeh, O., Mirzaee, M. R., Firoozabadi, B. & Hassani, K. 2014 Exact Modeling of Cardiovascular System Using Lumped Method p. 10.

Gorenoi, V., Schönermark, M. P. & Hagen, A. 2012 Ct coronary angiography vs. invasive coronary angiography in chd. *GMS Health Technology Assessment; 8:Doc02; ISSN 1861-8863* .

Hall, J. E. & Guyton, A. C. 2011 *Guyton and Hall Textbook of Medical Physiology*, 12th edn. Philadelphia, Pa: Saunders/Elsevier.

HeartFlow Cost 2019 Reducing the cost of care:provides significant savings to the healthcare system. https://www.heartflow.com/study-results, [Online; accessed 20-Feb-2019].

HeartFlow Inc. 2019*a* The heartflow analysis. https://www.heartflow.com/, [Online; accessed 10-Jan-2019].

HeartFlow Inc. 2019*b* The heartflow ffr-ct analysis. https://www.heartflow.com/heartflow-ffrct-analysis, [Online; accessed 20-Dec-2019].

Hoffman, M. 2018 ifr more cost-effective than ffr for patients requiring pci. https://www.hcplive.com/view/ifr-more-costeffective-than-ffr-for-patients-requiring-pci, [Online; accessed 15-Feb-2020].

Hoskins, P. R., Keevil, S. F. & Mirsadraee, S. 2016*a* Medical Imaging. In *Cardiovascular Biomechanics* (ed. P. R. Hoskins, P. Lawford & B. J. Doyle), pp. 163–191. New York, NY: Springer Berlin Heidelberg.

Hoskins, P. R., Lawford, P. & Doyle, B. J., ed. 2016*b* *Cardiovascular Biomechanics*. New York, NY: Springer Berlin Heidelberg.

Huang, X. & Tsechpenakis, G. 2009 *Medical image segmentation*. Cited By 13.

ICMR 2017 India: Health of the *nation's* states the india state-level disease burden initiative indian council of medical research public health foundation of india institute for health metrics and evaluation. https://www.healthdata.org/sites/default/files/files/policy_report/2017/India_Health_of_the_Nation$\%$27s_States_Report_2017.pdf, [online:accessed on 10-April-2019].

IFHP report 2019 ifhp comparative price report issued,for year 2017. https://healthcostinstitute.org/blog/entry/international-comparisons-of-health-care-prices-2017-ifhp-survey, [Online; accessed 15-Feb-2020].

Igarashi, A., Fujito, K., Hirano, M. & Fukuda, T. 2013 Cost minimization analysis of beta-blocker at the time of ct imaging for suspected of coronary heart disease in japan. *Journal of medical economics* **17**.

India Healthcare Tourism 2020 Cost of medical treatment & duration. http://www.indiahealthcaretourism.com/average_cost_of_treatment.php, [Online accessed 13 April-2020].

Innolitics 2016 Dicom standard browser by innolitics,2016-2019 innolitics, llc. https://dicom.innolitics.com/ciods, [accessed 10-Oct-2018].

ITK 2019 ITK - Segmentation & Registration Toolkit. https://itk.org/, [accessed on 10-April-2019].

Japan HeartFlow 2016 Heartflow ffrct approved for use in japan, 2016. https://cardiovascularnews.com/heartflow-ffrct-approved-for-use-in-japan/, [Online; accessed 20-Dec-2019].

Japan NCGM 2020 Central hospital of the national center for global health medicine. `http://www.hosp.ncgm.go.jp/en/inpatient/070/index.html`, [Online accessed 13 April-2020].

Jiang, X., Zhang, R. & Nie, S. 2012 Image Segmentation Based on Level Set Method. *Physics Procedia* **33**, 840–845.

Johnson, N. P., Johnson, D. T., Kirkeeide, R. L., Berry, C., De Bruyne, B., Fearon, W. F., Oldroyd, K. G., Pijls, N. H. & Gould, K. L. 2015 Repeatability of Fractional Flow Reserve Despite Variations in Systemic and Coronary Hemodynamics. *JACC: Cardiovascular Interventions* **8** (8), 1018–1027.

Kalra, A. 2018 Chapter 9 - developing fe human models from medical images. In *Basic Finite Element Method as Applied to Injury Biomechanics* (ed. K.-H. Yang), pp. 389 – 415. Academic Press.

Kaptoge, S., Pennells, L., De Bacquer, D., Cooney, M. T., Kavousi, M., Stevens, G., Riley, L. M., Savin, S., Khan, T., Altay, S., Amouyel, P., Assmann, G., Bell, S., Ben-Shlomo, Y., Berkman, L., Beulens, J. W., Björkelund, C., Blaha, M., Blazer, D. G., Bolton, T., Bonita Beaglehole, R., Brenner, H., Brunner, E. J., Casiglia, E., Chamnan, P., Choi, Y.-H., Chowdry, R., Coady, S., Crespo, C. J., Cushman, M., Dagenais, G. R., D'Agostino Sr, R. B., Daimon, M., Davidson, K. W., Engström, G., Ford, I., Gallacher, J., Gansevoort, R. T., Gaziano, T. A., Giampaoli, S., Grandits, G., Grimsgaard, S., Grobbee, D. E., Gudnason, V., Guo, Q., Tolonen, H., Humphries, S., Iso, H., Jukema, J. W., Kauhanen, J., Kengne, A. P., Khalili, D., Koenig, W., Kromhout, D., Krumholz, H., Lam, T., Laughlin, G., Marín Ibañez, A., Meade, T. W., Moons, K. G. M., Nietert, P. J., Ninomiya, T., Nordestgaard, B. G., O'Donnell, C., Palmieri, L., Patel, A., Perel, P., Price, J. F., Providencia, R., Ridker, P. M., Rodriguez, B., Rosengren, A., Roussel, R., Sakurai, M., Salomaa, V., Sato, S., Schöttker, B., Shara, N., Shaw, J. E., Shin, H.-C., Simons, L. A., Sofianopoulou, E., Sundström, J., Völzke, H., Wallace, R. B., Wareham, N. J., Willeit, P., Wood, D., Wood, A., Zhao, D., Woodward, M., Danaei, G., Roth, G., Mendis, S., Onuma, O., Varghese, C., Ezzati, M., Graham, I., Jackson, R., Danesh, J. & Di Angelantonio, E. 2019 World Health Organization cardiovascular disease risk charts: Revised models to estimate risk in 21 global regions. *The Lancet Global Health* **7** (10), e1332–e1345.

Karmonik, C., Brown, A., Debus, K., Bismuth, J. & Lumsden, A. B. 2014 Cfd challenge: Predicting patient-specific hemodynamics at rest and stress through an aortic coarctation. In *Statistical Atlases and Computational Models of the Heart. Imaging and Modelling Challenges* (ed. O. Camara, T. Mansi, M. Pop, K. Rhode, M. Sermesant & A. Young), pp. 94–101. Berlin, Heidelberg: Springer Berlin Heidelberg.

Kern, M. J., Sorajja, P. & Lim, M. J. 2018 *The Interventional Cardiac Catheterization Handbook*. Elsevier.

Kim, H. J., Vignon-Clementel, I. E., Coogan, J. S., Figueroa, C. A., Jansen, K. E. & Taylor, C. A. 2010 Patient-Specific Modeling of Blood Flow and Pressure in Human Coronary Arteries. *Annals of Biomedical Engineering* **38** (10), 3195–3209.

Kimura, T., Shiomi, H., Kuribayashi, S., Isshiki, T., Kanazawa, S., Ito, H., Ikeda, S., Forrest, B., Zarins, C. K., Hlatky, M. A. & Norgaard, B. L. 2015 Cost analysis of non-invasive fractional flow reserve derived from coronary computed tomographic angiography in Japan. *Cardiovascular Intervention and Therapeutics* **30** (1), 38–44.

Kincaid, E. 2018 Heartflow has raised $500 million for a test to detect heart disease. does it make patients better off? `https://www.forbes.com/sites/elliekincaid/2018/08/26/heartflow-has-raised-500-million-for-a-test-to-detect-heart-disease-does-it-make-patients-better-off/#2758`, [Online; accessed 20-Feb-2019].

Klabunde, R. E. 2011 *Cardiovascular Physiology Concepts-LWW (2011)*, 2nd edn. Lippincott Williams & Wilkins.

Klag, M. J. 2012 51 - epidemiology of cardiovascular disease. In *Goldman's Cecil Medicine (Twenty Fourth Edition)*, Twenty fourth edition edn. (ed. L. Goldman & A. I. Schafer), pp. 256 – 260. Philadelphia: W.B. Saunders.

Koo, B.-K., Erglis, A., Doh, J.-H., Daniels, D. V., Jegere, S., DeFrance, T., Lansky, A., Leipsic, J. & Min, J. K. 2011 Diagnosis of Ischemia-Causing Coronary Stenoses by Noninvasive Fractional Flow Reserve Computed From Coronary Computed Tomographic Angiograms. *Journal of the American College of Cardiology* **58** (19), 9.

Kruk, M., Wardziak, Ł., Demkow, M., Pleban, W., Pręgowski, J., Dzielińska, Z., Witulski, M., Witkowski, A., Rużyłło, W. & Kępka, C. 2016 Workstation-Based Calculation of CTA-Based FFR for Intermediate Stenosis. *JACC: Cardiovascular Imaging* **9** (6), 690–699.

Larobina, M. & Murino, L. 2014 Medical Image File Formats. *Journal of Digital Imaging* **27** (2), 200–206.

Levick, J. R. 1991 *An Introduction to Cardiovascular Physiology*. London ; Boston: Butterworths.

Lopes, R. D., Alexander, K. P., Stevens, S. R., Reynolds, H. R., Stone, G. W., Pina, I. L., Rockhold, F. W., Elghamaz, A., Lopez-Sendon, J. L., Farsky, P. S., Chernyavskiy, A. M., Diaz, A., Phaneuf, D., DeBelder, M. A., tong Ma, Y., Guzman, L. A., Khouri, M., Sionis, A., Hausenloy, D. J., Doerr, R., Selvanayagam, J. K., Maggioni, A. P., Hochman, J. S. & Maron, D. J. 2020 Initial invasive versus conservative management of stable ischemic heart disease patients with a history of heart failure or left ventricular dysfunction: Insights from the ischemia trial. *Circulation* **0** (0).

Lu, M. T., Ferencik, M., Roberts, R. S., Lee, K. L., Ivanov, A., Adami, E., Mark, D. B., Jaffer, F. A., Leipsic, J. A., Douglas, P. S. & Hoffmann, U. 2017 Noninvasive FFR Derived From Coronary CT Angiography. *CARDIOVASCULAR IMAGING* **10** (11), 9.

Mantero, S., Pietrabissa, R. & Fumero, R. 1992 The coronary bed and its role in the cardiovascular system: A review and an introductory single-branch model. *Journal of Biomedical Engineering* **14** (2), 109–116.

Margolis, D. J. A., Hoffman, J. M., Herfkens, R. J., Jeffrey, R. B., Quon, A. & Gambhir, S. S. 2007 Molecular imaging techniques in body imaging. *Radiology* **245** (2), 333–356, pMID: 17940297.

Marino, P. L. 2014 *The ICU Book*, 4th edn. LIPPINCOTT WILLIAMS & WILKINS.

Medwow 2018 Philips brilliance 64-slice ct-scanner. `http://www.medwow.com/med/ct-scanner/philips/brilliance-64-slice/8917.model-spec`, [accessed 01-Aug-2018].

Meijboom, W. B., Van Mieghem, C. A., van Pelt, N., Weustink, A., Pugliese, F., Mollet, N. R., Boersma, E., Regar, E., van Geuns, R. J., de Jaegere, P. J., Serruys, P. W., Krestin, G. P. & de Feyter, P. J. 2008 Comprehensive assessment of coronary artery stenoses: Computed tomography coronary angiography versus conventional coronary angiography and correlation with fractional flow reserve in patients with stable angina. *Journal of the American College of Cardiology* **52** (8), 636 – 643.

Min, J. K., Leipsic, J., Pencina, M. J., Berman, D. S., Koo, B.-K., van Mieghem, C., Erglis, A., Lin, F. Y., Dunning, A. M., Apruzzese, P., Budoff, M. J., Cole, J. H., Jaffer, F. A., Leon, M. B., Malpeso, J., Mancini, G. B. J., Park, S.-J., Schwartz, R. S., Shaw, L. J. & Mauri, L. 2012 Diagnostic Accuracy of Fractional Flow Reserve From Anatomic CT Angiography. *JAMA* **308** (12), 1237.

Min, J. K., Shaw, L. J. & Berman, D. S. 2010 The Present State of Coronary Computed Tomography Angiography. *Journal of the American College of Cardiology* **55** (10), 957–965.

Min, J. K., Taylor, C. A., Achenbach, S., Koo, B. K., Leipsic, J., Nørgaard, B. L., Pijls, N. J. & De Bruyne, B. 2015 Noninvasive Fractional Flow Reserve Derived From Coronary CT Angiography. *JACC: Cardiovascular Imaging* **8** (10), 1209–1222.

Moreno, C. & Bhaganagar, K. 2013 Modeling of Stenotic Coronary Artery and Implications of Plaque Morphology on Blood Flow. *Modelling and Simulation in Engineering* **2013**, 1–14.

Moschetti, K., Favre, D., Pinget, C., Pilz, G., Petersen, S. E., Wagner, A., Wasserfallen, J.-B. & Schwitter, J. 2014 Comparative cost-effectiveness analyses of cardiovascular magnetic resonance and coronary angiography combined with fractional flow reserve for the diagnosis of coronary artery disease. *Journal of Cardiovascular Magnetic Resonance* **16** (1), 13.

Murray, C. D. 1926 THE PHYSIOLOGICAL PRINCIPLE OF MINIMUM WORK APPLIED TO THE ANGLE OF BRANCHING OF ARTERIES. *The Journal of General Physiology* **9** (6), 835–841.

National Heart, Lung, and Blood Institute 2018 Atherosclerosis. `https://www.nhlbi.nih.gov/health-topics/atherosclerosis`, [accessed on 20-April-2019].

National Statistical Office India 2019 Press note on provisional estimate of annual national income 2018-19 and quaterly estimates of gross domestic product for the fourth quarter(q4) of 2018-19. http://mospi.nic.in/sites/default/files/press_release/PressNotePE2018-19-31.5.2019-Final.pdf.

NICE HeartFlow 2017 Heartflow ffrct for estimating fractional flow reserve from coronary ct angiography. https://www.nice.org.uk/guidance/mtg32/chapter/1-Recommendations, [Online; accessed 20-Dec-2019].

Nichols, W. W., Nichols, W. W. & McDonald, D. A., ed. 2011 *McDonald's Blood Flow in Arteries: Theoretic, Experimental, and Clinical Principles*, 6th edn. London: Hodder Arnold.

Nicoguaro,Wikipedia 2018 An illustration of the level-set method, Creative Commons Attribution 4.0 International. https://en.wikipedia.org/wiki/Level-set_method#/media/File:Level_set_method.png, [accessed on 20-April-2020].

Nørgaard, B. L. 2014 Diagnostic Performance of Noninvasive Fractional Flow Reserve Derived From Coronary Computed Tomography Angiography in Suspected Coronary Artery Disease. *Journal of the American College of Cardiology* **63** (12), 11.

Noumeir, R., Lemay, A. & Lina, J.-M. 2007 Pseudonymization of Radiology Data for Research Purposes. *Journal of Digital Imaging* **20** (3), 284–295.

OpenStax CNX 2013 Openstax, viscosity and laminar flow; poiseuilleâĂŹs law. http://cnx.org/contents/a4293fc2-4de2-4506-b890-a7abdeb70c16@4.

OTpedia 2019 Otpedia: Acr-nema. http://www.otpedia.com/entryDetails.cfm?id=31, [accessed 2-Feb-2019].

Pappano, A. J., Wier, W. G. & Levy, M. N. 2013 *Cardiovascular Physiology*, 10th edn. *Mosby Physiology Monograph Series* 10. Philadelphia, PA: Elsevier/Mosby.

Parisot, C. 2003 The basic structure of dicom,ge medical systems. http://www.ssrpm.ch/old/dicom/parisot1.pdf, [accessed 10-Oct-2018].

Park, S.-J., Kang, S.-J., Ahn, J.-M., Shim, E. B., Kim, Y.-T., Yun, S.-C., Song, H., Lee, J.-Y., Kim, W.-J., Park, D.-W., Lee, S.-W., Kim, Y.-H., Lee, C. W., Mintz, G. S. & Park, S.-W. 2012 Visual-Functional Mismatch Between Coronary Angiography and Fractional Flow Reserve. *JACC: Cardiovascular Interventions* **5** (10), 1029–1036.

Patel, M. R., Dai, D., Hernandez, A. F., Douglas, P. S., Messenger, J., Garratt, K. N., Maddox, T. M., Peterson, E. D. & Roe, M. T. 2014 Prevalence and predictors of nonobstructive coronary artery disease identified with coronary angiography in contemporary clinical practice. *American Heart Journal* **167** (6), 846–852.e2.

Pavone, P., Fioranelli, M. & Dowe, D. A. 2009 *CT Evaluation of Coronary Artery Disease*. Springer.

Philips CT website 2018 Philips brilliance 64-slice ct-scanner. https://www.usa.philips.com/healthcare/product/HC889407/diamond-select-brilliance-refurbished-64-channel-ct-scanner, [accessed 01-Aug-2018].

Phillips Medwow 2018 Phillips allura xper fd10 cath lab system. http://www.medwow.com/med/cath-lab/philips/allura-xper-fd10/34130.model-spec, [accessed 07-Aug-2018].

Pierce, E. 2019 Diagram of the human heart (cropped).svgm, gnu free doc. license. https://commons.wikimedia.org/wiki/File:Diagram_of_the_human_heart_(cropped).svg, [Online; accessed 10-January-2019].

Pijls, N. H., Fearon, W. F., Tonino, P. A., Siebert, U., Ikeno, F., Bornschein, B., van't Veer, M., Klauss, V., Manoharan, G., Engstrøm, T., Oldroyd, K. G., Ver Lee, P. N., MacCarthy, P. A. & De Bruyne, B. 2010 Fractional Flow Reserve Versus Angiography for Guiding Percutaneous Coronary Intervention in Patients With Multivessel Coronary Artery Disease. *Journal of the American College of Cardiology* **56** (3), 177–184.

Prabhakaran, D., Jeemon, P., Sharma, M., Roth, G. A., Johnson, C., Harikrishnan, S., Gupta, R., Pandian, J. D., Naik, N., Roy, A., Dhaliwal, R. S., Xavier, D., Kumar, R. K., Tandon, N., Mathur, P., Shukla, D. K., Mehrotra, R., Venugopal, K., Kumar, G. A., Varghese, C. M., Furtado, M., Muraleedharan, P., Abdulkader, R. S., Alam, T., Anjana, R. M., Arora, M., Bhansali, A., Bhardwaj, D., Bhatia, E., Chakma, J. K., Chaturvedi, P., Dutta, E., Glenn, S., Gupta, P. C., Johnson, S. C., Kaur, T., Kinra, S., Krishnan, A., Kutz, M., Mathur, M. R., Mohan, V., Mukhopadhyay, S., Nguyen, M., Odell, C. M., Oommen, A. M., Pati, S., Pletcher, M., Prasad, K., Rao, P. V., Shekhar, C., Sinha, D. N., Sylaja, P. N., Thakur, J. S., Thankappan, K. R., Thomas, N., Yadgir, S., Yajnik, C. S., Zachariah, G., Zipkin, B., Lim, S. S., Naghavi, M., Dandona, R., Vos, T., Murray, C. J. L., Reddy, K. S., Swaminathan, S. & Dandona, L. 2018 The changing patterns of cardiovascular diseases and their risk factors in the states of India: The Global Burden of Disease Study 1990–2016. *The Lancet Global Health* **6** (12), e1339–e1351.

Prasad, S., Harikrishnan, S., Sanjay, G., Abhilash, S., Bijulal, S., Kumar, M. K., Tharakan, J. & Ajit Kumar, V. 2017 Clinical Outcomes of patients with coronary artery disease who underwent FFR evaluation of intermediate coronary lesionS– COFFRS study. *Indian Heart Journal* **69** (4), 499–504.

Pryor, D., Hlatky, M. & Califf, R. 1991 Estimating the Likelihood of Severe Coronary Artery Disease. *The American Journal of Medicine* p. 10.

Raut, B. K., Patil, V. N. & Cherian, G. 2017 Coronary artery dimensions in normal Indians. *Indian Heart Journal* **69** (4), 512–514.

Rossmann, J., Berger, S. & Saloner, D. 2000 Influence of stenosis morphology on flow through severely stenotic vessels: Implications for plaque rupture. *Journal of biomechanics* **33**, 443–55.

Saikrishna, C., Talwar, S., Gulati, G. & Kumar, A. S. 2006 Normal coronary artery dimensions in Indians. *Indian Journal of Thoracic and Cardiovascular Surgery* **22** (3), 159–164.

Sanchis-Gomar, F., Perez-Quilis, C., Leischik, R. & Lucia, A. 2016 Epidemiology of coronary heart disease and acute coronary syndrome. *Annals of Translational Medicine* **4** (13), 256–256.

Sankaran, S., Esmaily Moghadam, M., Kahn, A. M., Tseng, E. E., Guccione, J. M. & Marsden, A. L. 2012 Patient-Specific Multiscale Modeling of Blood Flow for Coronary Artery Bypass Graft Surgery. *Annals of Biomedical Engineering* **40** (10), 2228–2242.

Sciola, M. I., Morris, P. D., Gosling, R., Lawford, P. V., Hose, D. R. & Gunn, J. P. 2018 The impact of Objective Mathematical Analysis during Fractional Flow Reserve measurement: Results from the OMA-FFR study. *EuroIntervention* **14** (8), 935–941.

Sengottuvelu, G., Chakravarthy, B., Rajendran, R. & Ravi, S. 2016 Clinical usefulness and cost effectiveness of fractional flow reserve among Indian patients (FIND study): Study of FFR Among Indian Patients. *Catheterization and Cardiovascular Interventions* **88** (5), E139–E144.

Shi, Y., Lawford, P. & Hose, R. 2011 Review of Zero-D and 1-D Models of Blood Flow in the Cardiovascular System. *BioMedical Engineering OnLine* **10** (1), 33.

SJICR 2019 Sri jayadeva institute of cardiovascular sciences and research: Procedure charges: Billing. `http://www.jayadevacardiology.com/procedure_charges.html`, [Online; accessed 27-December-2019].

SJM manual 2020 Sjm manual. `https://manuals.sjm.com/~/media/manuals/product-manual-pdfs/0/2/0249b90f-f4b4-409d-8dcf-5a1ab899478a.pdf`, [accessed Jan-2020].

Spencer, M. P. & Reid, J. M. 1979 Quantitation of carotid stenosis with continuous-wave (C-W) Doppler ultrasound. *Stroke* **10** (3), 326–330.

St. Jude global 2018 Pressure wire aeris with agile tip. `https://www.sjmglobal.com/en-int/professionals/resources-and-reimbursement/technical-resources/vascular/intravascular-diagnostics-and-imaging/intravascular-sensors-ffr-measurement/pressurewire-aeris-with-agile-tip-technology-wireless-ffr-measurement`, [accessed 07-Aug-2018].

Tanaka, N., Kohsaka, S., Murata, T., Akasaka, T., Kadota, K., Uemura, S., Amano, T., Shiode, N., Morino, Y., Fujii, K., Hikichi, Y. & Nakamura, M. 2019 Treatment strategy modification and its implication on the medical cost of fractional flow reserve-guided percutaneous coronary intervention in Japan. *Journal of Cardiology* **73** (1), 38–44.

Taylor, C. A., Fonte, T. A. & Min, J. K. 2013 Computational Fluid Dynamics Applied to Cardiac Computed Tomography for Noninvasive Quantification of Fractional Flow Reserve. *Journal of the American College of Cardiology* **61** (22), 2233–2241.

Tonino, P. A. L., Fearon, W. F., Oldroyd, K. G., Leesar, M. A. & MacCarthy, P. A. 2010 Angiographic Versus Functional Severity of Coronary Artery Stenoses in the FAME Study. *Journal of the American College of Cardiology* **55** (25), 6.

Tonino, P. A. L., Siebert, U., Manoharan, G. & MacCarthy, P. A. 2009 Fractional Flow Reserve versus Angiography for Guiding Percutaneous Coronary Intervention. *n engl j med* p. 12.

UK FFR-CT 2019 Nhs england innovation and technology payment: Heartflow itp flyer. `https://www.ahsnnetwork.com/wp-content/uploads/2019/04/Heartflow-ITP-flyer.pdf`, [Online accessed 13 April-2020].

Updegrove, A., Wilson, N. M., Merkow, J., Lan, H., Marsden, A. L. & Shadden, S. C. 2017 SimVascular: An Open Source Pipeline for Cardiovascular Simulation. *Annals of Biomedical Engineering* **45** (3), 525–541.

Uus, A. 2016 Patient-Specific Blood Flow Modelling in Diagnosis of Coronary Artery Disease. PhD thesis, City, University of London Institutional Repository.

Vignon-Clementel, I., Figueroa, C., Jansen, K. & Taylor, C. 2010 Outflow boundary conditions for 3D simulations of non-periodic blood flow and pressure fields in deformable arteries. *Computer Methods in Biomechanics and Biomedical Engineering* **13** (5), 625–640.

Vignon-Clementel, I. E., Alberto Figueroa, C., Jansen, K. E. & Taylor, C. A. 2006 Outflow boundary conditions for three-dimensional finite element modeling of blood flow and pressure in arteries. *Computer Methods in Applied Mechanics and Engineering* **195** (29-32), 3776–3796.

VTK 2019 VTK-The Visualization Toolit. `https://vtk.org/`, [accessed on 10-April-2019].

Waller, B. F., Orr, C. M., Slack, J. D., Pinkerton, C. A., Van Tassel, J. & Peters, T. 1992 Anatomy, histology, and pathology of coronary arteries: A review relevant to new interventional and imaging techniques-Part I. *Clinical Cardiology* **15** (6), 451–457.

Whittaker, A. & Curzen, N. 2013 What has the RIPCORD trial told us about using fractional flow reserve for diagnostic angiography? *Interventional Cardiology* **5** (6), 593–596.

Wootton, D. M. & Ku, D. N. 1999 Fluid mechanics of vascular systems, diseases, and thrombosis. *Annual Review of Biomedical Engineering* **1** (1), 299–329, pMID: 11701491.

World Health Organization 2016 Global health estimates 2016: Deaths by cause, age, sex, by country and by region, 2000- 2016. `http://www.who.int/healthinfo/global_burden_disease/estimates/en/`, [Online; accessed 10-January-2019].

Wu, S. P., Ringgaard, S., Oyre, S., Hansen, M. S., Rasmus, S. & Pedersen, E. M. 2004 Wall shear rates differ between the normal carotid, femoral, and brachial arteries: An in vivo MRI study. *Journal of Magnetic Resonance Imaging* **19** (2), 188–193.

Zarins, C. K., Taylor, C. A. & Min, J. K. 2013 Computed Fractional Flow Reserve (FFTCT) Derived from Coronary CT Angiography. *Journal of Cardiovascular Translational Research* **6** (5), 708–714.

Zhou, Y., Kassab, G. S. & Molloi, S. 1999 On the design of the coronary arterial tree: A generalization of Murray's law. *Physics in Medicine and Biology* **44** (12), 2929–2945.

Zimmermann, F. M., Omerovic, E., Fournier, S., Kelbæk, H., Johnson, N. P., Rothenbühler, M., Xaplanteris, P., Abdel-Wahab, M., Barbato, E., Høfsten, D. E., Tonino, P. A. L., Boxma-de Klerk, B. M., Fearon, W. F., Køber, L., Smits, P. C., De Bruyne, B., Pijls, N. H. J., Jüni, P. & Engstrøm, T. 2019 Fractional flow reserve-guided percutaneous coronary intervention vs. medical therapy for patients with stable coronary lesions: Meta-analysis of individual patient data. *European Heart Journal* **40** (2), 180–186.